



Universidad  
del País Vasco

Euskal Herriko  
Unibertsitatea

FACULTY  
OF ENGINEERING  
BILBAO  
UNIVERSITY  
OF THE BASQUE  
COUNTRY

# 3D printable polylactide-based functional systems with enhanced radiopacity and biological activity

Naroa Sadaba Larraona

Supervisors

Ester Zuza Hernandez

Jone Muñoz Ugartemendia

Bilbao, April 2021



ZIBIO Group, Department of Mining-Metallurgy Engineering and  
Materials Science

School of Engineering

Bilbao

Spain

Institute for Medicines iMed.Ulisboa,

Faculty of Pharmacy

Lisbon

Portugal

And

Institute of Biophysik

Universität für Bodenkultur Wien

Vienna

Austria





A mis padres Rafael y Puy



## TABLE OF CONTENTS





## Table of Contents

Summary .....	15
Resumen.....	21
CHAPTER 1:INTRODUCTION .....	29
1.1. Hard tissue engineering: Bone fixation devices .....	29
1.2. Manufacturing of scaffolds for bone tissue engineering: Material extrusion 3D printing.....	32
Polylactides for bone tissue engineering .....	39
Objectives .....	45
Bibliography .....	48
CHAPTER 2: REHOLOGICAL ANALYSIS OF POLYLACTIDE INKS FOR 3D PRINTING .....	65
2.1. Introduction.....	65
2.2. Printing process: 3D Bioplotter.....	67
2.3. Analysis of the fluid flow .....	70
2.4. Welding between layers or filaments .....	77
2.5. FINAL GEOMETRY OF THE SCAFFOLD.....	86
2.6. CONCLUSION .....	90
2.7. Material and experimental method .....	92
2.8. Bibliography .....	93
CHAPTER 3: RADIOPAQUE MATERIAL FOR 3D PRINTING .....	105
3.1. Introduction .....	105
3.2. Radiopaque particles addition: Properties of materials .....	109

3.3.	3D printing of radiopaque materials.....	121
3.4.	Viability of radiopaque materials for biomedical applications .....	124
3.5.	Conclusion .....	132
3.6.	Material and experimental methods .....	133
3.7.	Bibliography .....	139
CHAPTER 4: POLYLACTIDE BASED 3D PRINTABLE MATERIALS WITH BIOLOGICAL PERFORMANCE.....		153
4.1.	Introduction .....	153
4.2.	Synthesis and characterization of PLA-DA.....	157
4.3.	3D printing of PLA/PLA-DA blends .....	169
4.4.	Biological activity of PLA/PLA-DA scaffolds .....	171
4.5.	Conclusion .....	181
4.6.	Material and experimental method.....	182
4.6.1.	Materials .....	182
4.6.2.	Synthesis of L-Lactide .....	182
4.6.3.	Characterization of the PLA-DA polymer .....	183
4.6.4.	Characterization of blends .....	185
4.6.5.	Biological activity characterization .....	186
4.7.	Reference .....	188
General conclusion .....		199
APPENDIX .....		203
A1.	List of Figures.....	205
A2.	List of Tables .....	205

A3. Symbols and Abbreviations .....	205
Curriculum Vitae .....	213



## SUMMARY/RESUMEN



## Summary

In recent years biomaterials, and especially bioresorbable polymers, have become very popular in medical devices and scaffolds for tissue engineering. Tissue engineering has gained great interest due to the increase in life quality that entails the restoration of damaged tissue, more specifically bone tissue.

The development of bioresorbable polymeric materials for bone regeneration emerged to avoid a second surgical intervention for removal of metallic implants once the healing process is completed, or to avoid the problems caused by metallic implants such as rejection, sensitivity to the metallic components or weakening of the restored bone, a phenomenon known as stress-shielding.

Bioresorbable polymers do not require a second surgery, since they are reabsorbed as the tissue is restored. Therefore, the use of these materials represents a significant economic and social advance.

For an implant to be suitable for application in the field of bone tissue engineering, it must fulfil the following characteristics:

- It must be biocompatible to avoid adverse reactions in the human body.
- It must degrade and promote tissue integration, so it should be a porous material with adequate interconnection between them.
- It must have appropriate mechanical properties to the intended application site and handling.
- It must be easily to process to achieve the desired geometry and structure.
- It must be economically cost-effective.

Poly lactide (PLA) and its compounds are one of the most frequently adopted biodegradable polymers in the manufacture of scaffolds for bone fixation systems. PLA is a semi-crystalline thermoplastic polymer, with a glass transition temperature ( $T_g$ )  $\sim 60$  °C and melting temperature ( $T_m$ )  $\sim 180$  °C that is obtained by ring-opening polymerization (ROP) of L-lactide. Despite the fact that PLA shows adequate modulus of elasticity and mechanical strength, it is very brittle which limits its use in bone fixation devices. Furthermore, from a clinical point of view, breakage of a bone fixation device may cause further dislocation of the fractured bone, in addition to the presence of loose material. This loose material could cause irritation or some kind of adverse reaction, and would be very difficult to localize, since PLA is not visible to X-Rays. On the other hand, PLA lacks biological properties which makes its application difficult, since sometimes the body rejects the material or the cells do not integrate well along the scaffold. For rejection to occur, an inflammation is generated first, with subsequent infection that causes this scaffold to have to be removed.

As a solution to these drawbacks, the work of this doctoral thesis focuses on improving radiopacity and toughness, as well as, biological activity of PLA based scaffolds.

Initially, special attention is given to solution 3D printing. Subsequently, the thesis focuses on obtaining composite materials that show improve radiopacity and toughness, by means of addition of radiopaque particles. For this purpose, barium sulfate ( $BaSO_4$ ) particles are a good alternative as they are approved by the *Food and Drug Administration* (FDA).

Dopamine and its polymer polydopamine are used to enhance drug attachment/release. (Poly)dopamine is a universal adhesive inspired by



mussel adhesion that readily interacts with organic and inorganic substances, due to the possibility of pi-pi interaction of the aromatic ring as well as the hydroxyls of the catechol. It exhibits excellent properties as a coating, protective layer of materials. Therefore, (poly)dopamine is an ideal candidate to be combined with biodegradable polymers to increase drug adhesiveness. One of the main novelties of the thesis work is that, although it is usually used as a coating, it is also incorporated into the PLA polymeric chain conferring such properties to the chain itself.

To contextualize the PhD work, **chapter 1** provides an introduction to tissue engineering and in particular to bone tissue engineering. Next, scaffold processing techniques are described, here a brief overview on conventional techniques is given but mainly focuses on the different techniques offered by additive manufacturing (AM). It will be explained more deeply the extrusion-based 3D printing, since it is the one selected in this thesis for printing the PLA and PLA based materials. Finally, it discusses the use of different materials for bone tissue engineering and describes the advantages and disadvantages of PLA.

This thesis is divided into two main blocks: the first block consists of the fabrication of the scaffolds (chapter 2) and the second block of the improvement of the mechanical properties of PLA and drug attachment/release (biological activity) (chapter 3 and chapter 4, respectively).

In the first block of this thesis (**chapter 2**), PLA inks are studied to be 3D printed in the solution printing mode. Therefore, this chapter focuses on solution printing, different solvents are used to obtain PLA inks and a rheological study is carried out, which allows obtaining a model for 3D

printing. By means of this model, the printer parameters are obtained. In addition, the bond strength between the layers and filaments and the final geometry of the 3D printed part are analyzed.

The second part of this thesis focuses on PLA improvements. The first part of **chapter 3** is devoted to the improvement of the radiopacity and toughness of PLA. BaSO<sub>4</sub> particles are added to the PLA matrix, bringing radiopacity and toughness to the system simultaneously, due to a proper use of particle size papers (*"High Toughness Biodegradable Radiopaque Composites Based On Polylactide And Barium Sulphate"* and *"Understanding The Toughness Mechanism Prompted By Submicron Rigid Particles In Polylactide/Barium Sulfate Composites"*). Once these properties are improved, the second part focuses on improving the biological activity by drug adsorption and release. For this purpose, these particles are coated with polydopamine, so that the drugs can be adsorbed by the material for their subsequent release in the human body (paper *"Benefits Of Polydopamine As Particle/Matrix Interface In Polylactide/PD-BaSO<sub>4</sub> Scaffolds"*).

In Chapter 4, another strategy to improve the biological activity response of PLA are developed. The first part focuses on the synthesis of PLA using dopamine as an initiator. This polymerization in itself is already novel, since it is carried out in a single step and without the protection of the catechol alcohols (paper *"Catechol End-Functionalized Polylactide By Organocatalyzed Ring-Opening Polymerization"*). Once this new material has been obtained, the adsorption and drug release of the PLA with dopamine and the antibacterial activity are analyzed. A cellular study is also performed to demonstrate that the material and the amount of drug introduced in it are not toxic for the cells.

To conclude, **it shows** the conclusions of the contributions achieved in this work, the improvement of PLA toughness, radiopacity and the biological activity with a comprehensive study of controlled drug adsorption/release.

In view of the results, although there is still a long way to go, there is no doubt that the advances obtained in this research line will allow to obtain tailor-made "ad hoc" devices which are more efficient, economical, easily processable and quicker to obtain

.

## Resumen

En los últimos años los biomateriales, y en especial los polímeros bioreabsorbibles, han adquirido gran popularidad en dispositivos médicos y en andamios (*scaffolds*) para ingeniería de tejidos. Este último campo ha cobrado gran interés debido al aumento de calidad de vida que supone para la sociedad la restauración de tejido dañado, más en concreto el tejido óseo.

El desarrollo de los materiales poliméricos bioreabsorbibles para regeneración ósea, surgió debido a que, los implantes metálicos necesitan una segunda intervención quirúrgica para la eliminación de los dispositivos una vez terminado el proceso de curación, o para evitar los problemas causados por los implantes metálicos como el rechazo, sensibilidad a los componentes metálicos o el debilitamiento del hueso restaurado, fenómeno conocidos como *stress-shielding*.

Los polímeros bioreabsorbibles no necesitan de una segunda cirugía, ya que se van reabsorbiendo a medida que el tejido se va restaurando. Por lo tanto, el uso de estos materiales supone un avance económico y social notables.

Para que un ímplate sea adecuado para su aplicación en el campo de la ingeniería de tejidos óseos, debe tener las siguientes características:

- Debe ser biocompatible para evitar reacciones adversas en el cuerpo humano;
- Debe degradarse y promover la integración del tejido, por lo que conviene que sea un material poroso con adecuada interconexión entre ellos;
- Debe contener unas propiedades mecánicas adecuadas al lugar de aplicación y la manipulación previstos;

- Debe ser fácilmente procesable para conseguir la geometría y estructura deseada y
- Debe ser económicamente rentable.

La polilactida (PLA) y sus compuestos, son uno de los polímeros biodegradables más frecuentemente adoptados en la fabricación de andamios para los sistemas de fijaciones óseas. El PLA es un polímero termoplástico semicristalino, con una temperatura de transición vítrea ( $T_g$ )  $\sim 60$  °C y temperatura de fusión ( $T_m$ )  $\sim 180$  °C que se obtiene por polimerización de apertura de anillo (ROP) de la L-lactida. A pesar del hecho de que el PLA muestra un adecuado módulo de elasticidad y resistencia mecánica, es muy frágil lo que limita su uso en los dispositivos de fijación ósea. Además, desde un punto de vista clínico, la rotura de un dispositivo de fijación ósea puede causar una nueva dislocación del hueso fracturado, además de la presencia de material suelto. Este material libre podría causar irritación o algún tipo de reacción adversa, y sería muy difícil de localizar, ya que, el PLA es transparente a los rayos X. Por otro lado, el PLA carece de propiedades biológicas lo que a veces dificulta su aplicación, puesto que, en ocasiones el cuerpo rechaza el material o las células no se integran bien a lo largo del andamio. lo que ocurre es que se genera una inflamación y posterior infección que hace que este andamio tenga que ser retirado

Como solución a estos inconvenientes, el trabajo de esta tesis doctoral se centra en mejorar la radiopacidad, y las propiedades tanto biológicas como mecánicas

Inicialmente se pone especial atención en la impresión 3D por solución del polímero. Posteriormente, la tesis se centra en la obtención de materiales compuestos que muestran radiopacidad y tenacidad, mediante mezclas

físicas con partículas radiopacas. Para este fin las partículas de sulfato de bario ( $\text{BaSO}_4$ ) son una buena alternativa ya que están aprobadas por la Administración de Medicamentos y Alimentos (*Food and Drug Administration*, FDA)

Para mejorar la adsorción/liberación de droga (actividad biológica) se usa la dopamina y su polímero polidopamina. La (poli)dopamina es un adhesivo universal inspirado en la adhesión de los mejillones que interactúa fácilmente con sustancias orgánicas e inorgánicas, debido a la posibilidad de interacción pi-pi del anillo aromático, así como de los hidroxilos del catecol. Presenta unas excelentes propiedades como recubrimiento, capa protectora de materiales. Por lo tanto, la (poli)dopamina es un candidato ideal para ser combinado con polímeros biodegradables para aumentar adhesividad de droga. Una de las novedades principales del trabajo de tesis es que, a pesar de usarse normalmente como recubrimiento, también se incorpora a la cadena polimérica del PLA confiriendo dichas propiedades a la propia cadena.

Para proporcionar contexto a esto, el **Capítulo 1** ofrece una introducción a la ingeniería de tejidos y en especial a la ingeniería de tejido ósea. Inicialmente se describen las técnicas de procesado de andamios, aquí se hace un breve resumen de las técnicas convencionales pero nos centramos en las diferentes técnicas que ofrece la metodología avanzada o la fabricación aditiva (AM). Y centrándonos en la impresión 3D en base extrusión, ya que será la seleccionada para la impresión de los materiales (compuestos) que se van a usar a lo largo de esta tesis. Finalmente se describe el uso de distintos materiales para ingeniería de tejidos óseo y enfocándose en el PLA, se explican las ventajas y desventajas de dicho material.

Esta tesis se divide en dos bloques principales: el primer bloque consta de la fabricación de los andamios (capítulo 2) y el segundo bloque consta de la mejora de las propiedades mecánicas y biológicas del PLA (capítulo 3 y capítulo 4, respectivamente).

En el primer bloque de esta tesis (**capítulo 2**), se realiza un estudio de impresión del PLA analizando la impresión 3D en disolución (tintas de PLA). Por ello en este capítulo se centra en la impresión por disolución, se usan diferentes disolventes para obtener las tintas de PLA y se realiza un estudio reológico, el cual permite obtener un modelo para la impresión 3D. Mediante este modelo, se obtienen los parámetros de la impresora. Además, se analizan la fuerza de unión entre las capas y filamentos y la geometría final de la pieza impresa mediante impresión 3D.

El segundo bloque de esta tesis se centra en las mejoras del PLA. La primera parte de **capítulo 3**, se ciñe a la mejora de la radiopacidad y la tenacidad del PLA. Las partículas de BaSO<sub>4</sub> se añaden a la matriz de PLA, aportándole radiopacidad y tenacidad al sistema simultáneamente, debido a un adecuado uso del tamaño de partículas.(artículos "*High Toughness Biodegradable Radiopaque Composites Based On Polylactide And Barium Sulphate*" y "*Understanding The Toughness Mechanism Prompted By Submicron Rigid Particles In Polylactide/Barium Sulfate Composites*") Una vez mejoradas estas propiedades, la segunda parte se enfoca en la mejora de la actividad biológica para la adsorción y liberación de fármacos. Para ello se recubrirán estas partículas con polidopamina, de este modo se consigue que los fármacos puedan ser adsorbidos por el material para su posterior liberación en el cuerpo humano (artículo "*Benefits Of Polydopamine As Particle/Matrix Interface In Polylactide/PD-BaSO<sub>4</sub> Scaffolds*").



En el **Capítulo 4** se desarrollan estrategias para mejorar la actividad biológica del PLA. La primera parte se centra en la síntesis de PLA con el uso de dopamina como iniciador. Esta polimerización de por sí ya es novedosa, puesto que se realiza en una única etapa y sin la protección de los alcoholes del catecol (artículo "*Catechol End-Functionalized Polylactide By Organocatalyzed Ring-Opening Polymerization*"). Una vez obtenido este nuevo material, se analizan la adsorción y liberación de fármaco del PLA con dopamina y la actividad antibacteriana. También se realiza un estudio celular para demostrar que el material y la cantidad de fármaco introducida en él, no son tóxicas para las células.

Para finalizar, se muestran las conclusiones de las contribuciones logradas en este trabajo, la mejora de la tenacidad, radiopacidad del PLA y la mejora de la actividad biológica con el estudio exhaustivo de la adsorción/liberación de medicamento controlada.

Lo que revela que, aunque todavía queda mucho camino por delante, no hay duda de que los avances obtenidos en esta línea permiten obtener dispositivos hechos a medida "ad hoc" los cuales son más eficaces, económicos, fácilmente procesables y rápidas de obtener.





# Chapter 1



## CHAPTER 1:INTRODUCTION

This introduction provides to the reader the general context of this thesis to facilitate understanding of the scope of this project. This thesis arose from the need to formulate new printable and functional polymeric systems based on polylactides (PLA) for tissue engineering, especially for bone fracture fixations.

This introduction includes an overview of the state of the art of bone fixations in tissue engineering (TE), as well as an overview of PLA and its most potential applications as bioresorbable fixations and its main drawbacks. Finally, the processing modes of this material will be analyzed, focused mainly on scaffolds fabrication which plays a very important role in tissue engineering.

### **1.1. Hard tissue engineering: Bone fixation devices**

Langer and Vacanti introduced the term tissue engineering (TE) as "an interdisciplinary field that applies the principles of engineering and life sciences to the development of biological substitutes that restore, maintain or improve tissue function" in 1993 [1]. Usually, TE requires a structural support device, known as a scaffold, for cell implantation and attachment. The scaffold is three-dimensional (3D), highly porous with an interconnected pore network which provides as an intermediary template/model for tissue regeneration [2]. In the general procedure of tissue engineering, the cells can be isolated from the patient, expanded *in vitro*, and seeded into a scaffold shortly before implantation [3], and regeneration is based on the subsequent deposition of an extracellular matrix (ECM) inside the body. The scaffold can be implanted also without cells (see Figure 1.1).

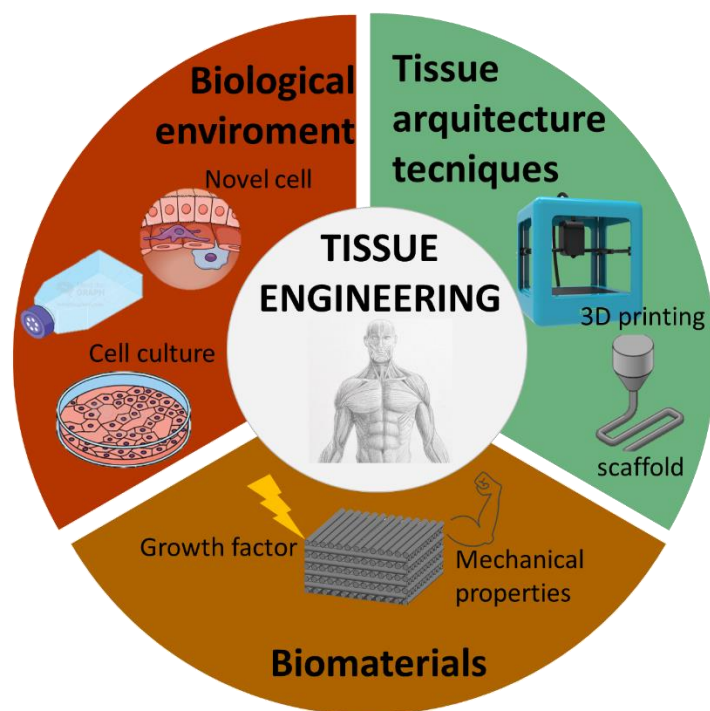


**Figure 1.1.** Areas involved in tissue engineering

Tissue engineering, like the human body, is classified into two main groups: (1) hard tissue engineering and (2) Soft tissue engineering. Hard tissues, also known as calcified tissues, are those containing calcium phosphate minerals such as bone and dental enamel, dentine and cement [4]. Soft tissues embraces the rest of the tissues/organs such as liver, lung, muscle, skin, nerves, blood vessels, cornea, heart valves, trachea and adipose tissues. Usually they consist of dense fibre network [5,6]. In the last decade researchers have investigated regeneration of both, hard tissue (bone [7,8]) and soft tissue (liver, heart valves and arteries, bladders, pancreas, nerves, corneas and other soft tissues [9]) and even the combination of both (skin-cartilage and bone-cartilage[10–12]). However, it has been demonstrated that bone has the highest possibility for regeneration among many other tissues in the body [13].

Throughout this thesis we will focus on osseous implants for hard tissue engineering.

Bone fixation devices have long been metallic, but these cause various complications, such as sensitization to components, corrosion, mutagenicity and interference with therapeutic irradiation, thermal sensitivity and palpability, but also bone fixation devices require a second intervention to remove them [14–16].

Ceramics such as hydroxyapatite (HA) or tricalcium sulfate (TCP) have also been used in bone stiffening engineering, these materials are more interesting than metallic ones due to their osteoconductive and osteoinductive properties, which help bone regeneration. However, they are very fragile materials and it is very difficult to predict their degradation. Moreover, their degradation can lead to a subproducts such as Ca and P which may cause cell death [17,18].

For all these reasons, bone fixation implants with biodegradable and bioresorbable materials have become of great interest which do not generate foreign particles for the human body, and avoid a second intervention.

Biodegradable polymers can be classified in two groups: natural biodegradable polymers and synthetic biodegradable polymers. The natural ones are those obtained from natural sources, such as collagen, chitosan, starch, hyaluronic acid. The main advantage of these polymers is their bioactive capacity, that is, their ability to interact with bone tissue. Their disadvantages are their limited mechanical properties and their difficulty of processing. Synthetic polymers are the most widely used in bone tissue engineering, due to their mechanical properties, versatility and

processability. Among them poly(carbonates), poly(phosphazenes), poly(anhydrides), poly(propylene fumarates) and poly( $\alpha$ -hydroxy acids) are found. The latter are the most widely used [16,19–21].

For an implant to be suitable for bone tissue engineering, the following characteristics must be fulfilled:

- To have interconnected pores of adequate scale to promote tissue integration and be easily manufactured in a variety of shapes and sizes [22–25]
- To be made of a biodegradable material with controlled biodegradation so that the regenerated tissue eventually replaces the scaffold.
- To have adequate surface chemistry to promote cellular adhesion, proliferation and differentiation.
- To possess adequate mechanical properties to suit the intended site of implantation and handling.
- To avoid adverse reactions in the human body.

These characteristics make the choice of the material and the manufacturing process of the implant or scaffold vital to succeed.

The following sections will introduce the two main aspects of this thesis: (1) the manufacturing of scaffolds by extrusion 3D printing and (2) the drawbacks to overcome in order to polylactides being used for bone tissue engineering.

### **1.2. Manufacturing of scaffolds for bone tissue engineering:**

#### **Material extrusion 3D printing**

In this section, the fabrication and processing of PLA scaffolds will be discussed. Despite being different techniques, the conventional methods of



scaffold fabrication such as solvent casting/particular leaching, gas foaming, emulsification, freeze-drying, phase separation and electrospinning. have the following limitations in common [26,27]:

- Difficulties in controlling pore size shape and interconnectivity.
- Poor mechanical properties (especially in electrospinning).
- Non-uniform structures, difficulty in reproducing complex geometries.

This means that these scaffolds do not achieve the desired success for bone fixation devices.

Advanced methodologies such as additive manufacturing (AM) eliminates the problems of the conventional processing techniques by introducing computer aid design (CAD). CAD allows to control both the geometry of the fixture and the geometry and size of the pore and its interconnectivity.

There are different printing methods but all of them share the same operation, in other words, all the 3D printers generate objects layer by layer. First, the geometry is designed in CAD, then the created design is divided into layers and finally the geometry and pore size is designed. This design is saved in a .STL file, taken to the 3D printer, which prints the object layer by layer. (Figure 1.2).

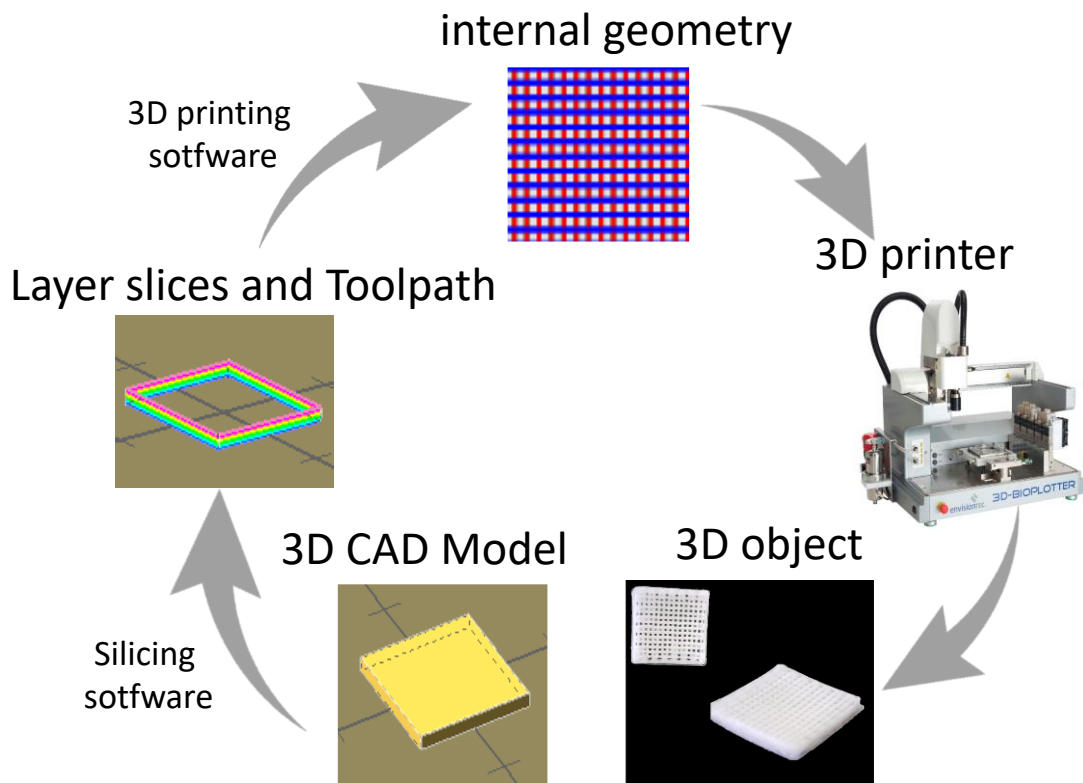


**Figure 1.2.** 3D printing process scheme, from the CAD model to the printed object

ASTM F2792-12a [28] standard divides the types of 3D printers according to the way of processing the material classifying them into seven groups (see Table 1.1).

**Table 1.1.** Additive manufacturing technologies overview according to ASTM F2792-12a

Process of AM	Process description	Type of 3D printing machine	Materials
Binder jetting (BJG)	Printing consists of a liquid adhesive agent that is selectively deposited to join powdered materials	binder jetting (BJG) and 3D printing (3DP)	ceramics and metal composites [32–34].
Directed energy deposition (DED)	This type of printer uses focused thermal energy, and is used to fuse materials by melting while depositing	directed light fabrication (DLF), direct metal deposition (DMD) and laser engineered shaping (LENS)	metal powders[32,35,36].
Powder bed fusion	This type of printer also uses thermal energy, but in this case the thermal energy selectively fuses regions of a powder bed	selective heat sintering (SHS), selective laser melting (SLM), electron beam melting (EBM) and direct metal laser sintering (DMLS)	Metals, high melting point polymers such as polyether ether ketone (PEEK) and polypropylene (PP) and ceramics[32,37–39].
Material jetting	In this process droplets of build material are selectively deposited. usually employed for bioprinting	inkjet printing(CIJ), multijet modelling (MJM), polyjet modelling (PJM), drop-on-demand (DoD)	ultra violet (UV)-curable photopolymers and hydrogels [40–42].
Sheet lamination	The process consist of bonded sheets of material to form an object.	ultrasonic additive manufacturing (UAM) and laminated object manufacturing (LOM).	Polymer like polyvinyl chloride (PVC), soft materials and bioink (cells and hydrogel) [43,44].
Vat photopolymerization	Liquid photopolymer in a vat is selectively cured by light-activated polymerization	stereolithography (SL), two-photon polymerization (2PP), digital light processing (DLP) and continuous liquid interface production (CLIP)	UV-curable photopolymers [45–47]
Material extrusion	Material is selectively dispensed through a nozzle or orifice	extrusion deposition modelling (FDM), direct ink writing (DIW).	thermoplastic such as polyester (PLA, PCL and their derivatives), polycarbonate (PC), acrylonitrile butadiene styrene (ABS), polystyrene (PS), Polyvinyl alcohol (PVA), as well as composite materials,[48–50].

According to table 1.1 the way to print PLA is through the extrusion process. Therefore, this thesis will be focused on extrusion 3D printing process. This printing process is describe in Figure 1.3a. A continuous PLA filament is fed and heated in a heating head where melts partly. Then the melt is extruded through a nozzle and the extruded filament is deposited on a platform, creating an object layer-by-layer [50]. The layers are bonded together because the material is still in a semi-liquid state when it is deposited [51], finally the layers solidify at room temperature.

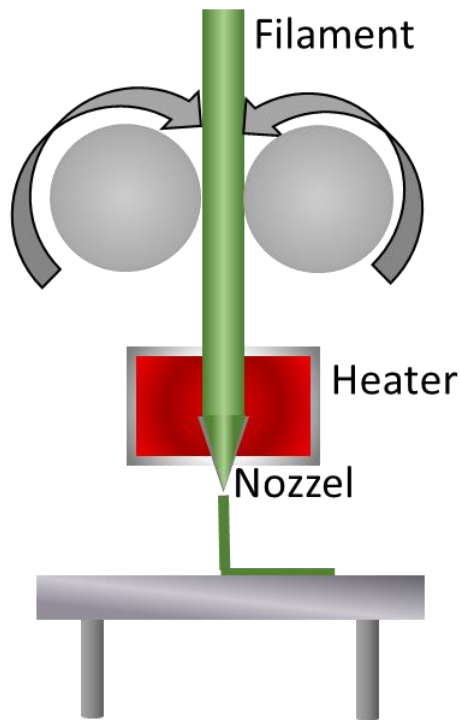


**Figure 1.3.** Schematic of the 3D printing process by material extrusion (FDM)

The mechanical properties and how the printing parameters (pore size, filament orientation, temperature and printing speed) affect the final properties of the objects have been analyzed in depth for PLA scaffolds printed by FDM [45,52]. Ferreira et al. and Tian et al. improve the mechanical properties of PLA by adding carbon fiber. Ferreira et al. added blended short carbon fibers with PLA to get a filament (PLA/carbon fiber) [53]., while Tian et al. did not generate a composite filament but modified the printing nozzle by adding material inputs. In this case they used one input for PLA and a second for carbon fiber, thus obtaining PLA scaffolds with continuous carbon fiber [54]. In other works the biological performance of the PLA scaffolds are

improved. For example, Milda Alksne et al. added hydroxyapatite (HA) to the PLA matrix to improve osteoinductive activity and to enhance bone formation [55]. Even Petra Arany et al. have managed to introduce drug (diclofenac) to the PLA scaffold [56], although it should be mentioned that they have not printed the PLA with the drug; first the PLA was printed by FDM and then the drug was added. The latest advance is the incorporation of multi-nozzle extrusion system so that different polymers can be printed simultaneously and multicomponent scaffolds can be achieved. D. Baca et al. printed typical FDM printing materials (polylactic acid (PLA), acrylonitrile butadiene styrene (ABS) and high impact polystyrene (HIPS)) with single nozzle and their combinations (PLA-ABS, ABS-HIPS, PLA-HIPS and PLA-HIPS-ABS) with multi-nozzle, they discovered that despite reducing the printing time the mechanical properties were not improved, as they reported problems at the interface of the different materials [57].

Despite being a simple, fast and low cost way of 3D printing and having advanced in terms of printing composite and multicomponent materials, it still has limitations, especially in bioprinting; high processing temperatures and material limitations do not allow to print hydrogels, encapsulated cells or polymer solutions [52]. Direct Ink Writing (DIW printers) do not show these limitations. The feeding system does not need a filament, thus any polymers printable by FDM, hydrogels, polymer solutions or even cells can be printed [20]. DIW printers consist of a cartridge where powder, pellets, solutions or hydrogels are introduced, the material is pushed pneumatically (but this may vary depending on the type of printer) through a nozzle (see Figure 1.4).

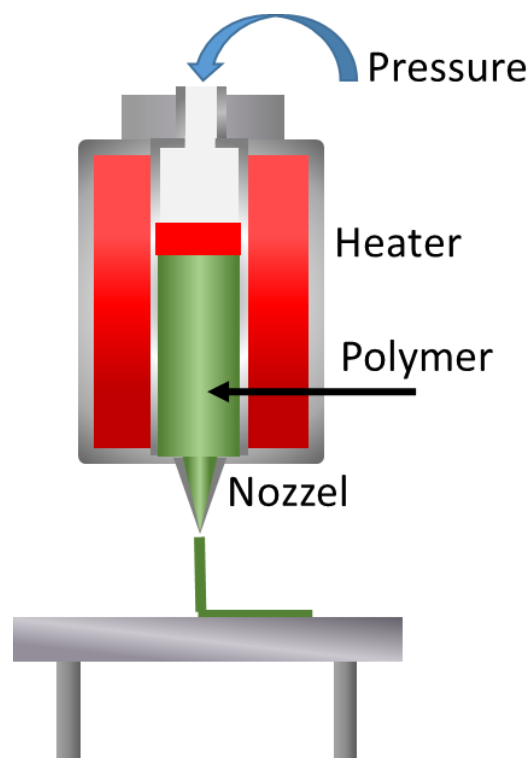


**Figure 1.4.** Schematic of the 3D printing process by material extrusion (DIW)

Using the DIW printer several works have been carried out to improve the biocompatibility or cell growth in PLA scaffolds. For example, Ritz et. al. added stromal-derived growth factors (SDF-1) to aid endothelial cell growth [58]. Roseti et al. reported how to improve the biocompatibility of PLA scaffolds by bioceramics (bioglass and HA)[20]. Other authors incorporate natural polymers to PLA to improve the biocompatibility. For example, Yeon et al. printed PLA/HA/SILK, the HA was used to improve osteogenic activity while the natural polymer (silk) was used to improve the biocompatibility of PLA, thus obtaining a PLA scaffold with improved biocompatibility and better bone regeneration[59]. Mengdi et al. printed PLA/cellulose acetate (CA) with 1-chloro-2,2,5,5-tetramethyl-4-imidazolidinone (MC); they also used a natural polymer (CA) to improve the biocompatibility of PLA and used a drug to prevent inflammation [60].

DIW printers not only allow the printing of PLA composites with enhanced biological activity, but also allow free-form printing, i.e. freeform spirals can be obtained, as the printing height increases above the nozzle size, they are able to be maintained by the evaporation of the solvent. Guo et al. analyzed the rheology of the PLA inks for each geometry and structure to be printed including free-form printing [61]. In addition, they studied the rheological and mechanical properties of the scaffolds obtained by DIW printing and they were the same as those of the FDM printers.

In this thesis, a 3D Bioplotter from Envisiontec, DIW type 3D printer, has been used to print PLA solutions, PLA composites and functionalized PLA blends for bone tissue engineering.

### **Poly lactides for bone tissue engineering**

Poly lactides (PLA) and its compounds are one of the most frequently used biodegradable polymers in bone fixation devices due to its mechanical properties (stiffness and strength) and the fact that they are bioresorbable. In addition, several studies have shown the use of these implants in bone fixation devices [62]. In this section, we will describe the properties and the main disadvantages of using PLA in bone fixation scaffolds.

PLA is a high strength and high modulus thermoplastic which can be easily processed by conventional (injection moulding, extrusion, compression moulding etc.) and advanced processing techniques such as additive manufacturing [63].

The monomer of polylactide, lactide acid (LA) can be obtained from natural sources such as corn, cassava, manioc, or sugar cane. It is traditionally produced by fermentation of sugars and their conversion into monomers after hydrolysis, but nowadays it can also be obtained by chemical reactions with products from non-renewable (petrochemical) sources.

PLA can be obtained by polycondensation, by azeotropic dehydration condensation by enzymatic polymerization [64,65]. or by ring opening polymerization (ROP) (see Figure 1.5)[66]. The most used technique is ROP as higher molecular weights can be synthesized. For medical applications in general, it is necessary to ensure that the PLA does not contain traces of materials derived from the synthesis process that are toxic or that are not bioresorbable. This is achieved by (1) purifying the PLA adequately, although this is sometimes complicated because removing traces can also degrade the polymer, and (2) by using organic catalysts [67–69].

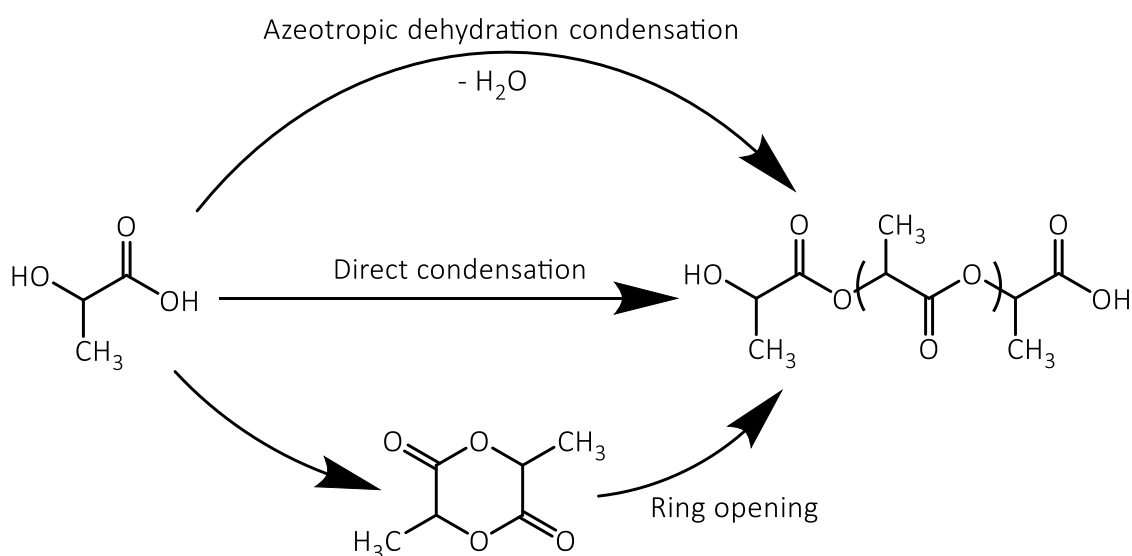


**Figure 1.5.** Different synthesis routes for the production of PLA. One of the characteristics of polylactides is that they are derived from lactide monomer, which is a chiral molecule. That is, it has two carbon atoms that give rise to two optically active configurations of lactide (L-lactide and D-lactide see Figure 1.6).

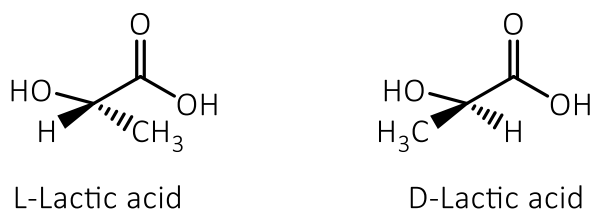
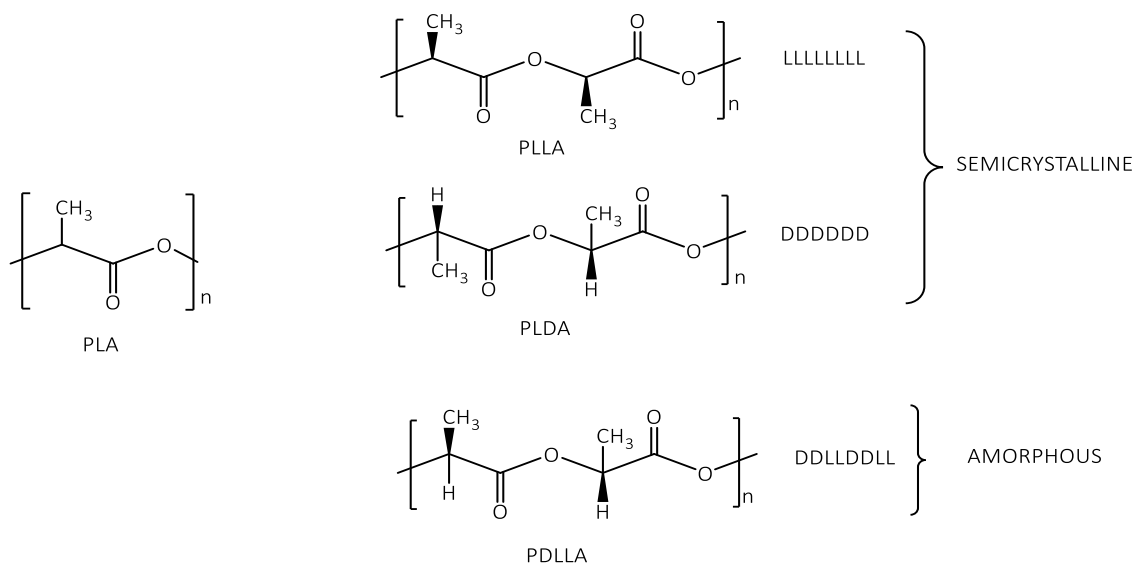


Figure 1.6. Enantiomers of lactic acid



The repeats of the LL-enantiomer give rise to poly(L-lactide) (PLLA), while the units of the DD-isomer give rise to poly(D-lactide) (PDLA). Stereoregular polylactides with pure L or D sequences in their chains usually crystallize in a pseudo-orthorhombic  $\alpha$ -shaped crystal [70–72]. However, when the two enantiomers of opposite configuration (L/D) are irregularly distributed in the polylactide backbone, the chain microstructure turns out to be stereo-irregular. When the same amount of L and D and are randomly located in the polylactide chain, a fully amorphous polylactide is obtained, then the polylactides can be considered as optically non-pure copolymers called poly(D,L-lactide) (PDLLA). [66,73]. PDLLA can be more or less crystalline depending on the placement and amount of the L- and D-enantiomers in the chain [74,75]. So the distribution of the LL, DD and DL repeat units determines the microstructure of the polymer chain that will be the basis for the thermal, mechanical and degradation properties of the polylactides [66]. Figure 1.7 illustrates the polymer configurations for PLA.



**Figure 1.7.** The three possible configurations of PLA chain.

In terms of thermal properties, the major difference is that PDLLA shows no crystallization or melting temperature, as expected since it is an amorphous polymer. But all semicrystalline PLA share the same temperatures  $T_g \sim 60^\circ\text{C}$ ,

$T_c \sim 100\text{ }^\circ\text{C}$  and  $T_f \sim 180\text{ }^\circ\text{C}$  [71,76]. Focused on mechanical properties, the semi-crystalline polymers show higher strength than the amorphous polymer, while the amorphous polymer has higher ductility than the semi-crystalline polymers. The semi-crystalline polymers (PLLA and PDLA) have a tensile modulus  $\sim 1800\text{ MPa}$ , a tensile strength  $\sim 60\text{-}70\text{ MPa}$  and an elongation at break of 7%. While the amorphous polymer PDLLA shows a tensile modulus  $\sim 1500\text{ MPa}$ , a tensile strength  $\sim 50\text{ MPa}$  and an elongation at break of 20%.

The microstructural features also affect the hydrolytic degradation of PLAs (see Figure 1.8). Semicrystalline enantiomers (PLLA and PDLA) degrade slower than the amorphous PLA (PDLLA), this is due to the fact that crystalline zones need more time to degrade than amorphous zones [77]. Finally Figure 1.8 shows the life cycle of lactide, as can be seen, the monomer can be recovered after polymerization.

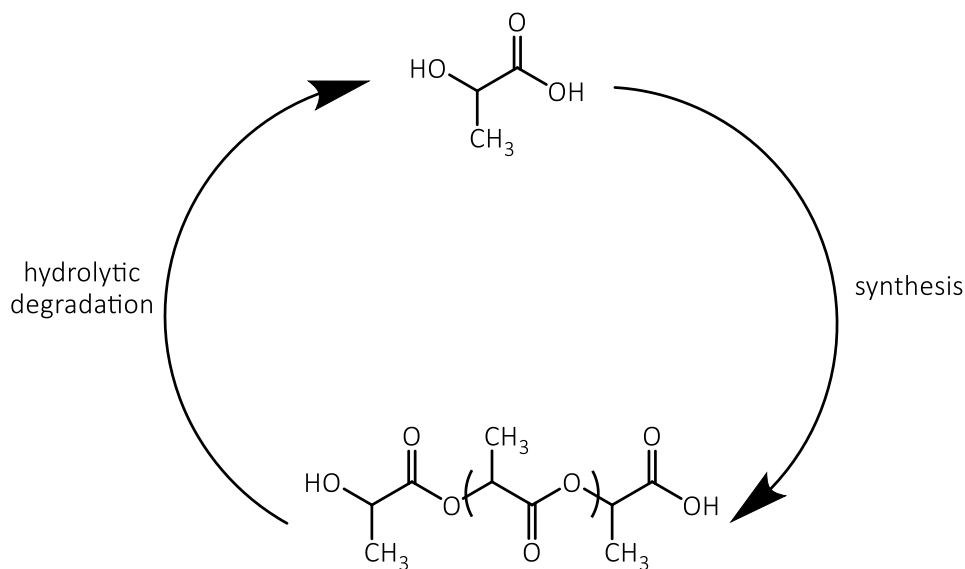


**Figure 1.8.** Life cycle of PLAs; synthesis and degradation. Thanks to the adjustable thermal, mechanical and biodegradation properties, PLA has been widely used in bone tissue engineering. However, PLA presents some drawbacks which will be discussed in the next section. The

need to overcome these disadvantages and improve some specific properties of PLA has been the reason why this thesis has been performed.

### **DRAWBACKS OF PLA**

In general PLA implants for bone tissue engineering show two main drawbacks: (1) the mechanical failure of the implants (2) the rejection of the implant due to adverse reactions to foreign bodies.

Mechanical failure due to implant failure can occur at the time of implantation or after implantation, i.e. when the implant is in service. In both cases, the failure is directly dependent on the mechanical properties of the PLA. As mentioned, PLA is a highly rigid and non-ductile material; its inherent fragility is one of its characteristics. If the implant breaks at the time of implantation the damage is repairable. However, when the implant breaks in use before fracture union, this might result in bone redisplacement and fragments of loose materials, which can cause irritation or adverse reactions [78,79]. In addition, these fragments are not visible to X-Rays. Conversely, metallic materials are radiopaque (opacity to X-Ray), in other words, electromagnetic radiation is not able to pass through the material making metals visible to X-rays. Therefore, as PLA is not radiopaque and thus, the evaluation of the damage is very complex.

To improve PLAs fragility different alternatives have been studied. In some works PLA is blended with another ductile polymer such as PCL and their copolymers like PLCL. Quiles-Carrillo et al. made PLA-based binary and ternary blends with poly( $\epsilon$ -caprolactone) (PCL) and thermoplastic starch (TPS), demonstrating that PLA-based ternary blends with relatively high PCL and low TPS contents improve both ductility and hardness [80]. Ugartemendia et al. added PLCL to improve the ductility of PLA by analyzing

different compositions. They found that the samples with less than 50 wt. % of PLCL composite had a behavior typical of thermoplastic polymers, although in this case they had lower tensile strength than PLA but significantly higher elongation at break. The rest of the compositions had a composition typical of thermoplastic elastomeric rubbers; they demonstrated how all the blends improved the ductility of PLA [77]. The toughness of PLA can also be improved with particles, plasticizing agents or polymers with small molecular weights. For example, Aliotta et al, added calcium carbonate particles to improve the ductility, in these cases the dispersion of the particles and the adhesion of this with the matrix play a great role to obtain this ductility [81]. Garcia-Gracia et al. used epoxidized karanja oil to act as a plasticizer in PLA, thus improving the elongation at break by up to 77% [82].

However, in most cases the stiffness of the material is also reduced and they are still invisible to X-Rays. To improve the radiopacity high mass element containing fillers must be added to obtain radiopaque composites; ferrous oxide ( $\text{Fe}_3\text{O}_4$ ) [83] and bismuth [84,85] have been previously reported as radiopaque polymer based composites. These particles have not been used with PLA since the matrix (PLA) undergoes degradation during processing [86], consequently the mechanical properties of PLA worsen. Therefore, if radiopacity is improved, ductility is not improved and, conversely, if ductility is improved, radiopacity is not improved.

Another problem with materials for bone tissue engineering is the adverse reactions, usually caused by the high crystallinity of PLA, which slows down hydrolytic degradation. To overcome this problem the crystallinity of the PLA is usually reduced by blending it with another amorphous polymers or low molecular weight polymers. In this way the amorphous phase is promoted

and the hydrolytic degradation [15,77]. There are also studies where PLA is blended with natural polymers such as collagen or silk not only to avoid adverse reactions but also to improve PLAs biodegradability [13,59,87]. This is due to the bioactive properties of natural polymers, which have better interactions with cells, obtaining improvements in the performance of the biological system [88].

Usually adverse reactions cause inflammation on the surrounding tissues. Incorporation of drugs could be a solution to prevent inflammation. There are different ways to carry the drug into the damage tissue. The incorporation of the drug nanoparticle of PLA-base is one of the option; once it is biodegraded the drug is released [89,90]. The drug can also be introduced into the pores of the scaffolds, however the drug is released suddenly and in uncontrolled way [91]. Another alternative is to adhere the drug into the PLA surface by functionalizing the surface with other chemical groups. One of the option is to use dopamine as an anchor for drugs. Dopamine is a catecholamine, which adheres to any type of surface. Taking advantage of the great adhesiveness of catecholamines there are several studies that asserted its effectiveness as anchor [92–96]. There are also studies where dopamine is chemically added to the polymer chain [97] , so that the drug can be added post processing.

Definitely, it is necessary to improve the mechanical properties, radiopacity and the drug attachment/release (biological activity) of PLA for bone tissue engineering. This fact is actually the guiding point why this thesis has been carried out.

## **Objectives**

Having underlined in the present chapter the advantages and disadvantages of the use of PLA in bone implants, this work will be focused on the design

of new radiopaque and functional implants for bone tissue regeneration and on their 3D fabrication methods.

In this sense, the work can be divided into two main sections: (1) 3D printing of PLA (chapter 2) (2) the improvement radiopacity, toughness and biological performance of PLA and PLA scaffolds (chapters 3 and 4).

In order to develop an efficient printing process, chapter 2 will describe the printing modes allowed by the 3D printer used in this thesis. It was observed that solution-printing was the most suitable mode to print PLA scaffolds. Therefore, throughout this chapter, different solvents and printing parameters will be analyzed, choosing the most suitable for printing PLA and its composites.

Continuing with the second part of the thesis, some properties of PLA will be improved. In chapter 3, barium sulfate particles are added to improve the radiopacity and its toughness. A polydopamine coating was added to the barium sulfate particles to promote drug attachment/release therefore to improve the (biological activity) of the material.

In Chapter 4 another alternative to improve the biological activity to PLA is reported. For this purpose a synthesis with organocatalysts will be carried out to add dopamine at the end of the PLA chain. The new PLA with dopamine will have the ability to adsorb and release drug without any coating after or before processing.

Finally, the results and the most relevant conclusions regarding the PLA printing mode and the properties and characteristics of the new PLA composites are discussed.

The steps followed to achieve these objectives are represented in the scheme of Figure 1.9.

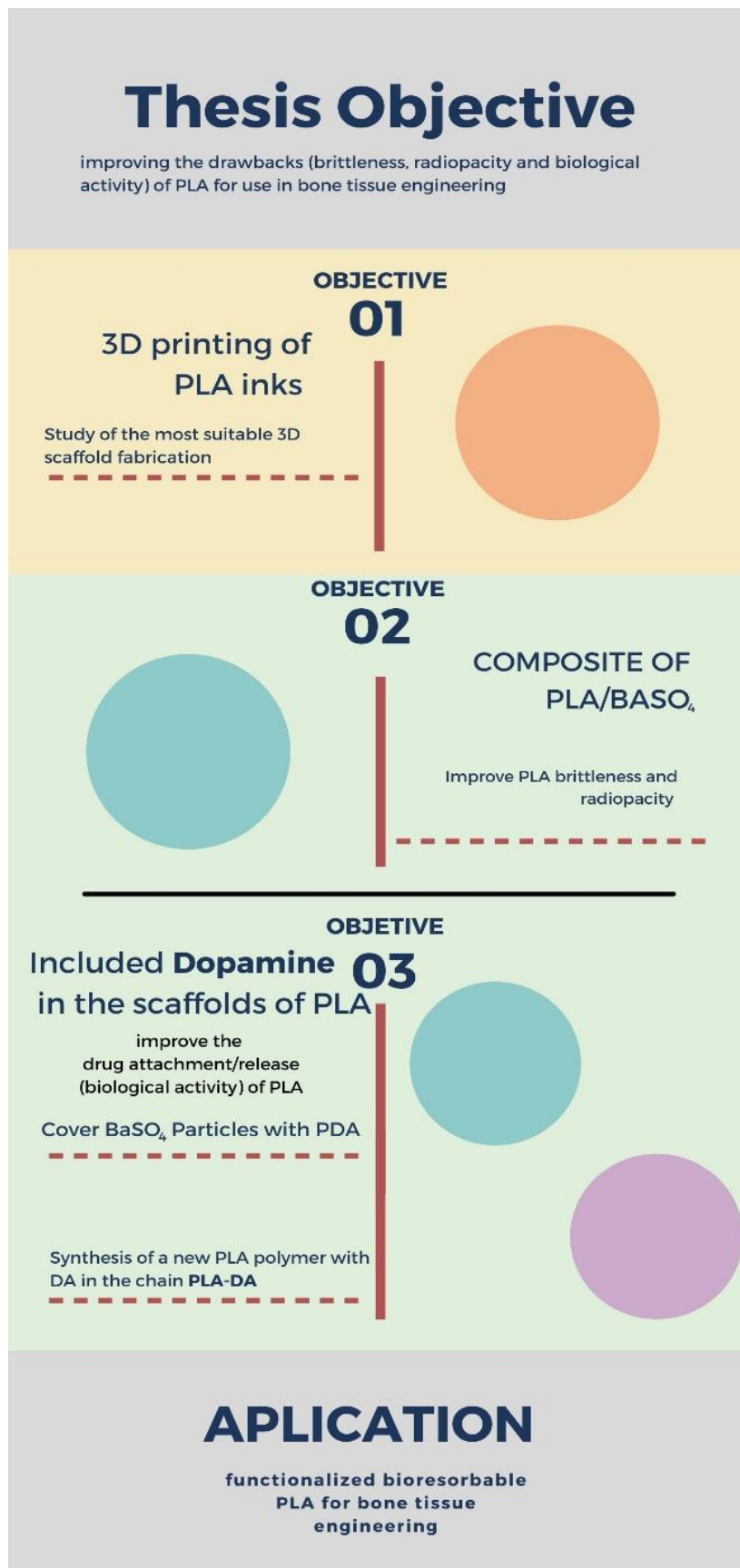


**Figure 1.9.** Scheme of the methodology that has been followed to achieved the objectives of the thesis

## Bibliography

1. Langer, R.; Vacanti, J.P. Tissue engineering. *Science (80-. )*. **1993**, *260*, 920–926, doi:10.1126/science.8493529.
2. Sultana, N. Scaffolds for tissue engineering. In *SpringerBriefs in Applied Sciences and Technology*; Springer Verlag, 2013; pp. 1–17.
3. Schultz, O.; Sittinger, M.; Haeupl, T.; Burmester, G.R. Emerging strategies of bone and joint repair. *Arthritis Res.* 2000, *2*, 433–436.
4. Zhang, K.; Wang, S.; Zhou, C.; Cheng, L.; Gao, X.; Xie, X.; Sun, J.; Wang, H.; Weir, M.D.; Reynolds, M.A.; et al. Advanced smart biomaterials and constructs for hard tissue engineering and regeneration. *Bone Res.* 2018, *6*, 1–15.
5. Landers, R.; Pfister, A.; Hübner, U.; John, H.; Schmelzeisen, R.; Mülhaupt, R. Fabrication of soft tissue engineering scaffolds by means of rapid prototyping techniques. *J. Mater. Sci.* **2002**, *37*, 3107–3116, doi:10.1023/A:1016189724389.
6. Kucinska-Lipka, J.; Gubanska, I.; Janik, H.; Sienkiewicz, M. Fabrication of polyurethane and polyurethane based composite fibres by the electrospinning technique for soft tissue engineering of cardiovascular system. *Mater. Sci. Eng. C* 2015, *46*, 166–176.
7. Kneser, U.; Schaefer, D.J.; Munder, B.; Klemm, C.; Andree, C.; Stark, G.B. Tissue engineering of bone. *Minim. Invasive Ther. Allied Technol.* 2002, *11*, 107–116.
8. Grémare, A.; Guduric, V.; Bareille, R.; Heroguez, V.; Latour, S.; L'heureux, N.; Fricain, J.C.; Catros, S.; Le Nihouannen, D. Characterization of printed PLA scaffolds for bone tissue engineering. *J. Biomed. Mater. Res. - Part A* **2018**, *106*, 887–894, doi:10.1002/jbm.a.36289.
9. Murphy, S. V.; Atala, A. 3D bioprinting of tissues and organs. *Nat. Biotechnol.*



- 2014, 32, 773–785.
10. Calejo, I.; Costa-Almeida, R.; Reis, R.L.; Gomes, M.E. A Physiology-Inspired Multifactorial Toolbox in Soft-to-Hard Musculoskeletal Interface Tissue Engineering. *Trends Biotechnol.* 2020, 38, 83–98.
  11. Seidi, A.; Ramalingam, M.; Elloumi-Hannachi, I.; Ostrovidov, S.; Khademhosseini, A. Gradient biomaterials for soft-to-hard interface tissue engineering. *Acta Biomater.* 2011, 7, 1441–1451.
  12. Patel, S.; Caldwell, J.-M.; Doty, S.B.; Levine, W.N.; Rodeo, S.; Soslowky, L.J.; Thomopoulos, S.; Lu, H.H. Integrating soft and hard tissues via interface tissue engineering. *J. Orthop. Res.* 2018, 36, 1069–1077, doi:10.1002/jor.23810.
  13. Chen, Y.; Mak, A.F.T.; Wang, M.; Li, J.; Wong, M.S. PLLA scaffolds with biomimetic apatite coating and biomimetic apatite/collagen composite coating to enhance osteoblast-like cells attachment and activity. *Surf. Coatings Technol.* 2006, 201, 575–580, doi:10.1016/j.surfcoat.2005.12.005.
  14. Busam, M.L.; Esther, R.J.; Obremsky, W.T. Hardware removal: Indications and expectations. *J. Am. Acad. Orthop. Surg.* 2006, 14, 113–120.
  15. Ugartemendia, J.M. In a search for tough polylactides for tissue regeneration - estudiosdeposgrado-graduondokoikasketak - Graduondoko Ikasketak - UPV/EHU Available online: <https://www.ehu.eus/eu/web/estudiosdeposgrado-graduondokoikasketak/-/in-a-search-for-tough-polylactides-for-tissue-regeneration> (accessed on Mar 12, 2021).
  16. Polo-Corrales, L.; Latorre-Esteves, M.; Ramirez-Vick, J.E. Scaffold design for bone regeneration. *J. Nanosci. Nanotechnol.* 2014, 14, 15–56.
  17. Dong, J.; Uemura, T.; Shirasaki, Y.; Tateishi, T. Promotion of bone formation using highly pure porous  $\beta$ -TCP combined with bone marrow-derived osteoprogenitor cells. *Biomaterials* 2002, 23, 4493–4502,

doi:10.1016/S0142-9612(02)00193-X.

18. Adams, C.S.; Mansfield, K.; Perlot, R.L.; Shapiro, I.M. Matrix regulation of skeletal cell apoptosis. Role of calcium and phosphate ions. *J. Biol. Chem.* **2001**, *276*, 20316–20322, doi:10.1074/jbc.M006492200.
19. Salah, M.; Tayebi, L.; Moharamzadeh, K.; Naini, F.B. Three-dimensional bio-printing and bone tissue engineering: technical innovations and potential applications in maxillofacial reconstructive surgery., doi:10.1186/s40902-020-00263-6.
20. Roseti, L.; Parisi, V.; Petretta, M.; Cavallo, C.; Desando, G.; Bartolotti, I.; Grigolo, B. Scaffolds for Bone Tissue Engineering: State of the art and new perspectives. *Mater. Sci. Eng. C* **2017**, *78*, 1246–1262.
21. Salgado, A.J.; Coutinho, O.P.; Reis, R.L. Bone Tissue Engineering: State of the Art and Future Trends. *Macromol. Biosci.* **2004**, *4*, 743–765, doi:10.1002/mabi.200400026.
22. Baptista, R.; Guedes, M. Morphological and mechanical characterization of 3D printed PLA scaffolds with controlled porosity for trabecular bone tissue replacement. *Mater. Sci. Eng. C* **2021**, *118*, 111528, doi:10.1016/j.msec.2020.111528.
23. Chen, H.; Han, Q.; Wang, C.; Liu, Y.; Chen, B.; Wang, J. Porous Scaffold Design for Additive Manufacturing in Orthopedics: A Review. *Front. Bioeng. Biotechnol.* **2020**, *8*, 609.
24. Hutmacher, D.W. Scaffold design and fabrication technologies for engineering tissues - State of the art and future perspectives. *J. Biomater. Sci. Polym. Ed.* **2001**, *12*, 107–124, doi:10.1163/156856201744489.
25. Hollister, S.J. Porous scaffold design for tissue engineering. *Nat. Mater.* **2005**, *4*, 518–524.
26. Mao, Y.; Xiong, Y.; Li, Q.; Chen, G.; Fu, W.; Tang, X.; Yang, L.; Li, J. 3D-Printed

- Patient-Specific Instrumentation Technique Vs. Conventional Technique in Medial Open Wedge High Tibial Osteotomy: A Prospective Comparative Study. *Biomed Res. Int.* **2020**, 2020, doi:10.1155/2020/1923172.
27. Szymczyk-Ziółkowska, P.; Łabowska, M.B.; Detyna, J.; Michalak, I.; Gruber, P. A review of fabrication polymer scaffolds for biomedical applications using additive manufacturing techniques. *Biocybern. Biomed. Eng.* 2020, 40, 624–638.
  28. ASTM F2792 - 12a Standard Terminology for Additive Manufacturing Technologies (Withdrawn 2015) Available online: <https://www.astm.org/Standards/F2792.htm> (accessed on Feb 28, 2021).
  29. Liao, J.; Cooper, D.R. The Environmental Impacts of Metal Powder Bed Additive Manufacturing. **2020**, doi:10.1115/1.4048435.
  30. Mao, Y.; Li, J.; Li, W.; Cai, D.; Wei, Q. Binder jetting additive manufacturing of 316L stainless-steel green parts with high strength and low binder content: Binder preparation and process optimization. *J. Mater. Process. Technol.* **2021**, 291, 117020, doi:10.1016/j.jmatprotec.2020.117020.
  31. Manotham, S.; Channasanon, S.; Nanthananon, P.; Tanodekaew, S.; Tesavibul, P. Photosensitive binder jetting technique for the fabrication of alumina ceramic. *J. Manuf. Process.* **2021**, 62, 313–322, doi:10.1016/j.jmapro.2020.12.011.
  32. Yang, Y.; Gong, Y.; Li, C.; Wen, X.; Sun, J. Mechanical performance of 316 L stainless steel by hybrid directed energy deposition and thermal milling process. *J. Mater. Process. Technol.* **2021**, 291, 117023, doi:10.1016/j.jmatprotec.2020.117023.
  33. Li, J.; Lin, X.; Yang, Y.; Wang, J.; Liu, J.; Guo, P.; Huang, W. Distinction in electrochemical behaviour of Ti6Al4V alloy produced by direct energy deposition and forging. *J. Alloys Compd.* **2021**, 860, 157912, doi:10.1016/j.jallcom.2020.157912.

34. Lohfeld, S.; Mchugh, P.E.; Caulfield, B.; Caulfield, B.; Mchugh, P.E.; Lohfeld, S. Title Dependence of mechanical properties of polyamide components on build parameters in the SLS process Dependence of mechanical properties of polyamide components on build parameters in the SLS process-NonCommercial-NoDerivatives 4.0 International <http://creativecommons.org/licenses/by-nc-nd/4.0>. **2007**, doi:10.1016/j.matprotec.2006.09.007.
35. Berretta, S.; Ghita, O.; Evans, K.E. Morphology of polymeric powders in Laser Sintering (LS): From Polyamide to new PEEK powders. *Eur. Polym. J.* **2014**, *59*, 218–229, doi:10.1016/j.eurpolymj.2014.08.004.
36. Chatham, C.A.; Long, T.E.; Williams, C.B. A review of the process physics and material screening methods for polymer powder bed fusion additive manufacturing. *Prog. Polym. Sci.* 2019, *93*, 68–95.
37. Zhu, W.; Ma, X.; Gou, M.; Mei, D.; Zhang, K.; Chen, S. 3D printing of functional biomaterials for tissue engineering. *Curr. Opin. Biotechnol.* 2016, *40*, 103–112.
38. Singh, M.; Haverinen, H.M.; Dhagat, P.; Jabbour, G.E. Inkjet printing-process and its applications. *Adv. Mater.* **2010**, *22*, 673–685, doi:10.1002/adma.200901141.
39. Saunders, R.E.; Derby, B. Inkjet printing biomaterials for tissue engineering: Bioprinting. *Int. Mater. Rev.* **2014**, *59*, 430–448, doi:10.1179/1743280414Y.0000000040.
40. Koch, L.; Brandt, O.; Deiwick, A.; Chichkov, B. Laser-assisted bioprinting at different wavelengths and pulse durations with a metal dynamic release layer: A parametric study. *Int. J. Bioprinting* **2017**, *3*, 42–53, doi:10.18063/IJB.2017.01.001.
41. Mekonnen, B.G.; Bright, G.; Walker, A. A study on state of the art technology of laminated object manufacturing (Lom). *Lect. Notes Mech. Eng.* **2016**, 207–

- 216, doi:10.1007/978-81-322-2740-3\_21.
42. Garcia, E.A.; Ayranci, C.; Qureshi, A.J. Material property-manufacturing process optimization for form 2 VAT-photo polymerization 3D printers. *J. Manuf. Mater. Process.* **2020**, *4*, doi:10.3390/jmmp4010012.
  43. Fiedor, P.; Pilch, M.; Szymaszek, P.; Chachaj-Brekiesz, A.; Galek, M.; Ortyl, J. Photochemical Study of a New Bimolecular Photoinitiating System for Vat Photopolymerization 3D Printing Techniques under Visible Light. *Catalysts* **2020**, *10*, 284, doi:10.3390/catal10030284.
  44. Peterson, G.I.; Schwartz, J.J.; Zhang, D.; Weiss, B.M.; Ganter, M.A.; Storti, D.W.; Boydston, A.J. Production of Materials with Spatially-Controlled Cross-Link Density via Vat Photopolymerization. *ACS Appl. Mater. Interfaces* **2016**, *8*, 29037–29043, doi:10.1021/acsami.6b09768.
  45. Khodaei, M.; Amini, K.; Valanezhad, A. Fabrication and Characterization of Poly Lactic Acid Scaffolds by Fused Deposition Modeling for Bone Tissue Engineering. *J. Wuhan Univ. Technol. Mater. Sci. Ed.* **2020**, *35*, 248–251, doi:10.1007/s11595-020-2250-4.
  46. Ranjan, N.; Singh, R.; Ahuja, I.P.S.; Kumar, R.; Singh, J.; Verma, A.K.; Leekha, A. On 3D printed scaffolds for orthopedic tissue engineering applications. *SN Appl. Sci.* **2020**, *2*, doi:10.1007/s42452-020-1936-8.
  47. Guo, S.-Z.; Heuzey, M.-C.; Therriault, D. Properties of Polylactide Inks for Solvent-Cast Printing of Three-Dimensional Freeform Microstructures. **2014**, *30*, doi:10.1021/la4036425.
  48. Chen, Q.; Mangadlao, J.D.; Wallat, J.; De Leon, A.; Pokorski, J.K.; Advincula, R.C. 3D printing biocompatible polyurethane/poly(lactic acid)/graphene oxide nanocomposites: Anisotropic properties. *ACS Appl. Mater. Interfaces* **2017**, *9*, 4015–4023, doi:10.1021/acsami.6b11793.
  49. Przekop, R.E.; Kujawa, M.; Pawlak, W.; Dobrosielska, M.; Sztorch, B.; Wieleba, W. Graphite Modified Polylactide (PLA) for 3D Printed (FDM/FFF)

- Sliding Elements. *Polymers (Basel)*. **2020**, *12*, 1250, doi:10.3390/polym12061250.
50. Dudek, P. FDM 3D printing technology in manufacturing composite elements. *Arch. Metall. Mater.* **2013**, *58*, 1415–1418, doi:10.2478/amm-2013-0186.
51. Davis, C.S.; Hillgartner, K.E.; Han, S.H.; Seppala, J.E. Mechanical strength of welding zones produced by polymer extrusion additive manufacturing. *Addit. Manuf.* **2017**, *16*, 162–166, doi:10.1016/j.addma.2017.06.006.
52. Xie, Z.; Gao, M.; Lobo, A.O.; Webster, T.J. 3D bioprinting in tissue engineering for medical applications: The classic and the hybrid. *Polymers (Basel)*. **2020**, *12*.
53. Ferreira, R.T.L.; Amatte, I.C.; Dutra, T.A.; Bürger, D. Experimental characterization and micrography of 3D printed PLA and PLA reinforced with short carbon fibers. *Compos. Part B Eng.* **2017**, *124*, 88–100, doi:10.1016/j.compositesb.2017.05.013.
54. Tian, X.; Liu, T.; Yang, C.; Wang, Q.; Li, D. Interface and performance of 3D printed continuous carbon fiber reinforced PLA composites. *Compos. Part A Appl. Sci. Manuf.* **2016**, *88*, 198–205, doi:10.1016/j.compositesa.2016.05.032.
55. Alksne, M.; Kalvaityte, M.; Simoliunas, E.; Rinkunaite, I.; Gendviliene, I.; Locs, J.; Rutkunas, V.; Bukelskiene, V. In vitro comparison of 3D printed polylactic acid/hydroxyapatite and polylactic acid/bioglass composite scaffolds: Insights into materials for bone regeneration. *J. Mech. Behav. Biomed. Mater.* **2020**, *104*, 103641, doi:10.1016/j.jmbbm.2020.103641.
56. Arany, P.; Papp, I.; Zichar, M.; Csontos, M.; Elek, J.; Regdon, G.; Budai, I.; Béres, M.; Gesztelyi, R.; Fehér, P.; et al. In Vitro Tests of FDM 3D-Printed Diclofenac Sodium-Containing Implants. *Molecules* **2020**, *25*, doi:10.3390/molecules25245889.

- 
57. Baca, D.; Ahmad, R. The impact on the mechanical properties of multi-material polymers fabricated with a single mixing nozzle and multi-nozzle systems via fused deposition modeling. *Int. J. Adv. Manuf. Technol.* **2020**, *106*, 4509–4520, doi:10.1007/s00170-020-04937-3.
58. Ritz, U.; Gerke, R.; Götz, H.; Stein, S.; Rommens, P.M. A new bone substitute developed from 3D-prints of polylactide (PLA) loaded with collagen i: An in vitro study. *Int. J. Mol. Sci.* **2017**, *18*, doi:10.3390/ijms18122569.
59. Yeon, Y.K.; Park, H.S.; Lee, J.M.; Lee, J.S.; Lee, Y.J.; Sultan, M.T.; Seo, Y. Bin; Lee, O.J.; Kim, S.H.; Park, C.H. New concept of 3D printed bone clip (polylactic acid/hydroxyapatite/silk composite) for internal fixation of bone fractures. *J. Biomater. Sci. Polym. Ed.* **2018**, *29*, 894–906, doi:10.1080/09205063.2017.1384199.
60. Zuo, M.; Pan, N.; Liu, Q.; Ren, X.; Liu, Y.; Huang, T.S. Three-dimensionally printed polylactic acid/cellulose acetate scaffolds with antimicrobial effect. *RSC Adv.* **2020**, *10*, 2952–2958, doi:10.1039/c9ra08916k.
61. Guo, S.Z.; Heuzey, M.C.; Therriault, D. Properties of polylactide inks for solvent-cast printing of three-dimensional freeform microstructures. *Langmuir* **2014**, *30*, 1142–1150, doi:10.1021/la4036425.
62. Lasprilla, A.J.R.; Martinez, G.A.R.; Lunelli, B.H.; Jardini, A.L.; Filho, R.M. Polylactic acid synthesis for application in biomedical devices - A review. *Biotechnol. Adv.* **2012**, *30*, 321–328.
63. Chiulan, I.; Frone, A.; Brandabur, C.; Panaitescu, D. Recent Advances in 3D Printing of Aliphatic Polyesters. *Bioengineering* **2017**, *5*, 2, doi:10.3390/bioengineering5010002.
64. Zhao, H.; Nathaniel, G.A.; Merenini, P.C. Enzymatic ring-opening polymerization (ROP) of lactides and lactone in ionic liquids and organic solvents: Digging the controlling factors. *RSC Adv.* **2017**, *7*, 48639–48648, doi:10.1039/c7ra09038b.

65. lassalle, veronica Enzymatic poly and co-polymerisation of lactic acid.
66. Singhvi, M.S.; Zinjarde, S.S.; Gokhale, D. V. Polylactic acid: synthesis and biomedical applications. *J. Appl. Microbiol.* 2019, *127*, 1612–1626.
67. Li, H.; Gu, L. Controllable synthesis of bio-based polylactide diols using an organocatalyst in solvent-free conditions. *J. Polym. Sci. Part A Polym. Chem.* **2018**, *56*, 968–976, doi:10.1002/pola.28974.
68. Mezzasalma, L.; Dove, A.P.; Coulembier, O. Organocatalytic ring-opening polymerization of L-lactide in bulk: A long standing challenge. *Eur. Polym. J.* 2017, *95*, 628–634.
69. Toshikj, N.; Robin, J.J.; Blanquer, S. A simple and general approach for the synthesis of biodegradable triblock copolymers by organocatalytic ROP from poly(lactide) macroinitiators. *Eur. Polym. J.* **2020**, *127*, 109599, doi:10.1016/j.eurpolymj.2020.109599.
70. Papadopoulos, L.; Klonos, P.A.; Terzopoulou, Z.; Psochia, E.; Sanusi, O.M.; Hocine, N.A.; Benelfellah, A.; Giliopoulos, D.; Triantafyllidis, K.; Kyritsis, A.; et al. Comparative study of crystallization, semicrystalline morphology, and molecular mobility in nanocomposites based on polylactide and various inclusions at low filler loadings. *Polymer (Guildf).* **2021**, *217*, 123457, doi:10.1016/j.polymer.2021.123457.
71. Sarasua, J.R.; Prud'homme, R.E.; Wisniewski, M.; Le Borgne, A.; Spassky, N. Crystallization and melting behavior of polylactides. *Macromolecules* **1998**, *31*, 3895–3905, doi:10.1021/ma971545p.
72. Södergård, A.; Stolt, M. Properties of lactic acid based polymers and their correlation with composition. *Prog. Polym. Sci.* 2002, *27*, 1123–1163.
73. Andreopoulos, A.G.; Hatzi, E.; Doxastakis, M. Synthesis and properties of poly(lactic acid). *J. Mater. Sci. Mater. Med.* **1999**, *10*, 29–33, doi:10.1023/A:1008887910068.



74. Sarasua, J.R.; Arraiza, A.L.; Balerdi, P.; Maiza, I. Crystallinity and mechanical properties of optically pure polylactides and their blends. *Polym. Eng. Sci.* **2005**, *45*, 745–753, doi:10.1002/pen.20331.
75. Urayama, H.; Kanamori, T.; Kimura, Y. Microstructure and Thermomechanical Properties of Glassy Polylactides with Different Optical Purity of the Lactate Units. *Macromol. Mater. Eng.* **2001**, *286*, 705, doi:10.1002/1439-2054(20011101)286:11<705::AID-MAME705>3.0.CO;2-Q.
76. Zuza, E.; Meaurio, E.; Sarasua, J.-R. Biodegradable Polylactide-Based Composites. In *Composites from Renewable and Sustainable Materials*; InTech, 2016.
77. Ugartemendia, J.M.; Larrañaga, A.; Amestoy, H.; Etxeberria, A.; Sarasua, J.R. Tougher biodegradable polylactide system for bone fracture fixations: Miscibility study, phase morphology and mechanical properties. *Eur. Polym. J.* **2018**, *98*, 411–419, doi:10.1016/j.eurpolymj.2017.11.040.
78. Baums, M.H.; Zelle, B.A.; Schultz, W.; Ernstberger, T.; Klinger, H.M. Intraarticular migration of a broken biodegradable interference screw after anterior cruciate ligament reconstruction. *Knee Surgery, Sport. Traumatol. Arthrosc.* **2006**, *14*, 865–868, doi:10.1007/s00167-006-0049-2.
79. Lembeck, B.; Wülker, N. Severe cartilage damage by broken poly-L-lactic acid (PLLA) interference screw after ACL reconstruction. *Knee Surgery, Sport. Traumatol. Arthrosc.* **2005**, *13*, 283–286, doi:10.1007/s00167-004-0545-1.
80. Quiles-Carrillo, L.; Montanes, N.; Pineiro, F.; Jorda-Vilaplana, A.; Torres-Giner, S. Ductility and Toughness Improvement of Injection-Molded Compostable Pieces of Polylactide by Melt Blending with Poly( $\epsilon$ -caprolactone) and Thermoplastic Starch. *Materials (Basel)*. **2018**, *11*, 2138, doi:10.3390/ma11112138.
81. Aliotta, L.; Cinelli, P.; Coltelli, M.B.; Lazzeri, A. Rigid filler toughening in PLA-

- Calcium Carbonate composites: Effect of particle surface treatment and matrix plasticization. *Eur. Polym. J.* **2019**, *113*, 78–88, doi:10.1016/j.eurpolymj.2018.12.042.
82. Garcia-Garcia, D.; Carbonell-Verdu, A.; Arrieta, M.P.; López-Martínez, J.; Samper, M.D. Improvement of PLA film ductility by plasticization with epoxidized karanja oil. *Polym. Degrad. Stab.* **2020**, *179*, 109259, doi:10.1016/j.polymdegradstab.2020.109259.
83. Chang, W.-J.; Pan, Y.-H.; Tzeng, J.-J.; Wu, T.-L.; Fong, T.-H.; Feng, S.-W.; Huang, H.-M. Development and Testing of X-Ray Imaging-Enhanced Poly-L-Lactide Bone Screws. *PLoS One* **2015**, *10*, e0140354, doi:10.1371/journal.pone.0140354.
84. Noor Azman, N.Z.; Musa, N.F.L.; Nik Ab Razak, N.N.A.; Ramli, R.M.; Mustafa, I.S.; Abdul Rahman, A.; Yahaya, N.Z. Effect of Bi<sub>2</sub>O<sub>3</sub> particle sizes and addition of starch into Bi<sub>2</sub>O<sub>3</sub>–PVA composites for X-ray shielding. *Appl. Phys. A* **2016**, *122*, 818, doi:10.1007/s00339-016-0329-8.
85. Abunahel, B.M.; Mustafa, I.S.; Noor Azman, N.Z. Characteristics of X-ray attenuation in nano-sized bismuth oxide/epoxy-polyvinyl alcohol (PVA) matrix composites. *Appl. Phys. A* **2018**, *124*, 828, doi:10.1007/s00339-018-2254-5.
86. Larrañaga, A.; Ramos, D.; Amestoy, H.; Zuza, E.; Sarasua, J.-R. Coating of bioactive glass particles with mussel-inspired polydopamine as a strategy to improve the thermal stability of poly(L-lactide)/bioactive glass composites. *RSC Adv.* **2015**, *5*, 65618–65626, doi:10.1039/C5RA09495J.
87. Wu, T.-Y.; Yang, M.-C.; Hsu, Y.-C. Improvement of cytocompatibility of polylactide by filling with marine algae powder. *Mater. Sci. Eng. C* **2015**, *50*, 309–316, doi:10.1016/J.MSEC.2015.02.020.
88. Nair, L.S.; Laurencin, C.T. Biodegradable polymers as biomaterials. *Prog. Polym. Sci.* **2007**, *32*, 762–798.

- 
89. Dong, Y.; Feng, S.S. Nanoparticles of poly(D,L-lactide)/methoxy poly(ethylene glycol)-poly(D,L-lactide) blends for controlled release of paclitaxel. *J. Biomed. Mater. Res. - Part A* **2006**, *78*, 12–19, doi:10.1002/jbm.a.30684.
90. Torchilin, V.P. Multifunctional nanocarriers. *Adv. Drug Deliv. Rev.* **2006**, *58*, 1532–1555.
91. Kamaly, N.; Xiao, Z.; Valencia, P.M.; Radovic-Moreno, A.F.; Farokhzad, O.C. Targeted polymeric therapeutic nanoparticles: Design, development and clinical translation. *Chem. Soc. Rev.* **2012**, *41*, 2971–3010, doi:10.1039/c2cs15344k.
92. Lee, H.; Dellatore, S.M.; Miller, W.M.; Messersmith, P.B. Mussel-Inspired Surface Chemistry for Multifunctional Coatings., doi:10.1126/science.1147241.
93. Moulay, S. Dopa/Catechol-Tethered Polymers: Bioadhesives and Biomimetic Adhesive Materials. *Polym. Rev.* **2014**, *54*, 436–513, doi:10.1080/15583724.2014.881373.
94. Ryu, J.H.; Messersmith, P.B.; Lee, H. Polydopamine Surface Chemistry: A Decade of Discovery. *ACS Appl. Mater. Interfaces* **2018**, *10*, 7523–7540.
95. Yeh, C.-H.; Chen, Y.-W.; Shie, M.-Y.; Fang, H.-Y. Poly(Dopamine)-Assisted Immobilization of Xu Duan on 3D Printed Poly(Lactic Acid) Scaffolds to Up-Regulate Osteogenic and Angiogenic Markers of Bone Marrow Stem Cells. *Materials (Basel)*. **2015**, *8*, 4299–4315, doi:10.3390/ma8074299.
96. Lee, H.; Dellatore, S.M.; Miller, W.M.; Messersmith, P.B. Mussel-inspired surface chemistry for multifunctional coatings. *Science (80-. )*. **2007**, *318*, 426–430, doi:10.1126/science.1147241.
97. Liu, Z.; Hu, B.H.; Messersmith, P.B. Acetonide protection of dopamine for the synthesis of highly pure N-docosahexaenoyldopamine. *Tetrahedron Lett.* **2010**, *51*, 2403–2405, doi:10.1016/j.tetlet.2010.02.089.

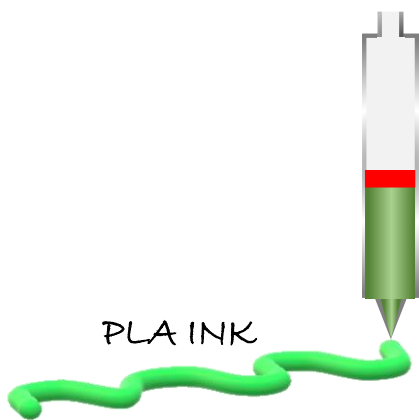


A large, solid orange circle is positioned on the left side of the page. Inside the circle, the text "Chapter 2" is written in a black, sans-serif font.

# Chapter 2



# Graphical abstract



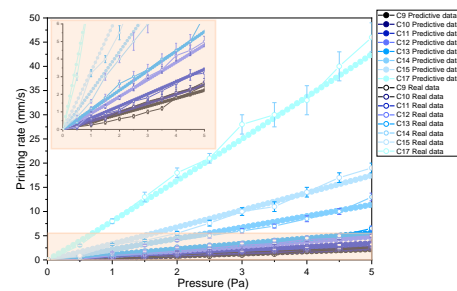
$$R_X = \left[ \frac{1 + \frac{R_0}{R_L} + \left(\frac{R_0}{R_L}\right)^2 - 3\left(\frac{R_0}{R_L}\right)^3}{1 + \frac{R_0}{R_L} + \left(\frac{R_0}{R_L}\right)^2} \right]^3$$

$$\mu = \frac{\Delta P R_0^4 R_X}{8VL^2q}$$

$$Q = \frac{\pi \Delta P R_0^4 R_X}{8\mu L}$$

$$V = \frac{\Delta P R_0^4 R_X}{8L^2q\eta_0} \left( \frac{P R_0^2}{(R_0 + R_L)\sqrt{\eta^2 + (R_0 - R_L)^2}} \right)^n$$

$$\sigma = \frac{P R_0^2}{(R_0 + R_L)\sqrt{\eta^2 + (R_0 - R_L)^2}}$$







## CHAPTER 2: REHOLOGICAL ANALYSIS OF POLYLACTIDE INKS FOR 3D PRINTING

3D printing, especially the solvent-extrusion 3D printing, is a very versatile fabrication technique which can be used to build different geometries such as filaments, parts and scaffolds by depositing a polymer solution ink layer by layer on a platform. This mode of printing is a great solution for polymers which have low thermal stability. In this chapter, a comprehensive characterization of the solvent-extrusion 3D printing process is presented. For this purpose poly(L-lactide) was solved in two different solvents; 1,4-Dioxane with a boiling point above room temperature and chloroform ( $\text{CHCl}_3$ ) with boiling point below room temperature. The flow behavior of the polymeric solutions, the filament welding and the morphology of the printed material were analyzed. A rheological model was developed to predict the optimal printing conditions (extrusion speed and printing pressure). It was observed that chloroform solutions followed better the model than 1,4-dioxane solutions. Welding analysis showed that less diluted solutions have better welds between filaments. The effect of solvent evaporation rate on final geometry and crystallization was also analyzed. The methodology developed in this chapter offers a new perspective for the fabrication of complex structures from polymer solutions and provides guidelines for optimizing the various parameters for 3D printing. Although this work is specific to bioplotting equipment (EnvisionTEC GmbH), the methodology described here can be applied to any type of micro-extrusion equipment.

### 2.1. Introduction

Additive manufacturing has gained importance over the last few years, especially the 3D printing. This advanced processing technique is commonly

used in tissue-engineering for scaffold fabrication as conventional techniques, such as, freeze-drying [1] particulate leaching [2,3], electrospinning [4], and thermally induced phase separation [5] are mainly process-dependent. In other words, by using conventional processing techniques the pore size and geometry, and also the interconnection between pores cannot be controlled. Therefore, 3D printing is a promising technique which allows to obtain complex geometries with controlled geometrical characteristics [6–8].

According to ASTM F2792-12a [9] there are seven different types of 3D printing: VAT photopolymerization, Power Bed Fusion (PBF), Binder Jetting, Material Jetting, Sheet lamination, Material extrusion and Directed energy deposition (DED)). Material extrusion is one of the most widely used due to its multiple solidification processes including pH, temperature change, solvent evaporation and photo-crosslinking [10–12]. These type of printers extrude and print the material layer by layer to reproduce a geometry previously designed in a computer-aided design (CAD) model [13,14]. In this work we use a 3D Bioplotter purchased by EnvisionTEC GmbH which allows to print the material in pellet form making the Bioplotter very versatile in terms of material selection and custom formulations [15].

Extrusion printing has been proved to be suitable for aliphatic polyester [16–18], such polylactides (PLA). PLA is biodegradable and biocompatible polymer widely available commercially nowadays. It shows suitable physicochemical and mechanical (high modulus and strength) properties for tissue engineering [19]. Moreover, as it is a thermoplastic polymer it is easy to process. [19–24]. However, the major drawback of working with PLA in melt extrusion 3D printing is its small thermal stability. Thermal degradation is a problem to overcome since it has a straight impact on printing conditions

and consequently on final printed parts [25]. In literature, few examples of how degradation affects the PLA printing process can be found. Findrik Balogová et. al. investigated the effect of moisture on material degradation and viscosity during printing of poly(lactide) (PLA)/polyhydroxybutyrate (PHB) blends [26]. Shubham Jain et. al. studied the degradation suffered by polylactide and copolyesters in 3D printing, this study shows how PLA loses a large amount of its molecular weight in 4 hours [25]. In other works stabilizers or chain extenders are added to avoid thermal degradation[27]. An alternative solution is to prepare PLA inks by dissolving the PLA in a solvent [28–30].

In this work two different PLA inks are formulated to avoid thermal degradation while printing. The inks are formulated by dissolving PLA in a low-boiling solvent (chloroform) and a high-boiling solvent (1,4-dioxane); two common solvents use to solved PLAs. A complete rheological study is carried out to optimize the printing conditions. The process-related viscosity of the PLA solutions are studied by means of a rotational rheometer. Welding between printed filaments are studied to show the strength of the printed part. The crystallization behavior of different inks are analyzed by differential scanning calorimetry (DSC) and the solvent evaporation kinetics by monitoring the reduction of the extruded filament weight over time. Finally, the morphological aspects are examined visually and by SEM microscopy.

## **2.2.Printing process: 3D Bioplotter**

In this work, a 3D Bioplotter from EnvisionTEC GmbH is used. The operation of this printer is based on the extrusion; compressed air pushes the melted (Figure 2.1a) or solved (Figure 2.1b) polymer placed in a cartridge through a conical needle generating a filament. The trajectory of the needle is

controlled by a programmed computer aided design/computer aided manufacturing (CAD/CAM) file, and in this way, the desired 3D structure it is generated layer by layer as shown in Figure 2.1.

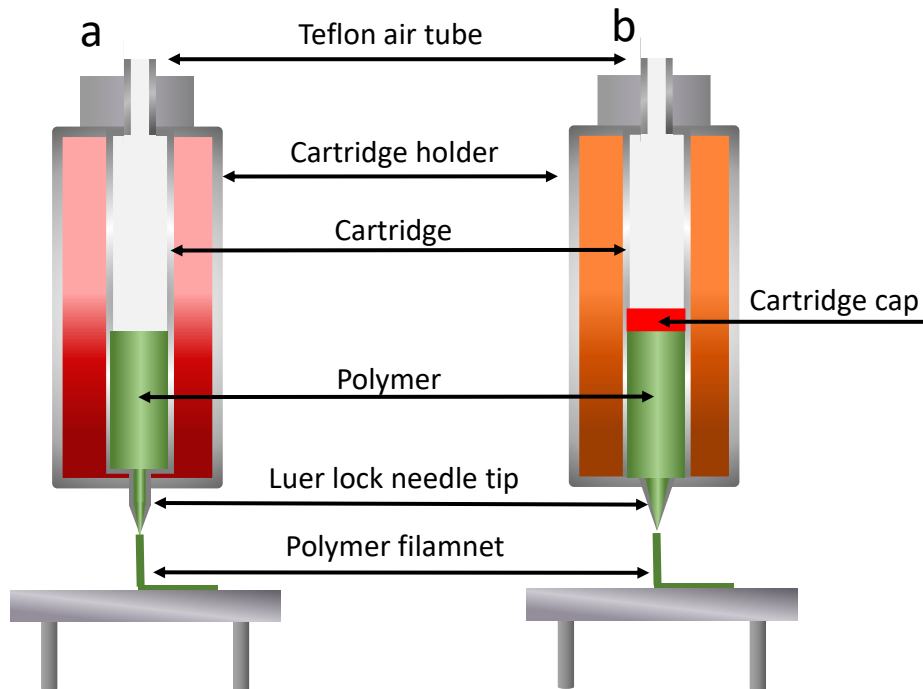


**Figure 2.1.** Schematic diagram of the 3D Bioplotter a) Melted polymer in a high temperature cartridge and b) polymer ink in low temperature cartridge.

The 3D Bioplotter used in this work allows printing at both high and low temperatures. It was corroborated that melt-printed PLA underwent a large molecular weight loss; in one hour, its molecular weight is reduced more than half. It was verified by GPC that PLA degrades in the print-head at high temperatures (see Figure 2.2). PLA is held for 30 minutes in the cartridge until complete melting before printing starts. Then, molecular weight of printed filaments are measured every 10 minutes by GPC. As the degradation proceeded, the viscosity of the melt decreased also. Consequently, the printing conditions had to be adjusted along the printing process, making impossible to print a scaffold properly.

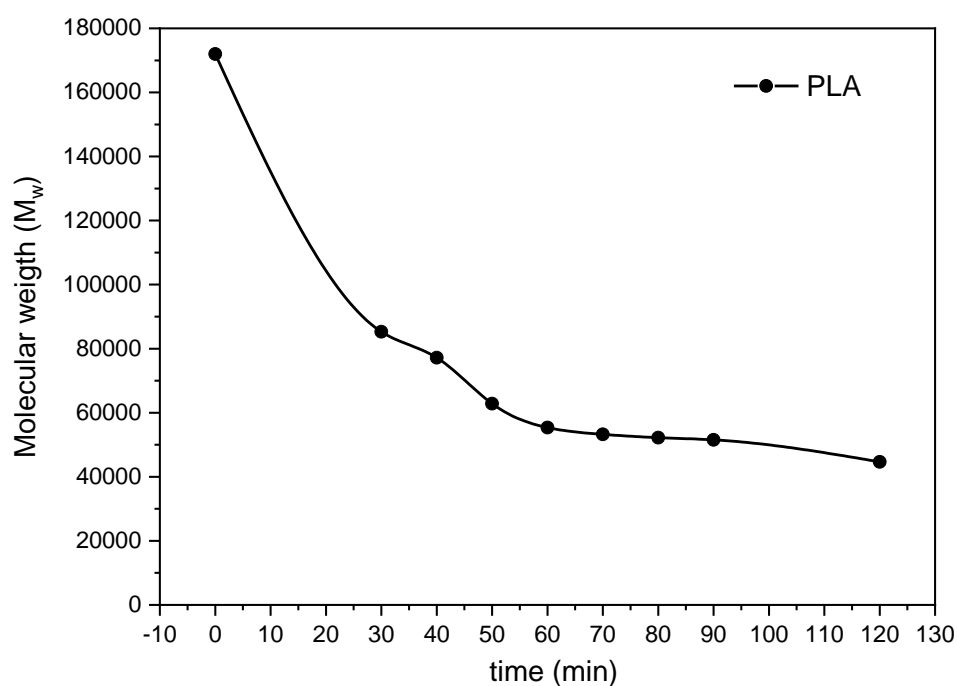


**Figure 2.2.** Molecular weight change during printing time. The temperature of the cartridge was 195 °C. To avoid thermal degradation, PLA is dissolved in chloroform and 1,4-dioxane, obtaining PLA inks for solution-printing (see Table 2.1).

**Table 2.1.** The solution of PLA with chloroform and 1,4-Dioxane. The wt. % of solution and the rename of de solution.

PLA (wt %)	Name (PLA/Dioxane)	Name (PLA/chloroform)
33.3	D8	C8
30.8	D9	C9
28.6	D10	C10
26.7	D11	C11
25	D12	C12
23.5	D13	C13
22.2	D14	C14
21.0	D15	C15
19.0	D17	C17

For PLA inks printing, a needle of 0.2 mm (inner diameter) is employed. PLA/Dioxane inks are printed at 50 °C and PLA/Chloroform solution at 22 °C.

In both cases, 30 minutes are waited prior to printing to avoid possible bubbles that may have formed when the ink was introduced into the cartridge.

The processing parameters (extrusion pressure, printing rate and temperature) were set in the Visual Machine software, which controls the 3D Bioplotter. To set these parameters rheological measurements are performed.

### **2.3. Analysis of the fluid flow**

One of the objectives of this work is to know, which solvent and which PLA ink was better for the manufacture of 3D scaffolds. For this purpose, the flow of the polymeric solutions inside the nozzle is analyzed. The solution must have a moderate viscosity, so that it can flow easily through the thin nozzle and give rise to a stable filament. For this purpose, the flow behavior of PLA solutions under two different operating conditions (i.e., printing rate and applied pressure) will be examined using a concentric cylinder analysis in continuous flow.

Figure 2.3 shows how all PLA solutions, both chloroform and 1,4-dioxane, exhibited Newtonian behavior in the range of low and moderate shear rates ( $10\text{-}1000\text{ s}^{-1}$ ) during the rotational rheometry tests. It was observed that at high shear rates, there is an instability of the flow of the solutions and the viscosity decreases sharply. On the other hand, it is observed how the PLA content influences the viscosity of the solutions. Under the same shear rate in the case of 1,4-dioxane solutions, it is observed that the most concentrated solution (D8) is almost two orders of magnitude higher than the most diluted solution (D15). In the case of chloroform this difference is smaller but shows the same behavior, the more concentrated solution (C9)

is almost one order of magnitude higher than the more dilute solution (C17). Furthermore, in the PLA solutions with 1,4-dioxane the shear rate increased slightly in all solutions if compared to the chloroform solutions, this is because the chloroform solutions are less elastic.

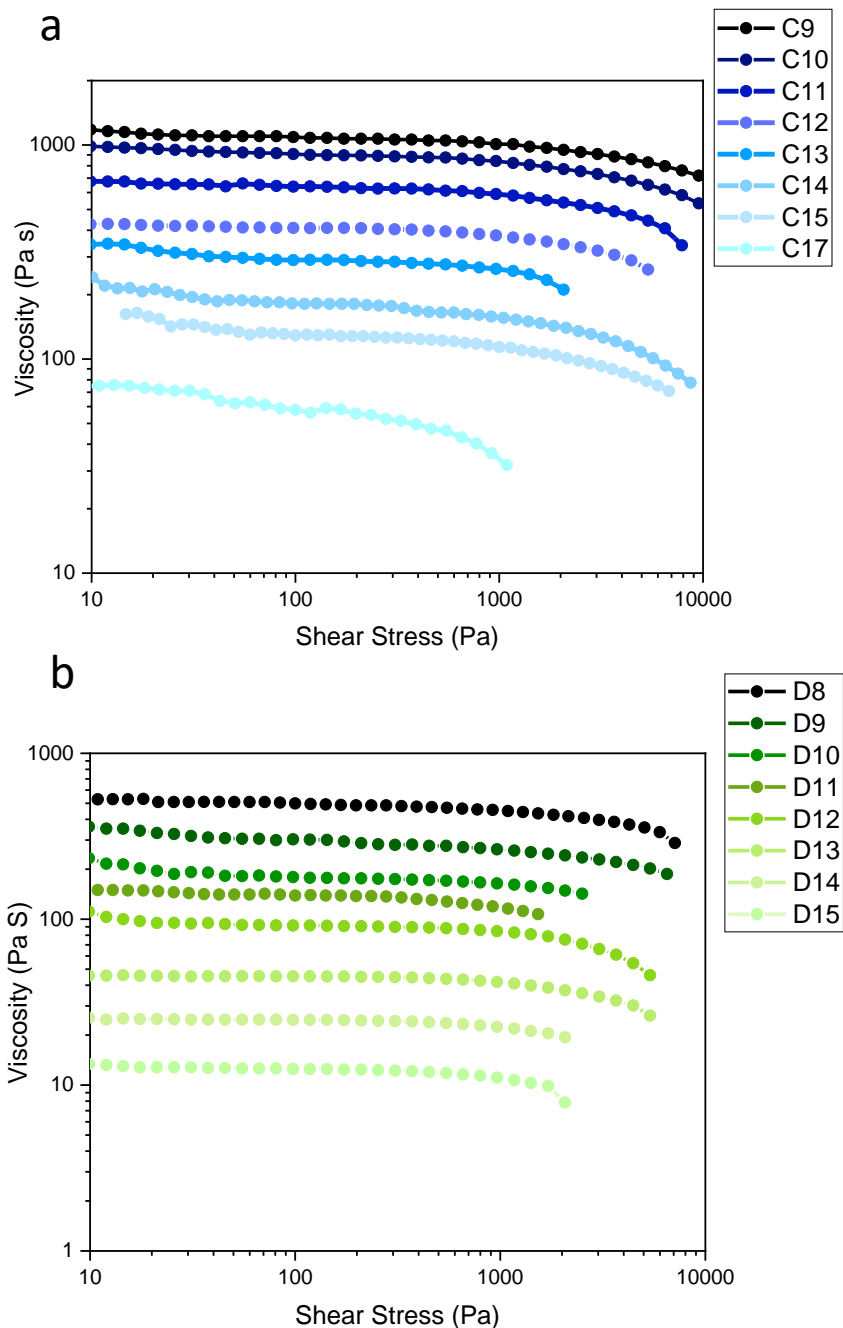


**Figure 2.3.** Viscosity as a function of shear rate for a) PLA solution in chloroform at room temperature and b) PLA solution in 1,4-Dioxane at 50 °C

The raw data obtained from Figure 2.3 were applied in the Reiner-Philippoff equation (equation 1).

$$\eta = \frac{\eta_0}{\left(1 + \frac{\sigma^2}{G}\right)^n} \quad (1)$$

Where,  $\eta$  is the viscosity of the sample,  $\eta_0$  is the viscosity at low shear rate, that is initial viscosity,  $\sigma$  is the shear stress,  $G$  is the shear modulus and  $n$  is the flow performance index.

The values of shear modulus ( $G$ ), initial viscosity ( $\eta_0$ ) and performance index ( $n$ ) are obtained (see Table 2.2). Then these values are used to obtain the printing parameters: printing rate and pressure for each PLA ink as explained below.



**Table 2.2.** Shear modulus ( $G$ ), initial viscosity ( $\eta_0$ ) and coporation index ( $n$ ) of PLA inks with chloroform and 1,4-dioxane.

	$G$ (Pa <sup>2</sup> )	$\eta_0$ (Pa s)	$n$
C9	1001180	1098	0.09
C10	935419	843	0.10
C11	378746	574	0.13
C12	3782100	411	0.18
C13	903315	290	0.13
C14	1112070	181	0.17
C15	1873240	129	0.13
C17	53679	76	0.08
D8	139796	366	0.16
D9	542164	189	0.10
D10	1648950	168	0.09
D11	859355	146	0.07
D12	238797	96	0.13
D13	71823	34	0.12
D14	504278	25	0.10
D15	139796	12	0.07

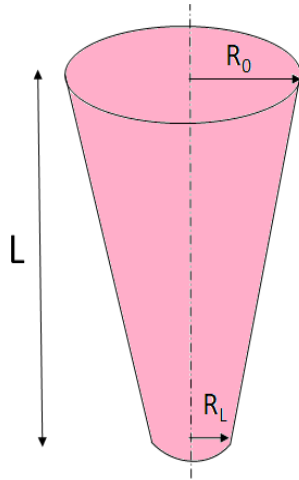
To obtain the printing values with the rheological data, the Reinner-Philippoff equation (equation 1) will be rewritten, for which the viscosity will be set as a function of the printing rate and the tension as a function of the printing pressure.

To write the viscosity as a function of printing rate, equation (2) [31] was used which describes the viscosity exerted in a truncated cone.

$$Q = \frac{\pi \Delta P R_0^4 R_x}{8\mu L} \quad (2)$$

here:

Q: Flow rate



L: Needle height

$R_L$ : Inner diameter of the needle end zone

$R_0$ : Inner diameter of the initial needle area

$\mu$ : Viscosity of PLA ink

$\Delta P$ : Change of pressure occurring in the needle

$$R_X = \left[ 1 - \frac{1 + \frac{R_0}{R_L} + \left(\frac{R_0}{R_L}\right)^2 - 3\left(\frac{R_0}{R_L}\right)^3}{1 + \frac{R_0}{R_L} + \left(\frac{R_0}{R_L}\right)^2} \right]; \quad R_X \text{ is the}$$

integration of the radius with the geometry variation.

In addition, the flow rate according to equation 3 can be defined as:

$$Q = \pi r_q \mathcal{V} \quad (3)$$

Considering that we are interested in the flow rate at the end of the needle  $r_q$  will be equal to  $R_L$ . Rewriting the flow rate of equation 2 by that of equation 3, we obtain the viscosity as a function of printing rate (equation 4).

$$\mu = \frac{\Delta P R_0^4 R_X}{8 \mathcal{V} L r_q^2} \quad (4)$$

To put stress as a function of pressure, we start with the definition of stress. Stress is the force exerted on a given area (equation 5).

$$\sigma = \frac{F}{S_L} \quad (5)$$

$S_L = \pi(R_0 + R_L)\sqrt{h^2 + (R_0 - R_L)^2}$ : the lateral surface of a truncated cone

$F = P \pi R_0^2$ : The force exerted at the needle inlet

Equation 7 defines stress as a function of pressure.

$$\sigma = \frac{P R_0^2}{(R_0 + R_L)\sqrt{h^2 + (R_0 - R_L)^2}} \quad (6)$$

Then equation 4 and equation 6 are substituted into the Reiner-Philippoff equation (equation (1)) and the printing rate as a function of printing pressure is obtained (equation 7).

$$V = \frac{\Delta P R_0^4 R_X \left( 1 + \frac{\left( \frac{P R_0^2}{(R_0 + R_L)\sqrt{h^2 + (R_0 - R_L)^2}} \right)^2}{G} \right)^n}{8Lr_q^2\eta_0} \quad (7)$$

Substituting the parameters obtained from the shear rate versus viscosity plot (Table 2.2) in equation 7, it gives an estimate of the printing rate for each printing pressure. Figure 2.4 shows the real values of pressure and printing rate and the values predicted by the rheological estimation for PLA inks in chloroform. It is shown that predictive rheological data are very similar to those obtained in the printer. Therefore, by means of rheological measurements one can predict the rate and pressure that will be needed in the printer.

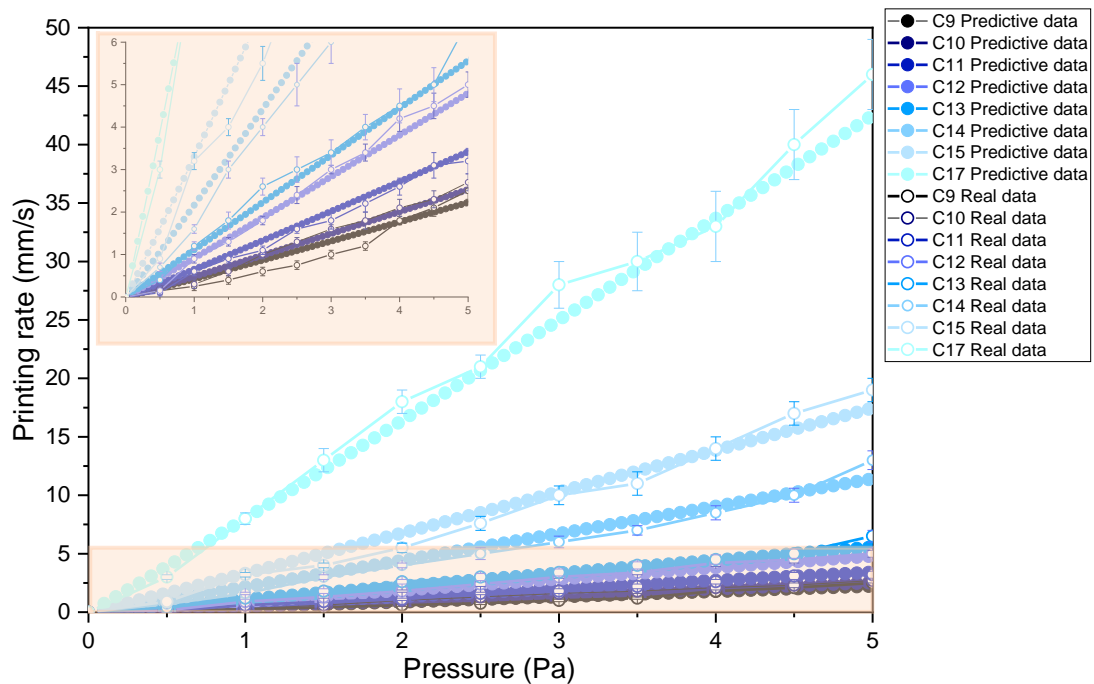


**Figure 2.4.** Printing pressure and rate of PLA inks in chloroform. Real data and predictive data.

Figure 2.5 shows the printing pressure and rate data for PLA inks in 1,4-dioxane. In this case it is observed that for very concentrated solutions the model resembles the real data, but for very dilute solutions the model does not fit. This might be due to the fact that the needle is not heated (Figure 2.1) and consequently a temperature gradient might exist which was not considered. This temperature gradient makes the viscosity in the needle to be higher than the one calculated in the rheology test. This is the reason why the printing rate and pressure data obtained from the rheological measurements are higher than the data obtained in the 3D printer. In more concentrated solutions, the times in which the flow is coming out of the needle is less, so the error is not so visible and the theoretical data are more similar to the real ones.

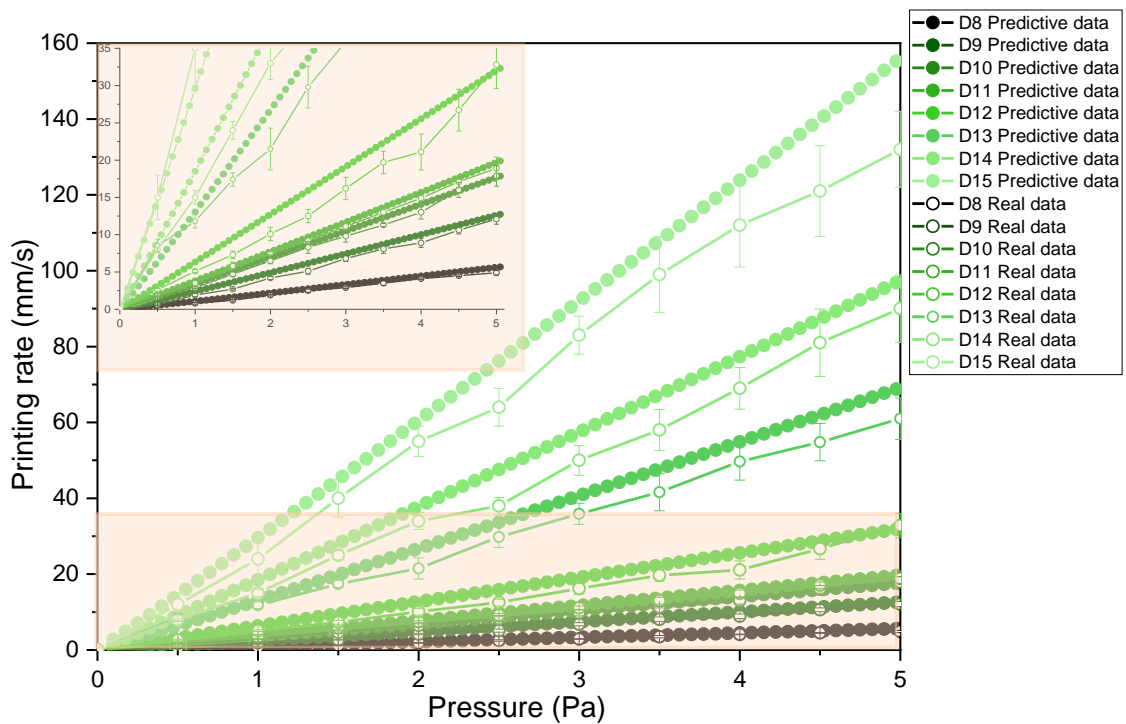


**Figure 2.5.** Printing pressure and rate of PLA inks in 1,4-dioxane. Real data and predictive data.

## 2.4. Welding between layers or filaments

For a correct use of 3D printing it is essential to know the variables that affect the welding or adhesion process of the layers or filaments that make up the final part (scaffold). For the adhesion between layers or filaments to be adequate, it is necessary that a diffusion process take place between the polymeric chains of the different layers or filaments. The welding process occurs in the terminal or flow zone, where the diffusion takes place between one layer of the polymer and another. It strongly depends on the temperature and the time of contact between layers, which are at the same time dependent on the structure of the polymer and molecular weight. Moreover, in the case of inks it also depends on the evaporation of the solvent.

Although the welding between layers is a very important parameter for a correct 3D printing, the literature on this subject is very limited [32–35], and

practically nonexistent for the case of inks, so the selection of good printing conditions can become a complex and laborious task.

Therefore, in this work the rheology applied to PLA inks will be the same as the one applied for polymer fusion, but to analyze the welding of PLA ink filaments we also analyzed the solvent evaporation, the crystallization of the inks and the mechanical properties of the welds.

In the case of the extrusion of molten materials for a weld to occur in the filaments we have to be located in the terminal zone or fluid zone [36], this means that the loss modulus has to be higher than the storage modulus ( $G'' > G'$ ).

The frequency at which PLA/Chloroform inks are process affects the welding between layers. Frequency sweeps tests (Figure 2.6) showed that at low frequencies all the inks are in the flow zone, but as the concentration increases the frequency decreases to a maximum of 20 Hz. Therefore, the most suitable frequencies to process PLA inks in chloroform are 1 to 10 Hz to ensure the inks are in the flow zone.

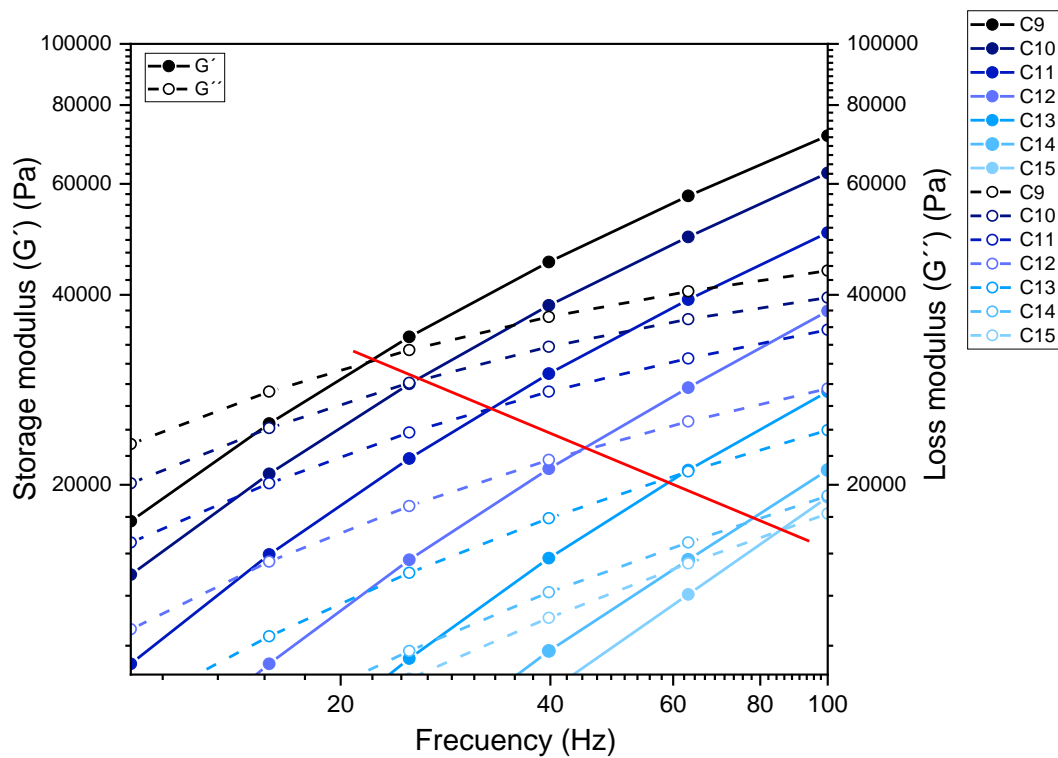


**Figure 2.6.** Frequency sweep for PLA inks in chloroform at 22 °C. The red line represents the cross-point between  $G'$  and  $G''$ . In the case of PLA/1,4-dioxane inks temperature gains importance. The more concentrated solutions (D8 and D9) are processed at 50 °C as they do not dissolve at room temperature. Therefore, 1,4-Dioxane frequency sweeps have been performed at two temperatures, one at 50 °C (

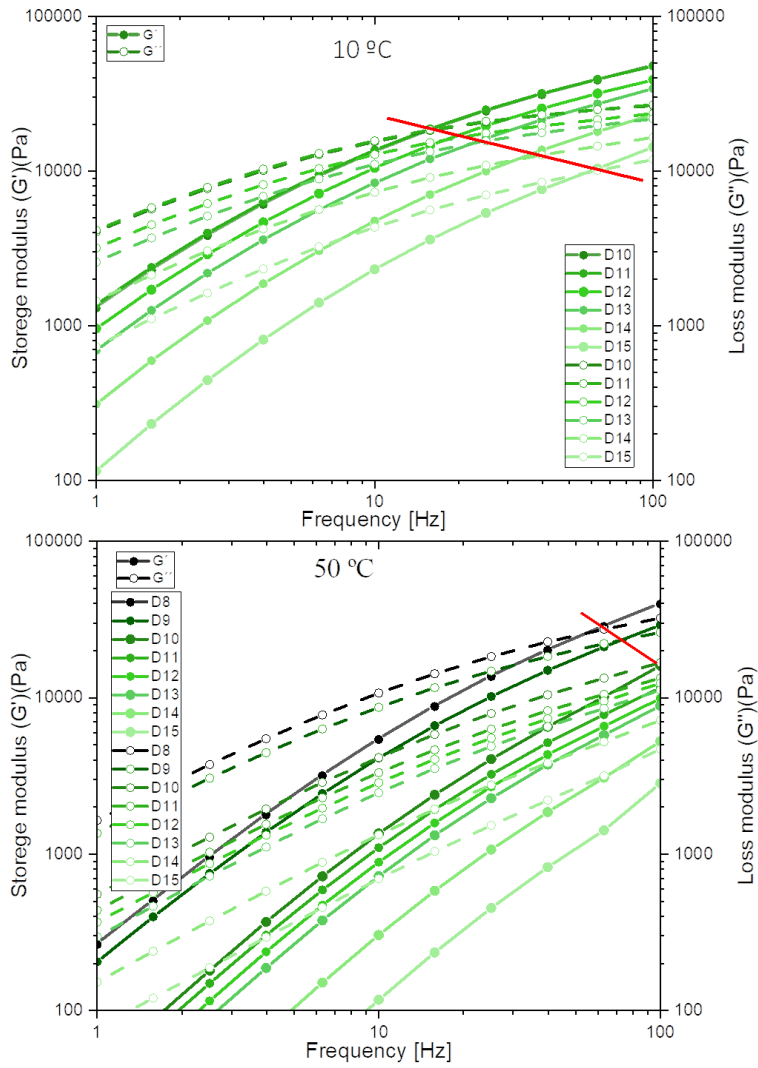


Figure 2.7 bottom) and the other one at 10 °C (



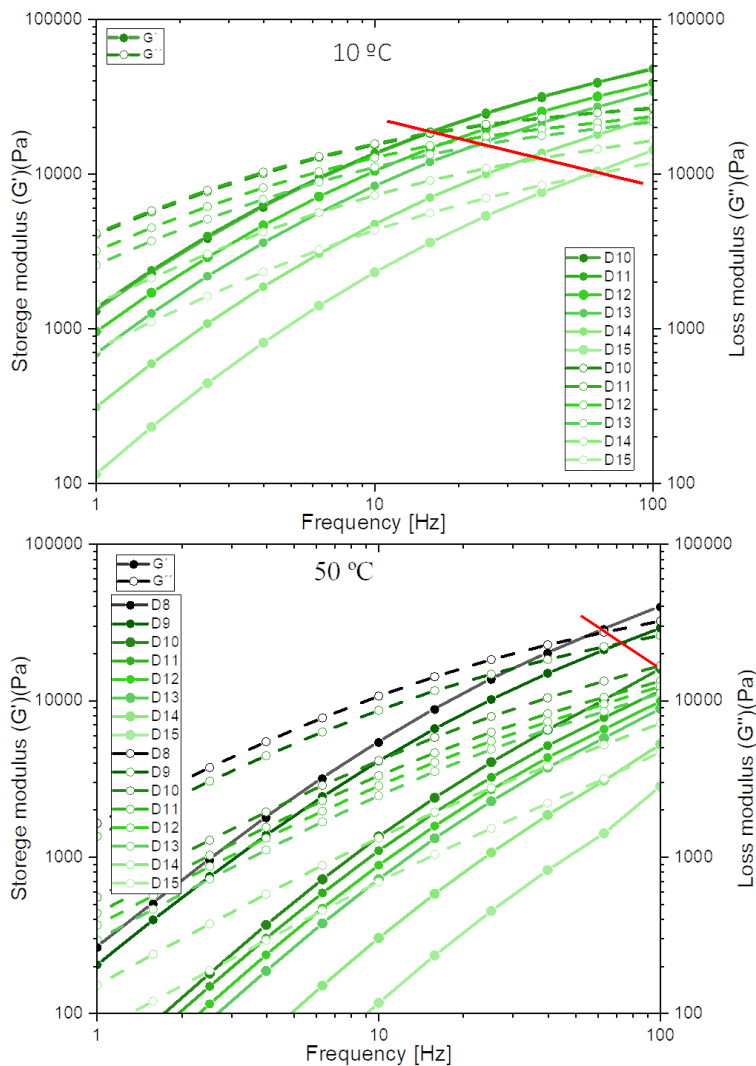
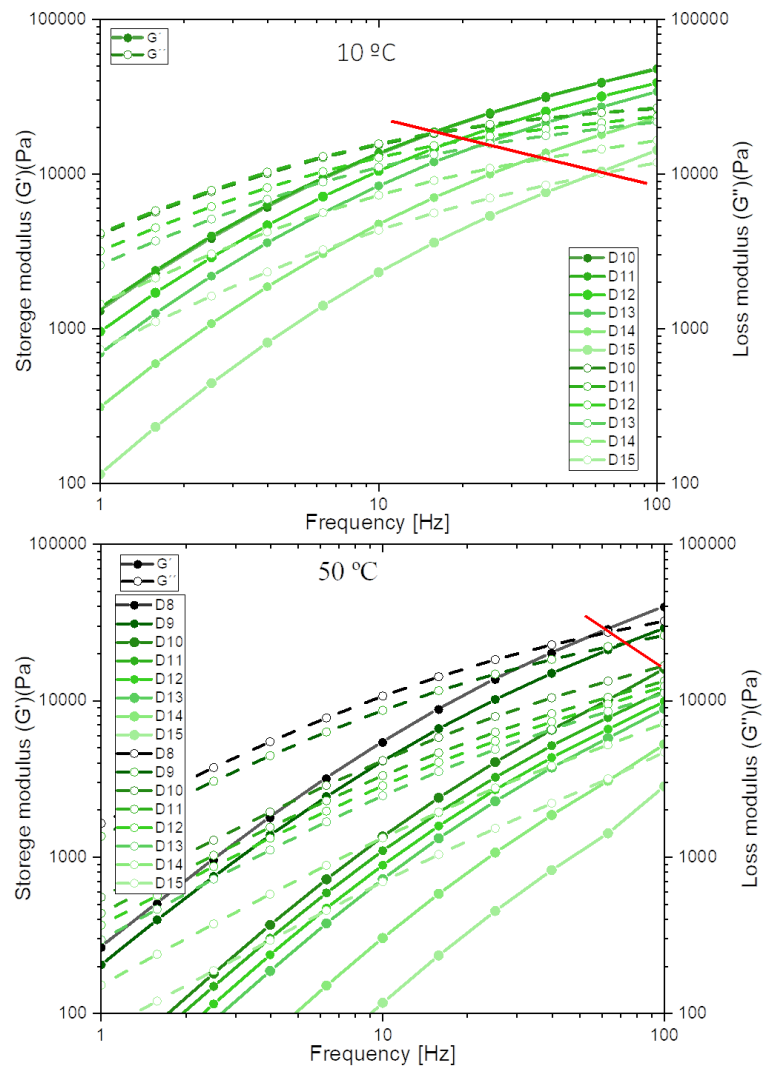


Figure 2.7 up). In the first case, inks are in the flow zone even at high frequencies (100 Hz). When the temperature is reduced to 10 °C, the frequencies also decrease. Moreover, as in the case of chloroform, when the concentration increases, the frequency decreases up to a maximum of 15 Hz. In view of the results obtained, the frequencies used for 1,4-dioxane will be the same as in the case of chloroform between 1 and 10 Hz.



**Figure 2.7.** Frequency sweep for PLA inks in 1,4-dioxane at 10 °C (up) and at 50 °C (bottom). The red line represents the cross-point between  $G'$  and  $G''$ .

Apart from the frequency, solvent evaporation and solvent evaporation mode play an important role in filament welding and the final geometry of the 3D printed part. Three different mechanisms take place in solvent removal: (1) flash vaporization, (2) diffusion within the filament and (3) convective transfer from the filament surface to the surrounding air [37–39]. Flash evaporation takes place near the nozzle tip due to a pressure drop after extrusion of the filament. The solvent molecules must then diffuse through the filament (internal diffusion) to evaporate at the air/filament interface (external convection).

Solvent evaporation was analyzed by monitoring the filament weight reduction as a function of time using a precision balance. Figure 2.8 shows the normalized solvent content with time evolution for 1 cm filaments and a 0.25 mm needle. The solutions used for this test were the most concentrated (C9 and D9) and the most dilute (C15 and D15) ones (see Figure 2.8). It was observed that solution concentration (C9 vs C15 and D9 vs D15) does not affect the evaporation mode of the solvent obtaining similar results regardless the solvent type.

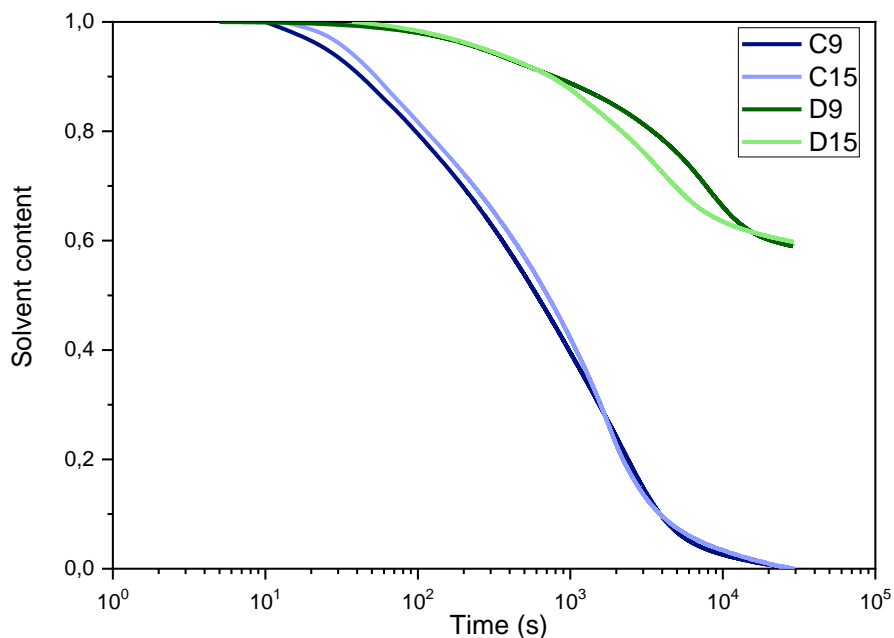


**Figure 2.8.** Normalized solvent content as a function of the time for C9, C15, D9 and D15 solutions. C#: Chloroform solutions and D#: 1,4-Dioxane solutions.

Attending to the curves shape, two differences are observed between chloroform and 1,4-dioxane: (1) Chloroform evaporates faster with a steeper slope, (2) Remaining 1,4-dioxane is observed after being evaporating at room temperature during 8 h. The latter will have consequences if large structures are wanted to built due to geometrical stability loss.

In view of this results in order to ensure a complete solvent removal the printed samples were introduced at 40 °C for C9 and C15 inks and at 60 °C for D9 and D15 inks. Samples were maintained at these temperatures overnight and reweighed to corroborate the total removal of the solvent.

Once the sample were completely dry welding process was analyzed following Chelsea S. David et al. developed method which measure weld forces based on mode III (“trouser tear”) fracture experiment [40]. Samples were prepared by printing eight filaments one on top of the other obtaining a height of 1.6 cm approximately. The length of the samples was varied from 8 mm to 150 mm. All layers were printed in the same direction with the extruder moving from left to right. In addition, a 25 mm wide piece of polytetrafluoroethylene (PTFE) tape was placed between filaments number 4 and 5 which is removed once the material is solidified to create a pre-crack. A summary of the specimen preparation process is shown in Figure 2.9.

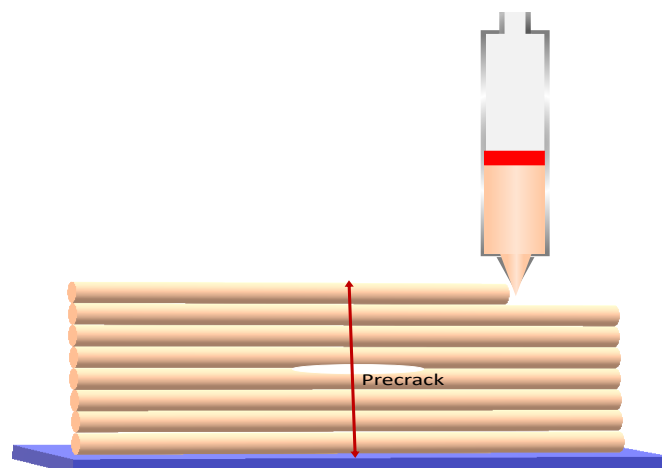


**Figure 2.9.** Schematic of simple specimen preparation for *trouser tearing* test.

Figure 2.10 show the propagation force versus filament length behavior for different PLA inks. Six to eight individual samples of each filament length were taken to calculate the propagation force.

A plastic deformation near or at the pre-crack and along the crack propagation was observed in all samples. The lengths of the specimens were analyzed before and after testing and an increase of about 7% was observed; this plastic deformation is typical of PLA [41,42]. However, neither the increase of the filament length nor the increase of the solvent concentration had any effect on the plastic deformation.

Solvent evaporation has a great effect on the crack propagation force or tearing strength. Rapid evaporation of the solvent leads to a weaker weld between filaments and so, to a lower tear strength (see Figure 2.10). Therefore, high concentration inks show better tearing strength than diluted ones. Moreover the roll of solvent evaporation is easily proved by printing filaments with different lengths. The longest samples (16 cm) show lower tearing strength than the shortest one (4 cm); it drops by almost an order of magnitude. The longer the sample is the more time is needed for printing and the more time has the solvent to evaporate before the next filament printing. Consequently, the welding between the two filaments is not strong.

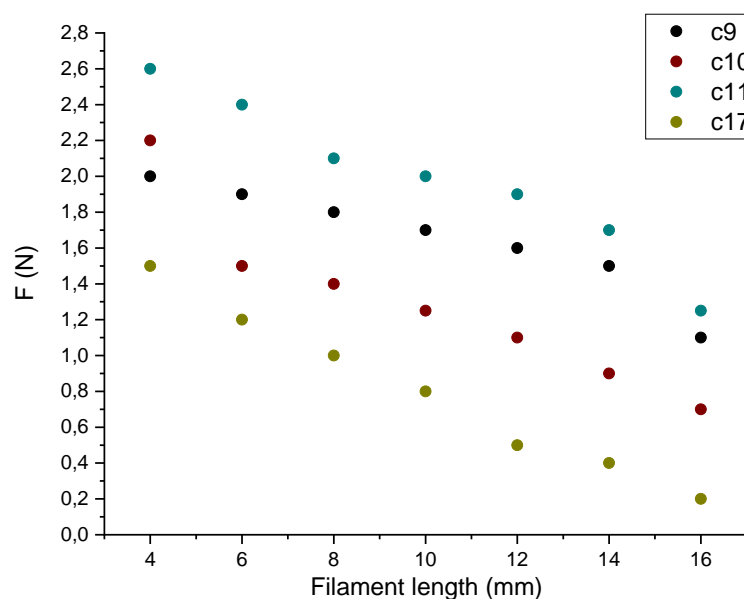


**Figure 2.10.** Propagation force obtained for different filament length on the samples (C9, C10, C11 and C17).

However, the sample with the highest amount of solvent is the one with the lowest tear strength. This happens because the filament shrunk due to a big loss of solvent and, thus the set point of the second filament changes, leaving a gap between them (see Figure 2.11 C17 and C15). Sample C11 shows the biggest weld layer and thus the highest tear strength in all filament lengths (Figure 2.11 C11). However, this thick weld layer causes the filament to deform and ultimately affects the final geometry of the part. The most concentrated solution (C9) is the most suitable in terms of filament shape and strength. In C9, the weld generated does not exceed 80% of the filament diameter, which means that the final height of the geometry is not affected and the bonding strength between the filaments is sufficient so that the filaments do not lose their adhesion to each other.

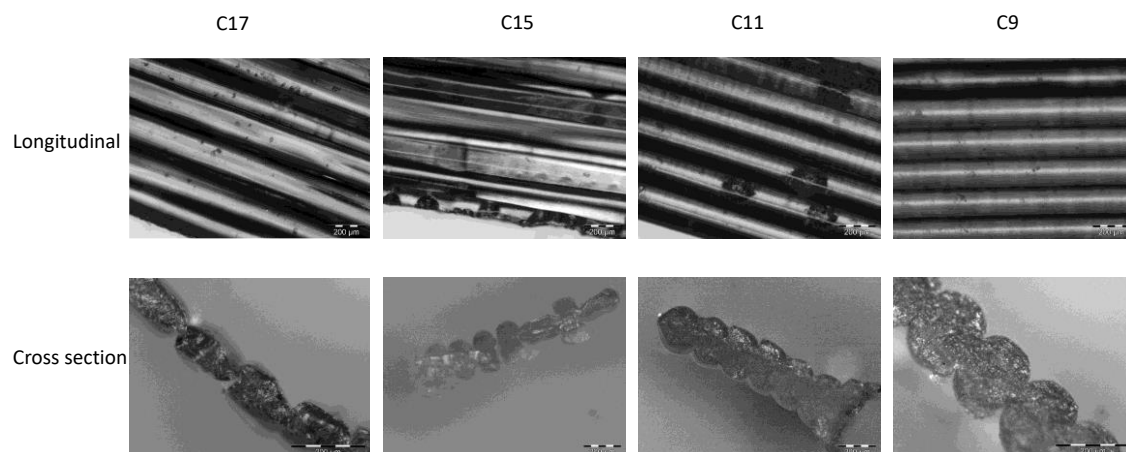


**Figure 2.11.** Longitudinal and cross section images of samples C17, C15, C11 and C9 for a filament length of 10 cm

For PLA/1,4-dioxane inks the more dilute samples could not be tested because they do not have sufficient stability to build the specimen (filament wall). Walls printed with D12 and D11 inks was not possible to test mechanically because the filaments had a complete union. That is, there was no filament separation where the crack could initiate. When placed for the tensile test, they broke before the crack propagation started. This happens

because the remaining or non-evaporated solvent in the filament (see Figure 2.12) diffusion between filaments is promoted.

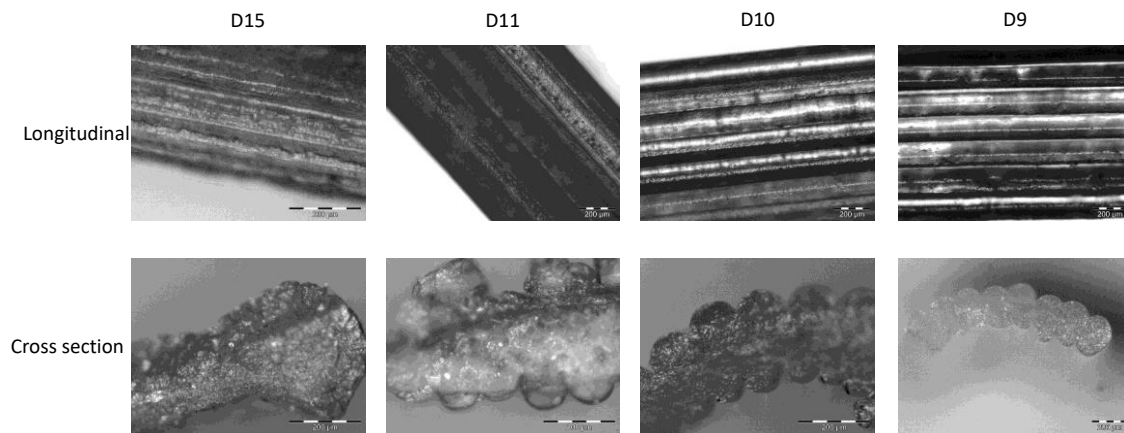


**Figure 2.12.** Longitudinal and cross section images of samples D15, D11, D10 and D9 for a filament length of 10 cm  
The largest weld was found for D10 ink which showed the highest crack propagation force or tearing strength (see Figure 2.13). In this case, as the solvent does not evaporate no geometrical instabilities were found. However, in diluted solutions, D14-D17, at certain level of height, the structure collapsed due to the weight of the filaments (see Figure 2.12).

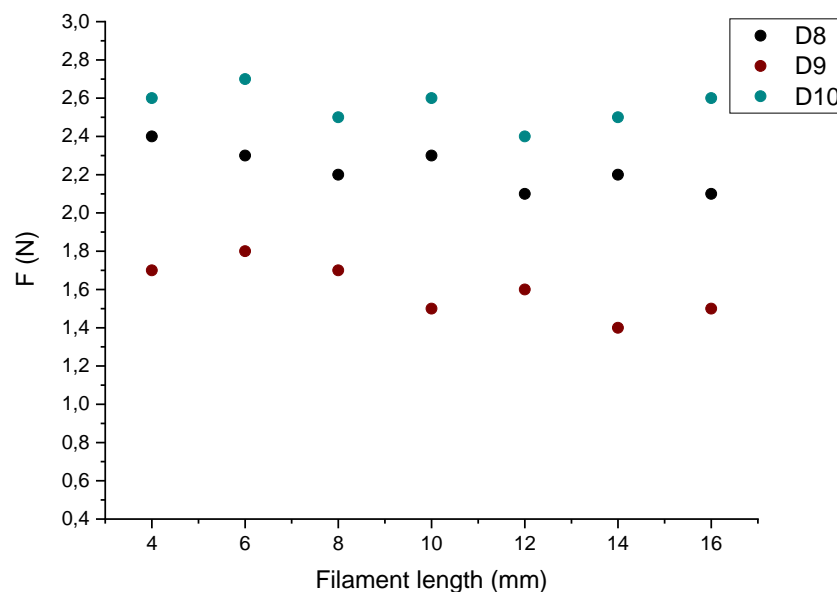
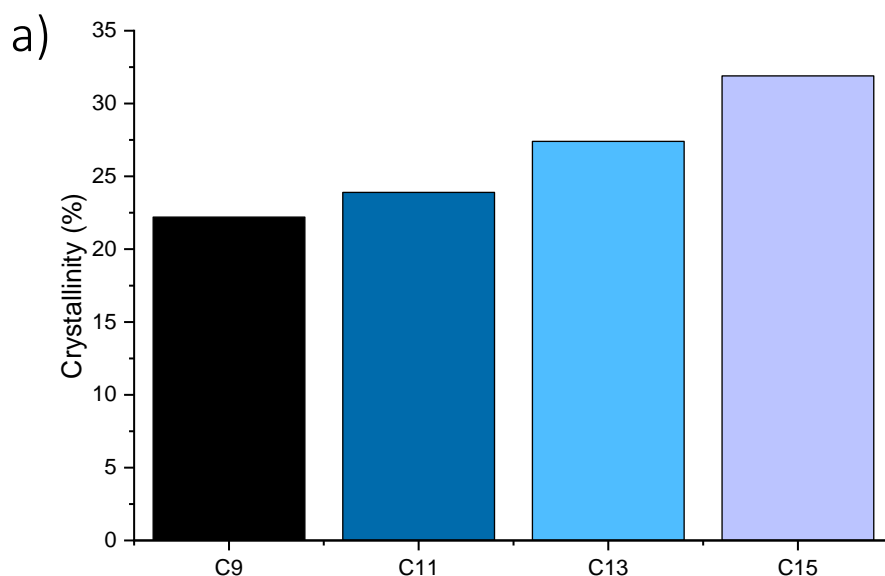


**Figure 2.13.** Propagation force obtained for different filament length on the samples (C9, D8, D9 and D10).

In contrast to PLA inks in chloroform, the filament length does not affect the crack propagation force which remains more or less constant over all filament lengths. Because 1,4-dioxane does not evaporate completely the generated welds are not as time dependent as in the case of chloroform samples. However, if too much weight is added to the structure by printing a different numbers of filaments then the structure might collapsed. In this sense the more concentrated dioxane solutions seem to reach an equilibrium; less solvent is trapped inside the filament making it stable and does not collapse with weight, and at the same time helps to generate a strong weld.

## 2.5.FINAL GEOMETRY OF THE SCAFFOLD

The crystallinity of the polymer is a factor that has to be considered regarding the geometry and final properties of the scaffold. The crystallization process can promote a shrinkage of the printed filaments and changes on the mechanical properties (more fragil samples). Therefore, a low crystallinity fraction is desired for scaffold printing. As shown in Figure 2.14 and **Error! Reference source not found.**, the crystallinity is analyzed as the dissolution concentration increases in both cases, i.e. in the PLA inks with chloroform and with 1,4-dioxane.



b)



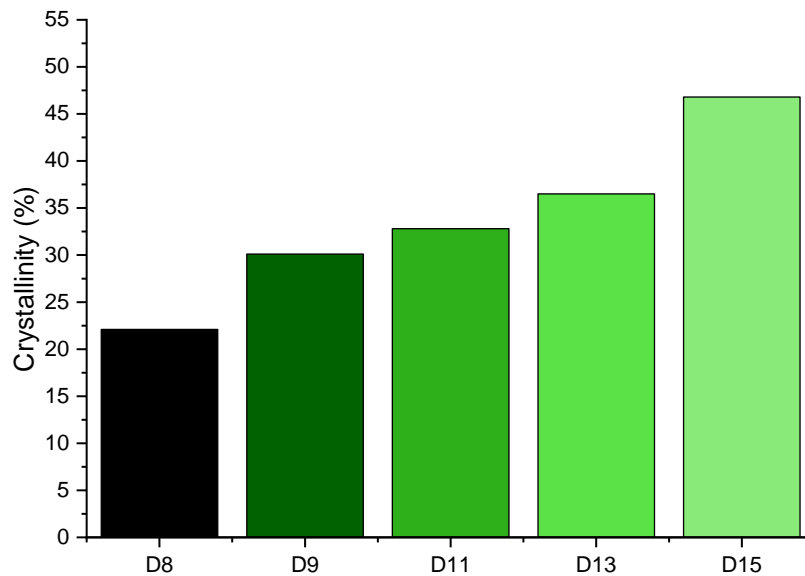


**Figure 2.14.** Crystallinity fraction for different (a) PLA/chloroform inks and (b) PLA/1,4-Dioxane inks.

It was observed an increase in crystallinity fraction as the concentration of the ink decreased (see Figure 2.14a). This occurs because the solvent makes the polymer chains more free and therefore they can be better rearranged. In any case, the difference in crystallization between the most dilute and the most concentrated concentration is not very large. A very similar results were found for PLA/1,4-Dioxane inks (see Figure 2.14b). Comparing the chloroform and 1,4-dioxane solutions, it is observed that the 1,4-dioxane solutions have higher crystallinity. Since this solvent does not evaporate immediately and it gives the polymer chains more time to rearrange.

In addition, SEM photographs were taken of the surfaces of the scaffolds to analyze the effect of solvent evaporation in solution (C14, C9, D11 and D8). In Figure 2 15 holes on the surface of the scaffold printed with diluted ink (C14) can be appreciated, while for the more concentrate one (C9) no sign of solvent evaporation on the surface is appreciated. Moreover, cross section analysis corroborated no signs of solvent evaporation.

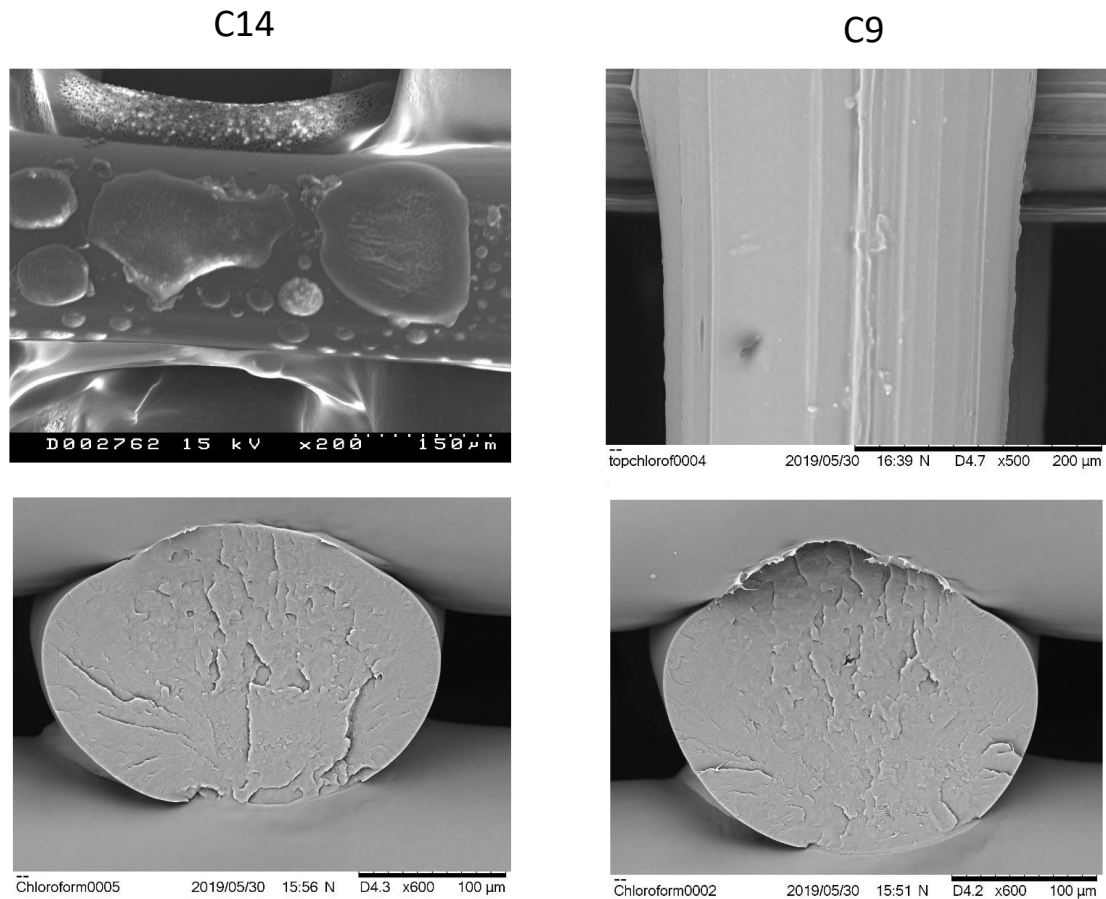


**Figure 2.15.** SEM images of PLA inks in chloroform, up images top view of scaffold and bottom images cross section of scaffolds. In the case of PLA/1,4-dioxane inks (Figure 2.16), D11 solution was the most diluted solution with which a scaffold could be printed. When analyzing the sample no signs of solvent evaporation was observed at the top of the scaffold, however, the cross section of the scaffold showed some micro-holes inside the filaments. For more concentrated inks (D8) evaporation occurred in the other way around; micro-hole were observed on the surface of the filament but not inside.

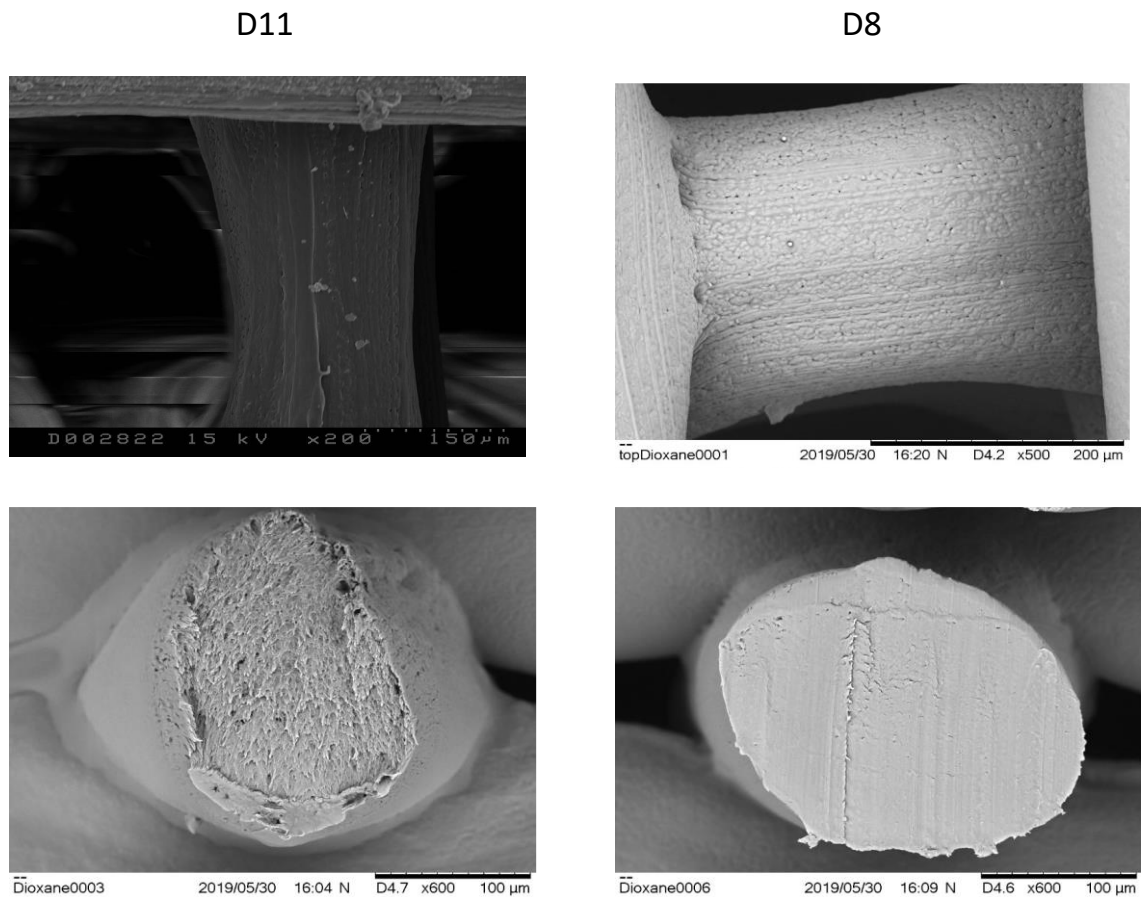


**Figure 2.16** SEM images of PLA inks in 1,4-dioxane, up images top view of scaffold and bottom images cross section of scaffolds. Once the scaffolds were printed, a visual analysis was carried out before and after solidifying steps. Both scaffolds (D8 and C9) exhibited a contraction in geometry, as expected due to the loss of volume. For C9 this contraction was not uniform; the contraction occurs while printing. Circular geometries ended up as conical shapes (see Figure 2.17a). After drying, no new contraction in the geometry was observed.

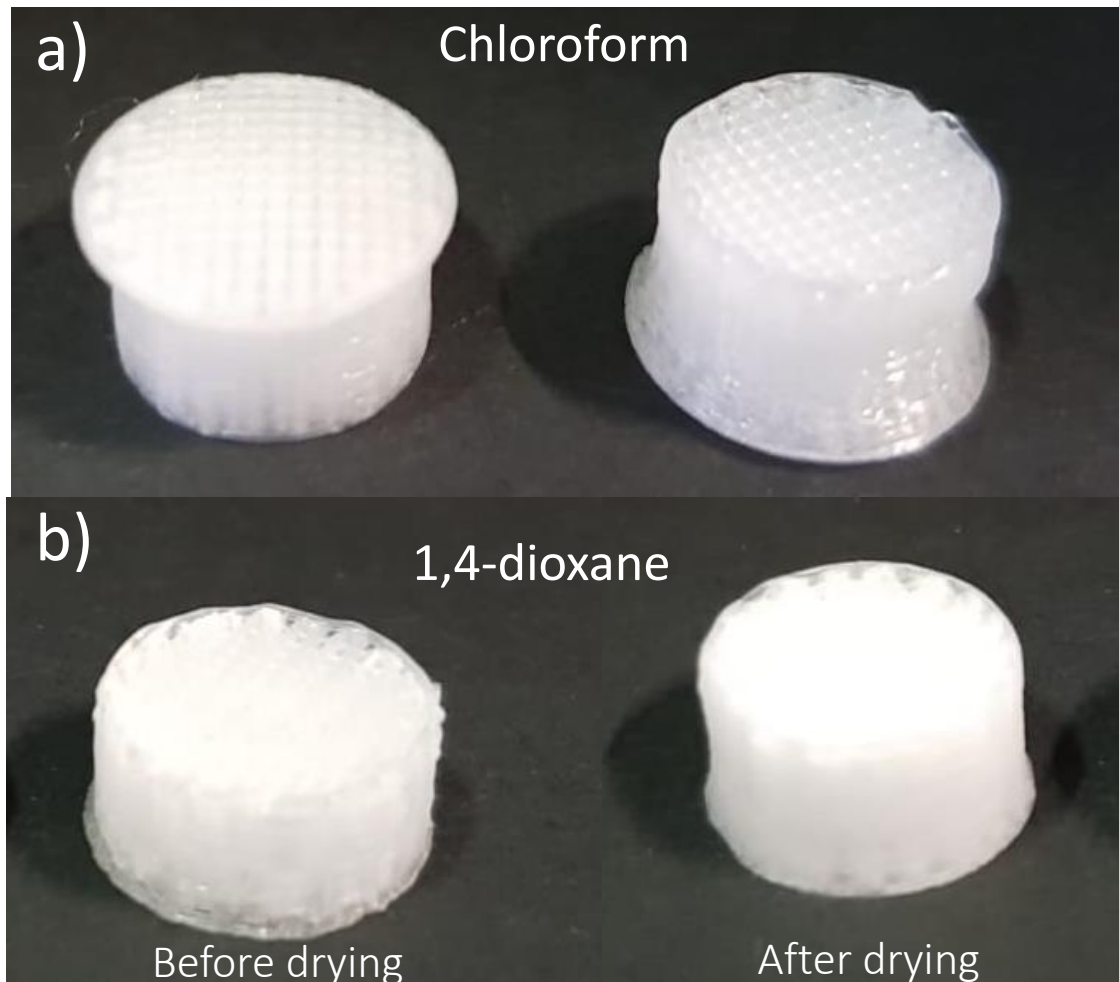


**Figure 2.17.** a) Image of C9 scaffold after printing process and b) image of D8 scaffold before and after drying.

For scaffold printed with D8 no contraction was observed during the printing process, as the solvent does not evaporate completely and helps the scaffold not to contract and maintain the geometry. Evaporation occurs after oven drying, but the sample shrinks uniformly (see Figure 2.17b). D8 scaffolds suffer a volume loss of 10 to 20% of their original volume. This factor will have to be taken into account when designing the part, since the final part will be smaller than the original one.

## 2.6.CONCLUSION

During this work, a rigorous 3D printing analysis was performed for PLA inks with chloroform and 1,4-dioxane. For this purpose, the work was divided

into three parts. In the first part the flow of the inks was analyzed and a model was obtained to help to calculate the printing parameters; in the second part the welding between the filaments was studied; and finally, in the third part the resulting geometry of the scaffold was analyzed.

In the first part, the 3D printer was modeled to obtain the printing parameters by using rheology. It was observed that 3D printing values of PLA/chloroform inks followed the model perfectly. However, PLA/ 1,4-Dioxane inks could only follow the model at high concentrations.

In the second part, the welding between filaments of different inks was analyzed. It was concluded that PLA inks in very diluted chloroform would be suitable for free printing of geometries, but not for making scaffolds, since they do not generate an adequate weld between the filaments. C9 ink was proved to be the most suitable in terms of welding and geometry stability. For PLA inks with 1,4-dioxane, the most diluted solutions were proved to be non-printable. The more concentrated dioxane solutions (D8) showed to reach an equilibrium between the solvent evaporation and welding without collapsing the geometry.

Finally, visual inspection of the geometries showed that the sample C9 suffered irregular contraction during printing which affected the final result, while in the sample D8 the contraction was regular along the whole part.

As a conclusion, it is considered that the D8 ink is the best for printing scaffolds, while the C9 ink could be suitable for parts with a maximum height of 4 mm.

## **2.7. Material and experimental method**

### **2.7.1. Materials and Solvents**

PLLA with a molecular weight of 100000 g/mol supplied by Purac was dissolved in two solvents, chloroform and 1,4-dioxane. (Both supplied by Sigma Aldrich)

### **2.7.2. Rheological Test**

The shear viscosity of the polymer solutions was characterized at 22 °C for chloroform solutions and at 50 °C for 1,4-Dioxane solutions using a rotational rheometer (MCR-502, Anton Paar) in a continuous flow (CC25 concentric cylinder geometry). The rheometer has a cap to prevent solvent evaporation. The shear rate ramp started from 10 s<sup>-1</sup> and increased until flow instabilities were observed at ~1000 s<sup>-1</sup>, where the viscosity dramatically decreased. Each polymer solution was tested under ambient pressure and three different test was carried out for each solutions. Frequency sweeps were also carried out on rotational rheometer (MCR-502, Anton Paar) in a oscillatory flow (CC25 concentric cylinder geometry) with a frequency change from 1 to 100 Hz.

### **2.7.3. Solvent Evaporation**

The solvent evaporation behavior of the polymeric inks was evaluated by directly depositing a 5 mm long filament on a glass substrate supported on a high precision balance (GH-202, A&D Engineering). D9 AND C9 composition were deposited with a 0.2 mm nozzle. The weight of the sample was recorded for 8 h. After this recording period, the sample was dried completely in an oven (G05053-10, Cole-Parmer) at 40 °C the chloroform sample and 60 °C the 1,4-Dioxane sample for 12 h and reweighed. The mass of the dried PLA was then used to calculate the solvent percentage in real time in the extruded filament.

#### 2.7.4. Mechanical test

The weld tear strength was determined by a Mode III fracture experiment ("trouser tearing"). In this technique, the average torsional tearing energy of a long, thin strip of material is determined. The experimental geometry and tear test parameters were modified from the ASTM D1938-14 test method reference standard [43].

#### 2.7.5. Differential scanning calorimetry

Thermal analysis was carried out with a DSC 2920 (Waters-TA Instruments) under a nitrogen atmosphere at a velocity of 20°C/min to verify the crystallinity of different solutions (1,4-Dioxane solutions and Chloroform solutions).

#### 2.7.6. Optical Microscopy and Scanning Electron Microscope (SEM)

The optical microscopy has been used to obtain the diameter of filament. And SEM has been used to analyze the surface of the 3D printed scaffolds.

### 2.8. Bibliography

1. Cardea, S.; Baldino, L.; Pisanti, P.; Reverchon, E. 3-D PLLA scaffolds formation by a supercritical freeze extraction assisted process. *J. Mater. Sci. Mater. Med.* **2014**, *25*, 355–362, doi:10.1007/s10856-013-5069-0.
2. Larrañaga, A.; Diamanti, E.; Rubio, E.; Palomares, T.; Alonso-Varona, A.; Aldazabal, P.; Martin, F.J.; Sarasua, J.R. A study of the mechanical properties and cytocompatibility of lactide and caprolactone based scaffolds filled with inorganic bioactive particles. *Mater. Sci. Eng. C* **2014**, *42*, 451–460, doi:10.1016/j.msec.2014.05.061.
3. Mukherjee, S.; Agarwal, M.; Bakshi, A.; Sawant, S.; Thomas, L.; Fujii, N.; Nair, P.; Kode, J. Chemokine SDF1 Mediated Bone Regeneration Using

- Biodegradable Poly(D,L-lactide- co-glycolide) 3D Scaffolds and Bone Marrow-Derived Mesenchymal Stem Cells: Implication for the Development of an “Off-the-Shelf” Pharmacologically Active Construct. *Biomacromolecules* **2020**, *21*, 4888–4903, doi:10.1021/acs.biomac.0c01134.
4. Mikes, P.; Horakova, J.; Saman, A.; Vejsadova, L.; Topham, P.; Punyodom, W.; Dumklang, M.; Jencova, V. Comparison and characterization of different polyester nano/micro fibres for use in tissue engineering applications. *J. Ind. Text.* **2021**, *50*, 870–890, doi:10.1177/1528083719848155.
  5. Yousefi, A.M.; Powers, J.; Sampson, K.; Wood, K.; Gadola, C.; Zhang, J.; James, P.F. In vitro characterization of hierarchical 3D scaffolds produced by combining additive manufacturing and thermally induced phase separation. *J. Biomater. Sci. Polym. Ed.* **2020**, doi:10.1080/09205063.2020.1841535.
  6. Mao, H.; Yang, L.; Zhu, H.; Wu, L.; Ji, P.; Yang, J.; Gu, Z. Recent advances and challenges in materials for 3D bioprinting. *Prog. Nat. Sci. Mater. Int.* **2020**, *30*, 618–634.
  7. Pekkanen, A.M.; Mondschein, R.J.; Williams, C.B.; Long, T.E. 3D Printing Polymers with Supramolecular Functionality for Biological Applications. *Biomacromolecules* **2017**, *18*, 2669–2687, doi:10.1021/acs.biomac.7b00671.
  8. Jaidev, L.R.; Chatterjee, K. Surface functionalization of 3D printed polymer scaffolds to augment stem cell response. *Mater. Des.* **2019**, *161*, 44–54, doi:10.1016/j.matdes.2018.11.018.
  9. ASTM F2792 - 12a Standard Terminology for Additive Manufacturing



- Technologies (Withdrawn 2015) Available online: <https://www.astm.org/Standards/F2792.htm> (accessed on Feb 28, 2021).
10. Wu, T.; Gray, E.; Chen, B. A self-healing, adaptive and conductive polymer composite ink for 3D printing of gas sensors. *J. Mater. Chem. C* **2018**, *6*, 6200–6207, doi:10.1039/c8tc01092g.
  11. Shahin-Shamsabadi, A.; Selvaganapathy, P.R. ExCeL: Combining extrusion printing on cellulose scaffolds with lamination to create in vitro biological models. *Biofabrication* **2019**, *11*, doi:10.1088/1758-5090/ab0798.
  12. Ligon, S.C.; Liska, R.; Stampfl, J.; Gurr, M.; Mülhaupt, R. Polymers for 3D Printing and Customized Additive Manufacturing. *Chem. Rev.* **2017**, *117*, 10212–10290.
  13. Gopi, S.; Kontopoulou, M. Investigation of thermoplastic melt flow and dimensionless groups in 3D bioplotting. *Rheol. Acta* **2020**, *59*, 83–93, doi:10.1007/s00397-019-01186-4.
  14. Gibson, I.; Rosen, D.; Stucker, B. *Additive manufacturing technologies: 3D printing, rapid prototyping, and direct digital manufacturing, second edition*; Springer New York, 2015; ISBN 9781493921133.
  15. O’Harra, K.; Sadaba, N.; Irigoyen, M.; Ruipérez, F.; Aguirresarobe, R.; Sardon, H.; Bara, J. Nearly Perfect 3D Structures Obtained by Assembly of Printed Parts of Polyamide Ionene Self-Healing Elastomer. *ACS Appl. Polym. Mater.* **2020**, *2*, 4352–4359, doi:10.1021/acsapm.0c00799.
  16. Chia, H.N.; Wu, B.M. Recent advances in 3D printing of biomaterials. *J. Biol. Eng.* **2015**, *9*, 4, doi:10.1186/s13036-015-0001-4.

17. Rashad, A.; Mohamed-Ahmed, S.; Ojansivu, M.; Berstad, K.; Yassin, M.A.; Kivijärvi, T.; Heggset, E.B.; Syverud, K.; Mustafa, K. Coating 3D Printed Polycaprolactone Scaffolds with Nanocellulose Promotes Growth and Differentiation of Mesenchymal Stem Cells. *Biomacromolecules* **2018**, *19*, 4307–4319, doi:10.1021/acs.biomac.8b01194.
18. Sadaba, N.; Larrañaga, A.; Orpella-Aceret, G.; Bettencourt, A.F.; Martin, V.; Biggs, M.; Ribeiro, I.A.C.; Ugartemendia, J.M.; Sarasua, J.R.; Zuza, E. Benefits of polydopamine as particle/matrix interface in polylactide/pd-baso4 scaffolds. *Int. J. Mol. Sci.* **2020**, *21*, 1–15, doi:10.3390/ijms21155480.
19. Grémare, A.; Guduric, V.; Bareille, R.; Heroguez, V.; Latour, S.; L'heureux, N.; Fricain, J.C.; Catros, S.; Le Nihouannen, D. Characterization of printed PLA scaffolds for bone tissue engineering. *J. Biomed. Mater. Res. - Part A* **2018**, *106*, 887–894, doi:10.1002/jbm.a.36289.
20. Drumright, R.E.; Gruber, P.R.; Henton, D.E. Polylactic Acid Technology. *Adv. Mater.* **2000**, *12*, 1841–1846, doi:10.1002/1521-4095(200012)12:23<1841::AID-ADMA1841>3.0.CO;2-E.
21. Sarasua, J.R.; Prud'homme, R.E.; Wisniewski, M.; Le Borgne, A.; Spassky, N. Crystallization and melting behavior of polylactides. *Macromolecules* **1998**, *31*, 3895–3905, doi:10.1021/ma971545p.
22. Hamad, K.; Kaseem, M.; Yang, H.W.; Deri, F.; Ko, Y.G. Properties and medical applications of polylactic acid: A review. *Express Polym. Lett.* **2015**, *9*, 435–455, doi:10.3144/expresspolymlett.2015.42.
23. Tajbakhsh, S.; Hajiali, F. A comprehensive study on the fabrication and

- properties of biocomposites of poly(lactic acid)/ceramics for bone tissue engineering. *Mater. Sci. Eng. C* **2017**, *70*, 897–912, doi:10.1016/J.MSEC.2016.09.008.
24. Singhvi, M.S.; Zinjarde, S.S.; Gokhale, D. V. Polylactic acid: synthesis and biomedical applications. *J. Appl. Microbiol.* 2019, *127*, 1612–1626.
25. Jain, S.; Fuoco, T.; Yassin, M.A.; Mustafa, K.; Finne-Wistrand, A. Printability and Critical Insight into Polymer Properties during Direct-Extrusion Based 3D Printing of Medical Grade Polylactide and Copolyesters. *Biomacromolecules* **2020**, *21*, 388–396, doi:10.1021/acs.biomac.9b01112.
26. Findrik Balogová, A.; Hudák, R.; Tóth, T.; Schnitzer, M.; Feranc, J.; Bakoš, D.; Živčák, J. Determination of geometrical and viscoelastic properties of PLA/PHB samples made by additive manufacturing for urethral substitution. *J. Biotechnol.* **2018**, *284*, 123–130, doi:10.1016/j.jbiotec.2018.08.019.
27. Poh, P.S.P.; Chhaya, M.P.; Wunner, F.M.; De-Juan-Pardo, E.M.; Schilling, A.F.; Schantz, J.-T.; van Griensven, M.; Hutmacher, D.W. Polylactides in additive biomanufacturing. *Adv. Drug Deliv. Rev.* **2016**, *107*, 228–246, doi:10.1016/J.ADDR.2016.07.006.
28. Navarro, J.; Calderon, G.A.; Miller, J.S.; Fisher, J.P. Bioinks for Three-Dimensional Printing in Regenerative Medicine. In *Principles of Regenerative Medicine*; Elsevier, 2019; pp. 805–830.
29. Guo, S.-Z.; Heuzey, M.-C.; Therriault, D. Properties of Polylactide Inks for Solvent-Cast Printing of Three-Dimensional Freeform Microstructures. **2014**, *30*, doi:10.1021/la4036425.
30. He, Y.; Wildman, R.D.; Tuck, C.J.; Christie, S.D.R.; Edmondson, S. An

- Investigation of the Behavior of Solvent based Polycaprolactone ink for Material Jetting. *Sci. Rep.* **2016**, *6*, 1–10, doi:10.1038/srep20852.
31. Bird, R.B.; Armstrong, R.C.; Hassager, O. Dynamics of polymeric liquids. Vol. 1, 2nd Ed. : Fluid mechanics 1987.
32. Yin, J.; Lu, C.; Fu, J.; Huang, Y.; Zheng, Y. Interfacial bonding during multi-material fused deposition modeling (FDM) process due to inter-molecular diffusion. *Mater. Des.* **2018**, *150*, 104–112, doi:10.1016/j.matdes.2018.04.029.
33. D’Amico, A.; Peterson, A.M. An adaptable FEA simulation of material extrusion additive manufacturing heat transfer in 3D. *Addit. Manuf.* **2018**, *21*, 422–430, doi:10.1016/j.addma.2018.02.021.
34. Xia, H.; Lu, J.; Tryggvason, G. Fully resolved numerical simulations of fused deposition modeling. Part II – solidification, residual stresses and modeling of the nozzle. *Rapid Prototyp. J.* **2018**, *24*, 973–987, doi:10.1108/RPJ-11-2017-0233.
35. Seppala, J.E.; Hoon Han, S.; Hillgartner, K.E.; Davis, C.S.; Migler, K.B. Weld formation during material extrusion additive manufacturing. *Soft Matter* **2017**, *13*, 6761–6769, doi:10.1039/c7sm00950j.
36. Barnes, H.A. (2000) A. *Introduction to Polymer Viscoelasticity, 4th Edition | Wiley*;
37. Guo, S.Z.; Heuzey, M.C.; Therriault, D. Properties of polylactide inks for solvent-cast printing of three-dimensional freeform microstructures. *Langmuir* **2014**, *30*, 1142–1150, doi:10.1021/la4036425.
38. Du, Z.; Yu, X.; Han, Y. Inkjet printing of viscoelastic polymer inks. *Chinese Chem. Lett.* **2018**, *29*, 399–404,

- doi:10.1016/j.ccllet.2017.09.031.
39. Guo, S.-Z.; Gosselin, F.; Guerin, N.; Lanouette, A.-M.; Heuzey, M.-C.; Therriault, D. Solvent-Cast Three-Dimensional Printing of Multifunctional Microsystems. *Small* **2013**, *9*, 4118–4122, doi:10.1002/smll.201300975.
40. Davis, C.S.; Hillgartner, K.E.; Han, S.H.; Seppala, J.E. Mechanical strength of welding zones produced by polymer extrusion additive manufacturing. *Addit. Manuf.* **2017**, *16*, 162–166, doi:10.1016/j.addma.2017.06.006.
41. Zuza, E.; Meaurio, E.; Sarasua, J.-R. Biodegradable Polylactide-Based Composites. In *Composites from Renewable and Sustainable Materials*; InTech, 2016.
42. Martínez De Arenaza, I.; Sadaba, N.; Larrañaga, A.; Zuza, E.; Sarasua, J.R. High toughness biodegradable radiopaque composites based on polylactide and barium sulphate. *Eur. Polym. J.* **2015**, *73*, 88–93, doi:10.1016/j.eurpolymj.2015.10.005.
43. ASTM D1938 - 14 Standard Test Method for Tear-Propagation Resistance (Trouser Tear) of Plastic Film and Thin Sheeting by a Single-Tear Method Available online: <https://www.astm.org/DATABASE.CART/HISTORICAL/D1938-14.htm> (accessed on Mar 3, 2021).



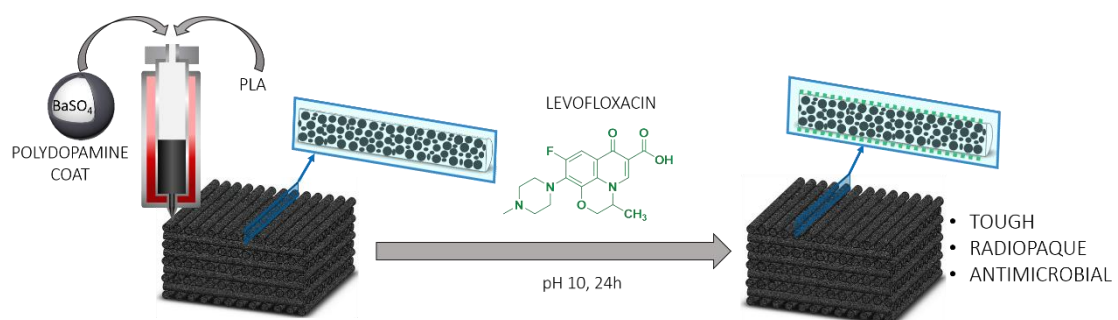


Chapter **3**





## Graphical abstract





---

## CHAPTER 3: RADIOPAQUE MATERIAL FOR 3D PRINTING

This chapter relates the advantages of the addition of inorganic and rigid radiopaque particles in a polylactide (PLA) matrix. After a deep contextualization of the materials used in this chapter, different aspects are described and separated in three parts: firstly, it is revealed the excellent influence in the mechanical properties, in which the presence of undermicron size particles increases impressively the ductility and the toughness of polylactides. Secondly, it is stated the printability of these systems for scaffold designing. Finally, it is demonstrated the viability of these composites as biomedical implants, in which the non-toxicity of the systems and their residues is assessed. Also the use of a new technology based on the capability of polydopamine coating to adsorb/release antimicrobial drugs as levofloxacin pointed out these composites as future trending biomedical devices.

### 3.1. Introduction

Polylactides are biodegradable polymers with great potential for the reconstruction of damaged tissues[1]. Especially in bone reconstruction for using as fixation devices of small size [2], due to their physical-chemical properties, as explained in chapter 1. In short, the drawbacks of PLA to be used in bone reconstruction as opposed to metals (e.g., stainless steels or titanium alloys), are transparency to X-ray and mechanical brittleness [3,4]. However, high mass elements containing fillers can be added to PLA to obtain radiopaque composites and improve its mechanical properties. Barium sulfate ( $\text{BaSO}_4$ ) [5–7], ferrous oxide ( $\text{Fe}_3\text{O}_4$ ) [8] and bismuth oxide ( $\text{Bi}_2\text{O}_3$ ) [9,10] have been previously reported as radiopaque composite

additives, being BaSO<sub>4</sub> currently the most commonly used in medical applications [11].

Inorganic particulate reinforcements can enhance the mechanical properties of polymers and confer additional filler-specific properties to the matrix [12]. It is also well known that the enhancement of mechanical properties directly related to strength (as elastic modulus, yield strength and ultimate strength) is much more noticeable with continuous fiber composites [13].

However continuous fiber formulations do not lend themselves well to free form manufacturing techniques such as extrusion, injection molding or, as it is the case, 3D printing [14–16]. Particularly, 3D printing is progressing very rapidly as an advanced manufacturing technique in the last decade, and research on particulate composites becomes a 'must'. Additionally, there are still challenges to be met in the development of new drug delivery systems for 3D printing. For this purpose in this work it is selected the versatility of dopamine and its polymer. To explore polydopamine properties related to the drug adsorption/desorption of an antibiotic drug (levofloxacin) two different approaches are followed: in chapter 3 polydopamine is used as coating of the particles of barium sulfate and in chapter 4 the dopamine molecule is used as the initiator in the polymerization of the lactide (LA) ring.

Polydopamine (PD) is a newfangled nature inspired adhesive usually used for immobilization of small molecules on materials surfaces as drugs and proteins for biomedical use [17]. In addition, it has been used for improving the thermal stability of composites [18] due to the fact that oxidative particles help in the early degradation of the matrix [8,19]. Accordingly, coating these particles with polydopamine, the matrix is

protected from thermal degradation in the blending and transformation processes [18]. As mentioned before in most cases promoted by its biomimetic adhesivity [20] it has been used in nanocapsules or nanocarriers [21,22]. Nevertheless, the main use of polydopamine is as substrate coating due to its ability and efficiency for conjugation with bioactive molecules as growth factors [23] and drugs [24]. Zhang et al. immobilize bone morphogenic protein 2 (BMP-2) and insulin-like growth factor 1 (IGF-1) on polydopamine coated scaffold, reducing the burst release of the factors and endowing long-term osteoconductivity [23]. Furthermore, titanium nanotubes have been coated with polydopamine to adsorb dexamethasone sodium phosphate, an anti-inflammatory and modulator of osteogenic differentiation, leading to slow, sustained and controlled drug release [24]. However, few publications have reported the use of polydopamine in polymer matrix composites reinforced with inorganic and radiopaque compounds. Almost all the publications referred to composites focus their research on dispersion and biocompatibility, for example, on boron nitride nanotubes [25], bioglass in polylactides [18] and multi-walled carbon nanotubes (MWCNT) in polyurethanes (PU) [26]. Few works have reported changes in mechanical properties of polymer composites due to polydopamine coating of the inorganic phase, one of them is that on polylactide reinforced by polydopamine functionalized halloysite nanotubes [27].

Previously, some efforts have been made to enhance different properties of polylactide implants [28]. Wu et al. improve antibacterial behavior filling polylactide with marine algae [29], while Cai et al incorporate silver-nanoparticles to obtain lower affinity for bacterial adhesion [30]. Other authors report the effect in hydrolytic degradation rate of different fillers as

titanium dioxide, multi-walled carbon nanotubes, surface-treated multi-walled carbon nanotubes, and graphene nanoplatelets [31]. Also, addition of bioactive ceramics as bioactive glass, hydroxyapatite and calcium phosphate has been reported in polylactide matrix composites for bone tissue regeneration [2]. Polylactide electrospinning membranes have been modified with chitosan and polydopamine coatings for improving the osteogenic activity [32]. However, the advantages of the combination of the versatile characteristics of the polydopamine coating on inorganic particles have not been previously published: improvement in mechanical properties, protection of matrix degradation under melt-processing and drug adhesion. In summary, this chapter highlights the versatility of inorganic radiopaque particles when coating them with polydopamine, because of the following reasons:

- Coated particle still remains X-ray visibility and mechanical properties.
- Coated particle protects the possible chemical interactions between particles and matrix.
- Coated particle improves adhesion at the interface matrix-particles, and consequently improves mechanical properties of composites.
- Coated particle favors adhesiveness of biologically active molecules on the surface of the composite.

Although this system is applicable for conventional composite processing techniques, all these characteristics give an expectant step in the way of the new/future bioactive formulations for 3D printable materials.

### 3.2. Radiopaque particles addition: Properties of materials

The sizes of barium sulfate ( $\text{BaSO}_4$ ) particles as well as the barium sulfate particles coated with polydopamine (PD- $\text{BaSO}_4$ ) are shown in **Figure 3.1**. In both cases there is a broad particle size: in the non-modified  $\text{BaSO}_4$  particles size was between 0.5-1.25  $\mu\text{m}$  being the average particle size of 0.75  $\mu\text{m}$ , while in the PD- $\text{BaSO}_4$  the size range from 1.25  $\mu\text{m}$  to 2.25  $\mu\text{m}$  being the average of 1.75  $\mu\text{m}$ . The increase in size of coated particle was due to two reasons: (1) the increment due to the coating itself and, (2) the increment owing to agglomeration during the coating process.

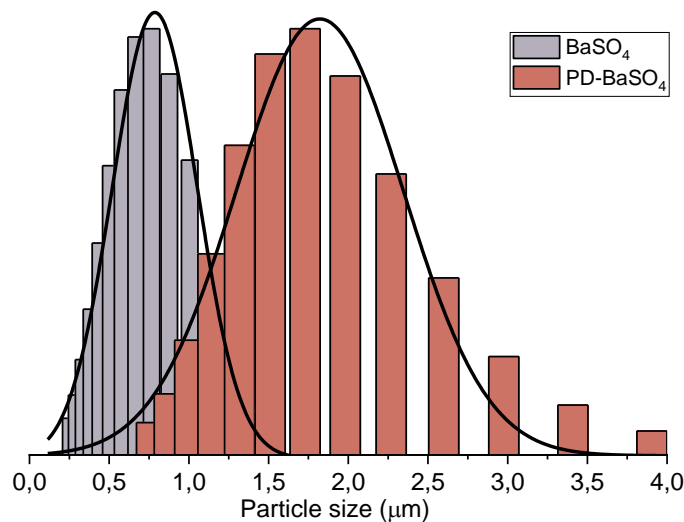


**Figure 3.1.** Particle size of  $\text{BaSO}_4$  (gray) and PD- $\text{BaSO}_4$  (pink). The 0.5, 1, 2, 5 and 10 wt.% of particle dispersion of  $\text{BaSO}_4$  and PD- $\text{BaSO}_4$  inside of the PLA matrix was analyzed by Transmission Electron Microscope (TEM). Although only the composites with 10 wt. % of  $\text{BaSO}_4$  and PD- $\text{BaSO}_4$  of particles composites are shown in the Figure 3.2, all composite have the same behavior. For particles of  $\text{BaSO}_4$  aggregates were not observed (Figure 3.2 a). These images reveal individual particles randomly and homogeneously dispersed as a consequence of the fine dispersion in the PLA matrix. However, for coated particles (PD- $\text{BaSO}_4$ ), there are small aggregates formed during the coating process (see Figure 3.2 b). Despite the small

aggregates in coating particle, the particles were randomly and homogeneously dispersed in the PLA matrix. It is well known that the dispersion of particles in the polymer matrix and interfacial interactions between the polymer matrix and particles are key factors influencing the physical properties of polymer composites.

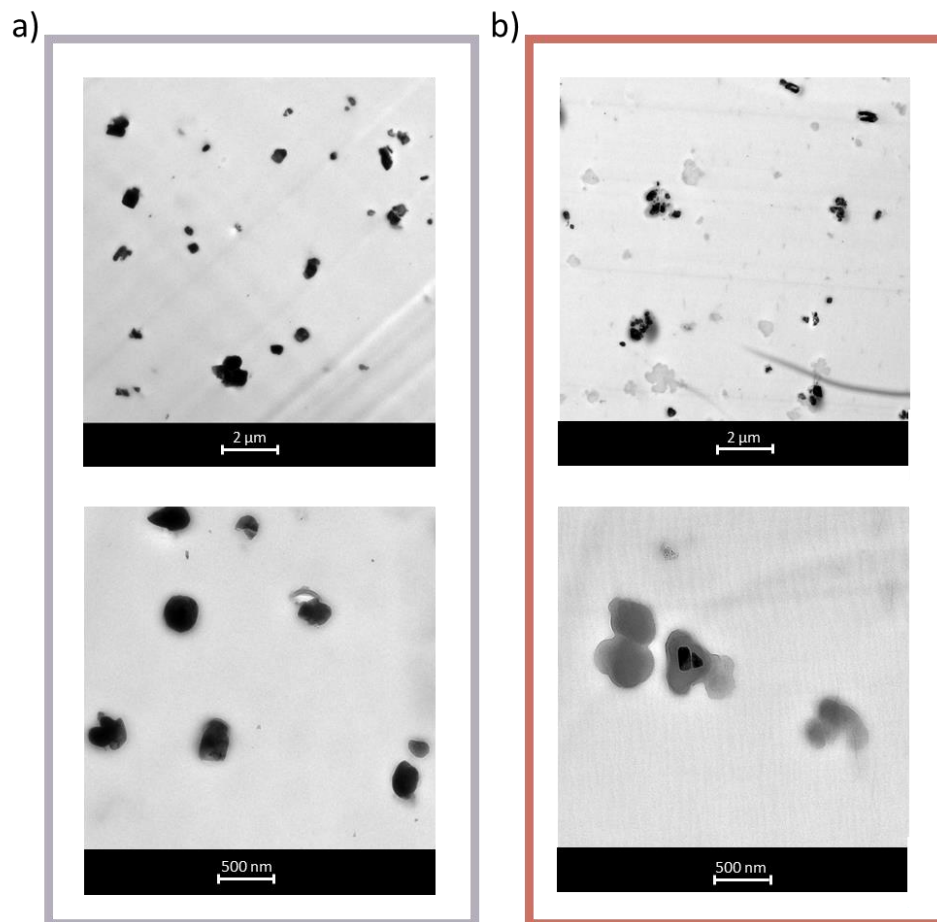


**Figure 3.2.** TEM microscopy images of composites containing 10 wt. % of particles of a) PLA/BaSO<sub>4</sub> and b) PLA/PD-BaSO<sub>4</sub>.



An increase in radiopacity (RO) could be observed when BaSO<sub>4</sub> or PD-BaSO<sub>4</sub> particles were added to the PLA matrix.

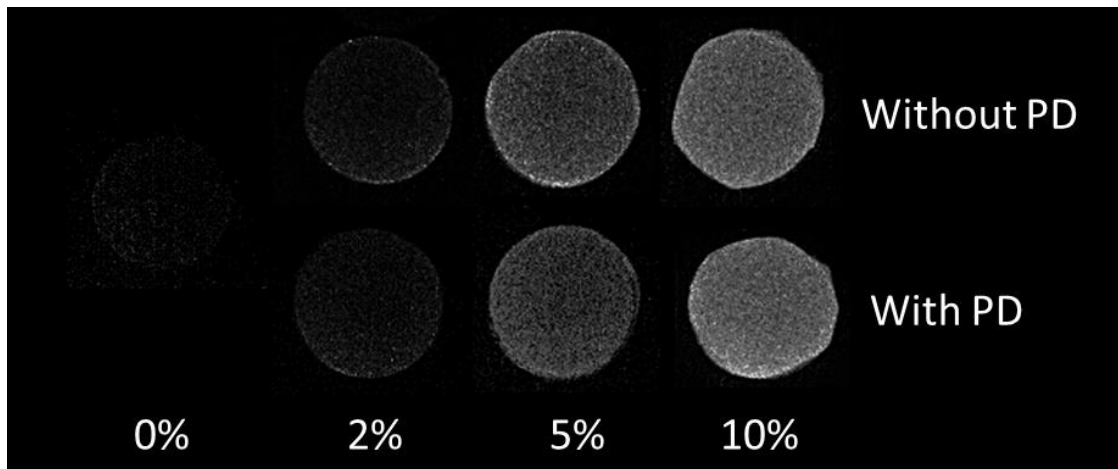
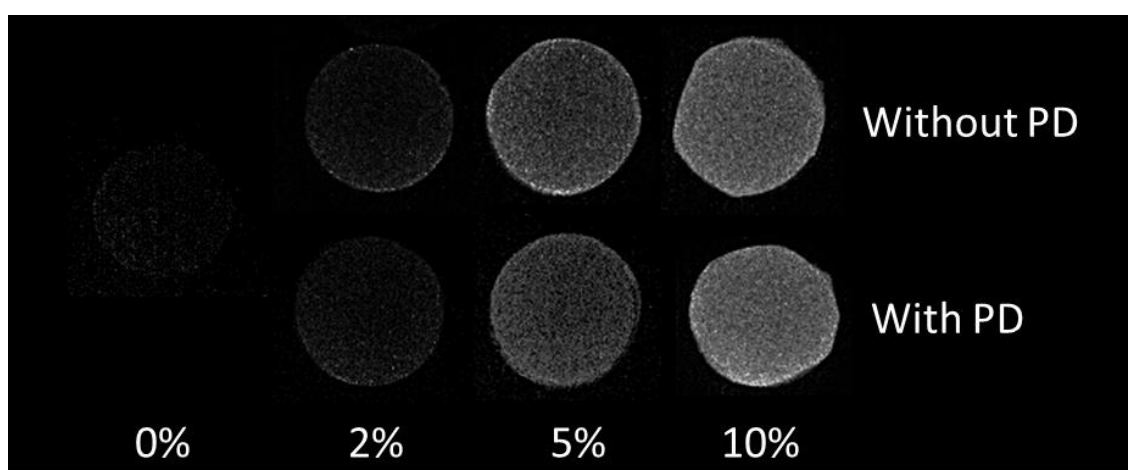


Figure 3.3 shows X-Ray radiographies of neat PLA, PLA/BaSO<sub>4</sub> and PLA/PD-BaSO<sub>4</sub> composite with 2, 5 and 10 wt. % of BaSO<sub>4</sub> and PD-BaSO<sub>4</sub> respectively. The analysis of the images calculated by equation 3.1 (section 3.6.3 Radiopacity). As expected, the percentages that have a greater amount of particles have a greater increase in RO (Table 3.1). In addition, it should be mentioned that both systems show the same radiopacity, therefore the dopamine coating does not affect the radiopacity of the composites.



**Figure 3.3.** X-radiographies neat PLA, PLA/BaSO<sub>4</sub> and PLA/PD-BaSO<sub>4</sub> composites with 2, 5 and 10 wt. % of BaSO<sub>4</sub> and PD-BaSO<sub>4</sub>.

**Table 3.1.** Radiopacity of composite PLA/BaSO<sub>4</sub> and PLA/PD-BaSO<sub>4</sub> for 2, 5 and 10 wt. % of BaSO<sub>4</sub> and PD-BaSO<sub>4</sub> respectively

Particles in wt %	0%	2%	5%	10%
PLA/BaSO <sub>4</sub>	-	3.1	5.2	15.1
PLA/PD-BaSO <sub>4</sub>	-	3.3	5.1	15.0

Thermal properties of neat PLA, PLA/BaSO<sub>4</sub> and PLA/PD-BaSO<sub>4</sub> composites containing 0.5, 1, 2, 5 and 10 wt.% of particles were evaluated by differential scanning calorimetry (DSC). The presence of BaSO<sub>4</sub> or PD-BaSO<sub>4</sub> in the composite did not favor the overall crystallinity of the PLA, whose values stayed practically constant. In particular, neat PLA shows 3.5 % of crystallinity, while composites with 10.0 wt.% of BaSO<sub>4</sub> 7.7 % and composites with 10 wt.% of PD-BaSO<sub>4</sub> 7.8%. After the processing composites were air-cooled and as the cooling rate was relatively fast, composites were practically in amorphous state with some imperfect crystals [33,34].

Analyzing thermal degradation of the materials, it could be concluded that the particles do not accelerate the thermal degradation of the material, whose values stayed practically constant. Specifically, the onset of thermal degradation temperature ( $t_d$ ) of neat PLA starts at 200 °C, while for composites with uncoted and coated BaSO<sub>4</sub> starts at 210 °C and 220 °C, respectively.

The tensile stress–strain curves and mechanical properties of neat polylactide and its composites (PLA/BaSO<sub>4</sub> and PLA/PD-BaSO<sub>4</sub>) were determined by tensile testing. Neat PLA does not reach a yield point and shows a typical brittle behavior, exhibiting around 9% of elongation before failure and 67 MPa of tensile strength. In contrast, both composites showed a clear yield point and an extended ductile behavior with a high increase in

elongation at break, this being accompanied with a moderate increase in the elastic modulus.

Other studies previously explained the great increase in the ductility with the addition of particles. Harrats et al. reported an increase in impact resistance upon addition of rigid particles [35]. Under uniaxial stress the rigid particles act as stress concentrators and are debonded from the matrix (Figure 3.4) [36]. The debonded particles leave voids in the matrix and activate shear yielding of the polymer. Moreover, when particles present a suitable size and good adhesion with the matrix, an increase in the elastic modulus and elongation is achieved. This works report the improvement of both stiffness and fracture toughness related to particle size between 0.7–1.9  $\mu\text{m}$  [37,38].

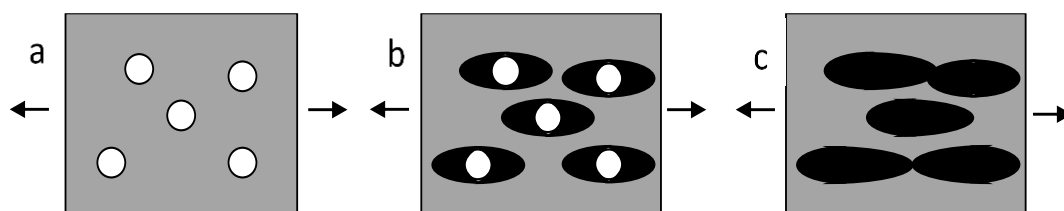


**Figure 3.4.** Stress concentrations in rigid particles (a) induce debonding (b) and shear yielding (c) mechanism.

Table 3.2 and Table 3.3 summarize the mechanical properties measured by tensile test of neat PLA and its composites PLA/BaSO<sub>4</sub> and PLA/PD-BaSO<sub>4</sub>. These values are plotted and compared in Figure 3.5. Although there is not a big difference between the mechanical properties (elastic modulus, tensile strength, ductility and toughness) of both composite systems, there is a remarkable increase comparing them with neat PLA.

For instance, by incorporating 5 and 10 wt.% of particles to neat PLA the tensile modulus increase by 20 % and 15%, whereas the tensile strength decrease by around 15% and 19 %, respectively. Similarly, when 2 and 10 wt.% of the coated particles are incorporated the tensile modulus increase

by 14% and 9%, whereas the tensile strength decrease by 7 % and 18%, respectively.

The most significant increase is observed in the values of the elongation at break ( $\epsilon_r$ ), and consequently in the toughness (TT).  $\epsilon_r$  reaches its maximum value when incorporating 5% wt. of BaSO<sub>4</sub> and 2% wt. of PD-BaSO<sub>4</sub> particles, recording an increase by 1416% and 1887%, respectively. The maximum was achieved sooner for the coated particles due to their bigger size which makes them to agglomerate more easily and reach breakage before.

As mentioned before, although there is not a big difference between coated and uncoated composites, it is relevant the difference between both systems in values of elongation and strength, and consequently, in tensile toughness. Composites reinforced with coated particles show higher values than with uncoated ones.

**Table 3.2.** Mechanical properties of neat PLA and PLA/BaSO<sub>4</sub> composites with respect to wt. % of BaSO<sub>4</sub>. E: tensile modulus,  $\sigma_y$ : tensile yield,  $\sigma_r$ : tensile strength,  $\epsilon_r$ : elongation at break and TT: tensile toughness.

BaSO <sub>4</sub> (%)	E (MPa)	$\sigma_y$ (MPa)	$\sigma_r$ (MPa)	$\epsilon_r$ (%)	TT (J/m <sup>3</sup> )
0	1243 ± 96	-	67.10 ± 0,5	9.17 ± 0,5	3.84 ± 0.6
0.5	1322±118	67.7±1.8	44.9±11	100.5±9.7	45.2±7.8
1	1373±163	67.6±3.1	51.7±4.8	114.8±6.0	52.0±2.6
2	1420±72	62.8±3.5	55.7±3.5	129.3±5.4	58.8±5.5
5	1498±105	68.8±2.2	56.8±4.6	139.0±9.6	67.6±6.6
10	1426±137	67.6±0.6	54.5±3.5	134.1±6.5	62.9±4.6

**Table 3.3.** Mechanical properties of neat PLA and PLA/PD-BaSO<sub>4</sub> composites with respect to wt. % of PD-BaSO<sub>4</sub> E: tensile modulus,  $\sigma_y$ : tensile yield,  $\sigma_r$ : tensile strength,  $\epsilon_r$ : elongation at break and TT: tensile toughness.

PD-BaSO <sub>4</sub> (%)	E (MPa)	$\sigma_y$ (MPa)	$\sigma_r$ (MPa)	$\epsilon_r$ (%)	TT (J/m <sup>3</sup> )
0	1243 ± 96	-	67.10 ± 0.5	9.17 ± 0.5	3.84 ± 0.6
0,5	1309 ± 51	78.7 ± 0.4	56.33 ± 5.4	132.19 ± 13.1	67.49 ± 6.1

1	1396 ± 109	77.7 ± 0.8	56.03 ± 4.8	146.26 ± 9.8	73.55 ± 4.6
2	1415 ± 86	78.4 ± 1.7	62.48 ± 5.2	182.18 ± 5.9	95.10 ± 1.7
5	1417 ± 49	75.7 ± 0.6	57.58 ± 5.8	171.87 ± 2.9	85.95 ± 0.8
10	1350 ± 124	74.1 ± 0.8	55.25 ± 4.3	154.56 ± 8.6	76.20 ± 2.8

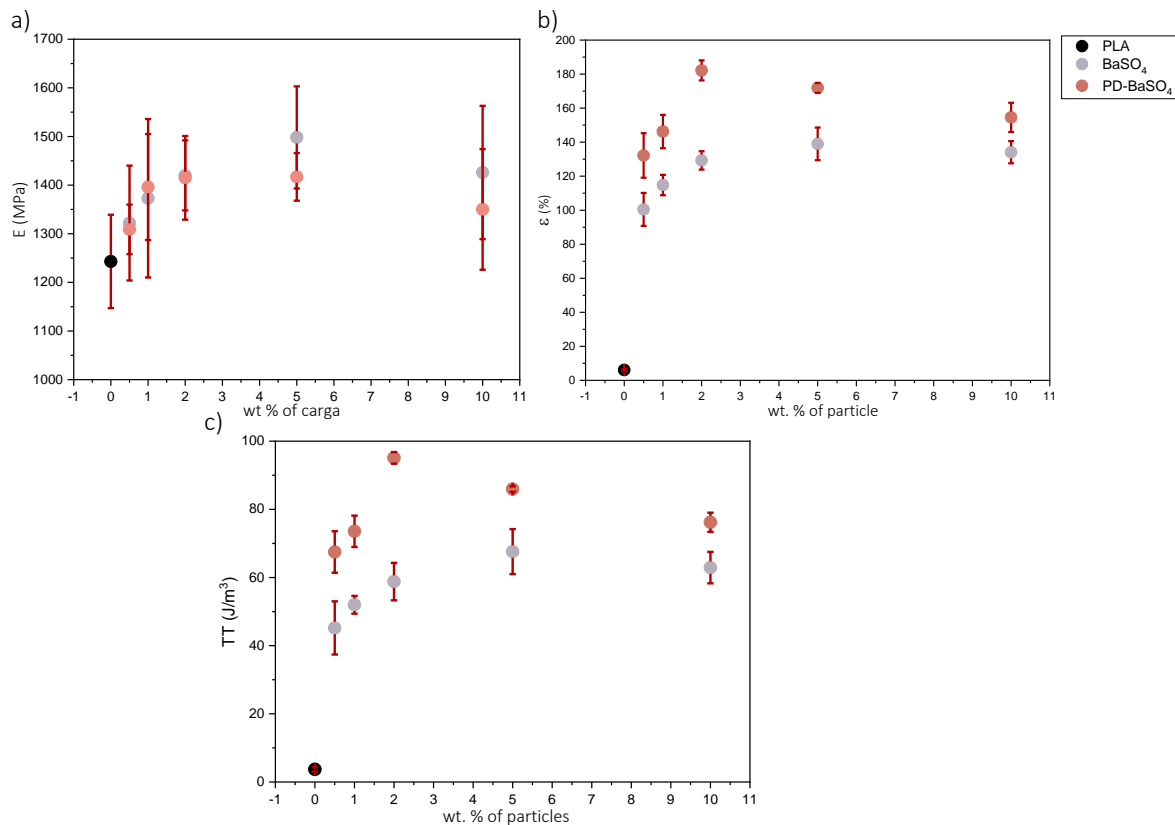


**Figure 3.5.** Values obtained from tensile stress-strain behavior of neat PLA, PLA/BaSO<sub>4</sub> and PLA/PD-BaSO<sub>4</sub> composites with 0.5, 1.0, 2.0, 5.0 and 10.0 wt. % of particles. a) Tensile modulus b) elongation at break and c) tensile toughness.

For further studies composites having 10 wt.% of BaSO<sub>4</sub> and PD-BaSO<sub>4</sub> particles were analyzed. It was concluded that among all compositions these composites present the optimal properties of radiopacity and high toughness.

Tensile toughness was measured as the area under the stress-strain curves for fracture and corresponds to the work required per unit volume. For composites having 10 wt.% of BaSO<sub>4</sub> and PD-BaSO<sub>4</sub> the tensile toughness increased by 1538% and 1884%, respectively. These results are explained by

a slight increase in strength and dramatic improvement in ductility. As shown in Figure 3.6 composites showed stress whitening (Figure 3.6 red arrow) and necking (Figure 3.6 red circle) immediately after the yield point, indicating the formation of crazes and/or voids. Crazing and shear yielding proceed simultaneously during the stretching of the composites and both contribute to the large elongation before failure of the composites [39].

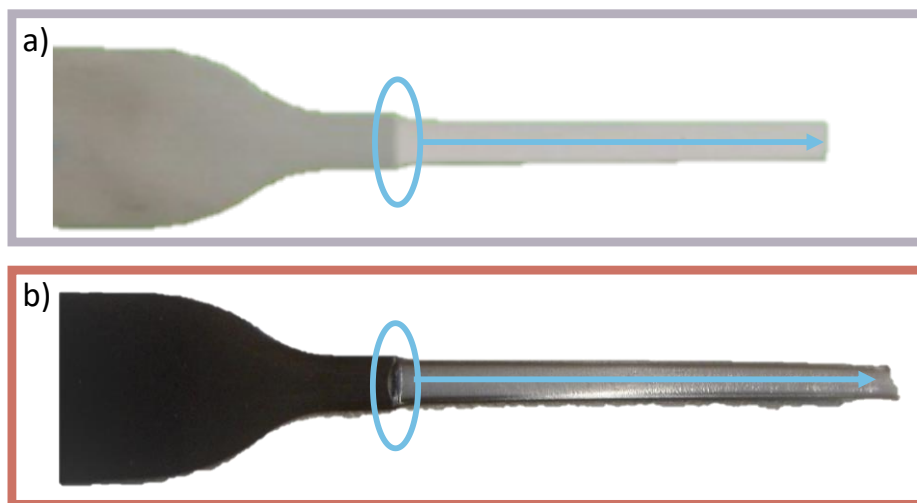


**Figure 3.6.** Tensile test specimen after a tensile test, (a) PLA/BaSO<sub>4</sub> 10 wt. % of BaSO<sub>4</sub> and (b) PLA/PD-BaSO<sub>4</sub> 10 wt. % of PD-BaSO<sub>4</sub>. Blue arrows represent stress whitening and blue circles the necking.

The tensile test specimens were tested and once broken, they were cryogenically cut longitudinally in the stress whitening zone and this section was observed by scanning electron microscope (SEM). In Figure 3.7 SEM images show a good dispersion of the BaSO<sub>4</sub> particles and the numerous voids that those particles created along the matrix (pointed with blue circle in Figure 3.7). Based on SEM observations debonding and crack deflection between the matrix and BaSO<sub>4</sub> particles were proposed as the toughening mechanism attributed to PLA/BaSO<sub>4</sub> composites.

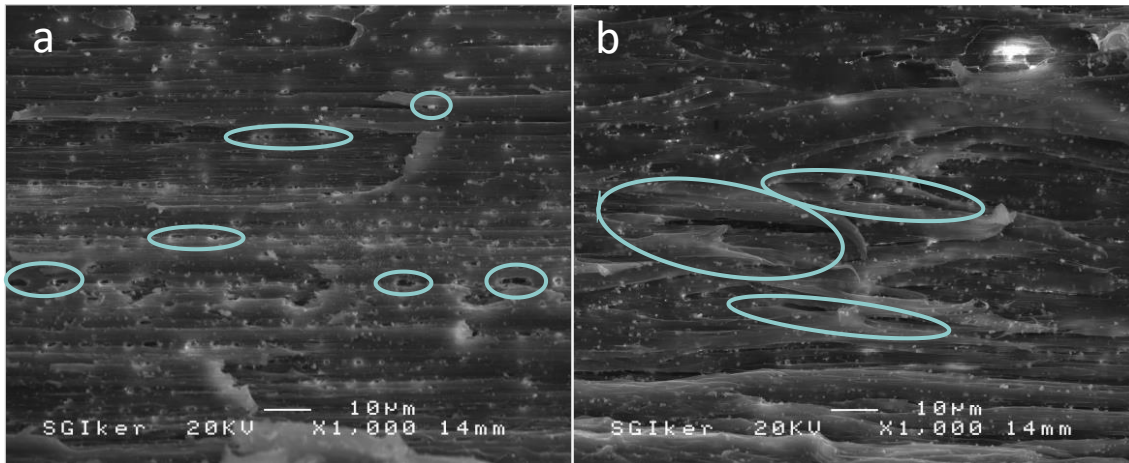


**Figure 3.7.** SEM images of PLA/BaSO<sub>4</sub> composites with (a) 5 and (b) 10 wt.% of BaSO<sub>4</sub>. blue circle pointed voids created by particles.

Moreover, previous researchers explained the relevance of the size of the fillers and the good dispersion along the matrix as the reason for the high deformation values obtained [40,41]. Thio et al. reported an increase in toughness attributed to the previously explained mechanism when CaCO<sub>3</sub> particles of 0.7 μm were added in isotactic polypropylene. However, when particle sizes were smaller (0.07 μm) or larger (3.5 μm) only an increase in the modulus was observed [42]. Zuiderduin et al. studied the effect of CaCO<sub>3</sub> particle size and the surface treatment of the particles on toughening properties [37]. They found that the stearic acid treated CaCO<sub>3</sub> particles of 0.7 μm showed the best properties.

In our work, a dramatic improvement in PLA toughness was observed incorporating BaSO<sub>4</sub> particles with particle size of 0.75-1 μm. When large aggregates with critical size were presented in the matrix, the voids created by debonding were not stable and grew to a size where crack initiation occurs. The creation of a stable free volume at the particle size level leads to high energy adsorption by shear yielding and consequently to high toughness. In the case of the PLA/PD-BaSO<sub>4</sub> composite, the same increase in deformation capacity is observed again as in the PLA/BaSO<sub>4</sub> [3,5].

In order to prove the existence of voids, SEM images of the stress whitening zone were taken. Figure 3.8 shows the fracture surface of composite with 10 wt.% of coated barium sulfate particles. High deformation capability showing threads that are thinner than a micrometer can be observed, typical of a ductile fracture. In any case, particles are observed along these thin threads (red and dot-line arrows). Moreover, some threads seem to be anchored and stretched between radiopaque particles (white and straight arrows). This behavior is characteristic of composites presenting good adhesion, in our case, attributed to the interactions that are established between ester groups of polylactide with alcohol groups of polydopamine [20,43]. In view of the results, radiopaque particles act as fixed points that under external stress help the matrix to be deformed.

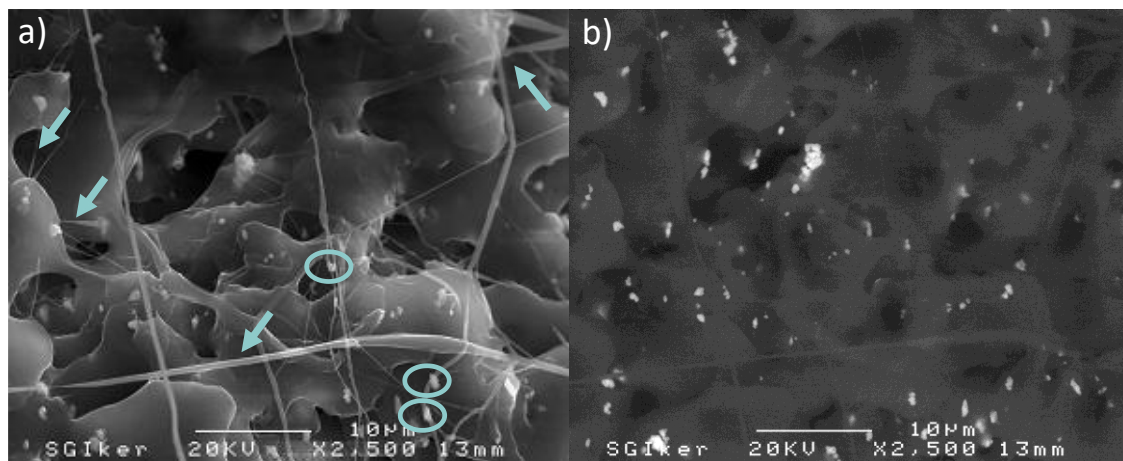


**Figure 3.8.** SEM image of PLA/PD-BaSO<sub>4</sub> composite 10 wt.% of PD-BaSO<sub>4</sub> taken with dispersion of (left) secondary electrons and (right) backscattered electrons. Blue arrows pointed anchored and stretched threads between particles and blue circle particles in threads.

In this sense, particles could act as discontinuities in polymer matrix and therefore they can be considered as voids or defects present within the polymer structure when the material is subjected under tensile conditions [44]. When a particle is subjected to mechanical stress, elongation of voids occurs in the stress direction and elliptical holes and a fibrillated matrix is



developed. Therefore, mechanism initiated by debonding of particles continues with craze formation and finally resulting in high deformation values.

For a better understanding of this peculiar composite system, tests of fracture toughness has been conducted with uncoated particles. As fracture toughness reflects, the improvement in toughness is due to the energy absorbed by the material during the cracking process ahead and behind the crack tip (see Figure 3.9). Accordingly, particular attention must be placed in the submicron size and round shape of the fillers. These well dispersed submicron voids favor the activation of intrinsic and extrinsic mechanisms. The main success of this work is that high deformation of a brittle matrix is achieved without the need of incorporating a rubber phase.

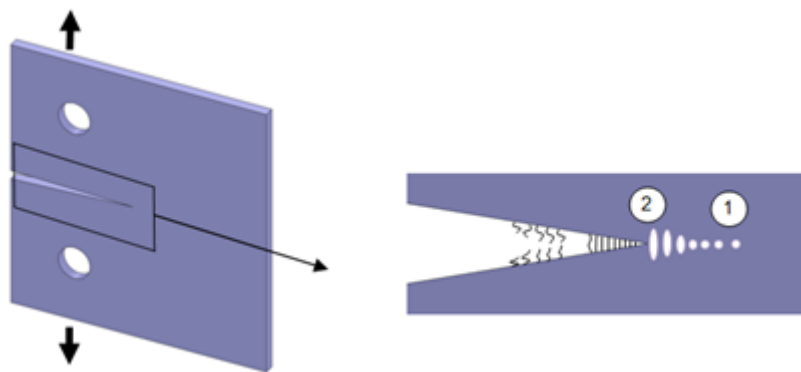


**Figure 3.9.** Schematic representation of the steps involved in crazing process. 1) earlier stage: debonding and cavitation of the voids; 2) advanced stage: deformed voids initiate craze formation.

The presence of submicron particles of  $\text{BaSO}_4$  increased the dissipated energy in the plastic deformation of the polymer matrix and induces the crack to propagate as fibrillated crazes, resulting in a five-fold increase of the energy required to fracture the composite with respect to the neat PLA (see Figure 3.10). More specifically the force to initiate crack propagation ( $F_{\text{max}}$ ) is about 25% greater in PLA/ $\text{BaSO}_4$  compared to neat PLA. Since the

nonlinear regions of the sample are large no estimation of fracture toughness is given. Instead, a work of fracture (WOF) was calculated by dividing the area under the force-displacement curve by the cross section of the ligament of material ahead of the notch (cracked material). Therefore, the work of fracture measures the energy necessary to propagate the crack and, also, the energy necessary to break the material. The WOF of PLA/BaSO<sub>4</sub> is five times higher than the WOF. of neat PLA, which is a remarkable improvement by any standard.

It is hypothesized that this improvement of toughness is due to the energy absorbed by the material ahead and behind the crack tip. In addition to the usual plastic deformation of PLA matrix, PLA/BaSO<sub>4</sub> composite can deform from the debonding of the particle and growth of the cavities; a micro-mechanism which is similar to epoxies toughening with rubber particles [45], but in this case with the presence of rigid particles.

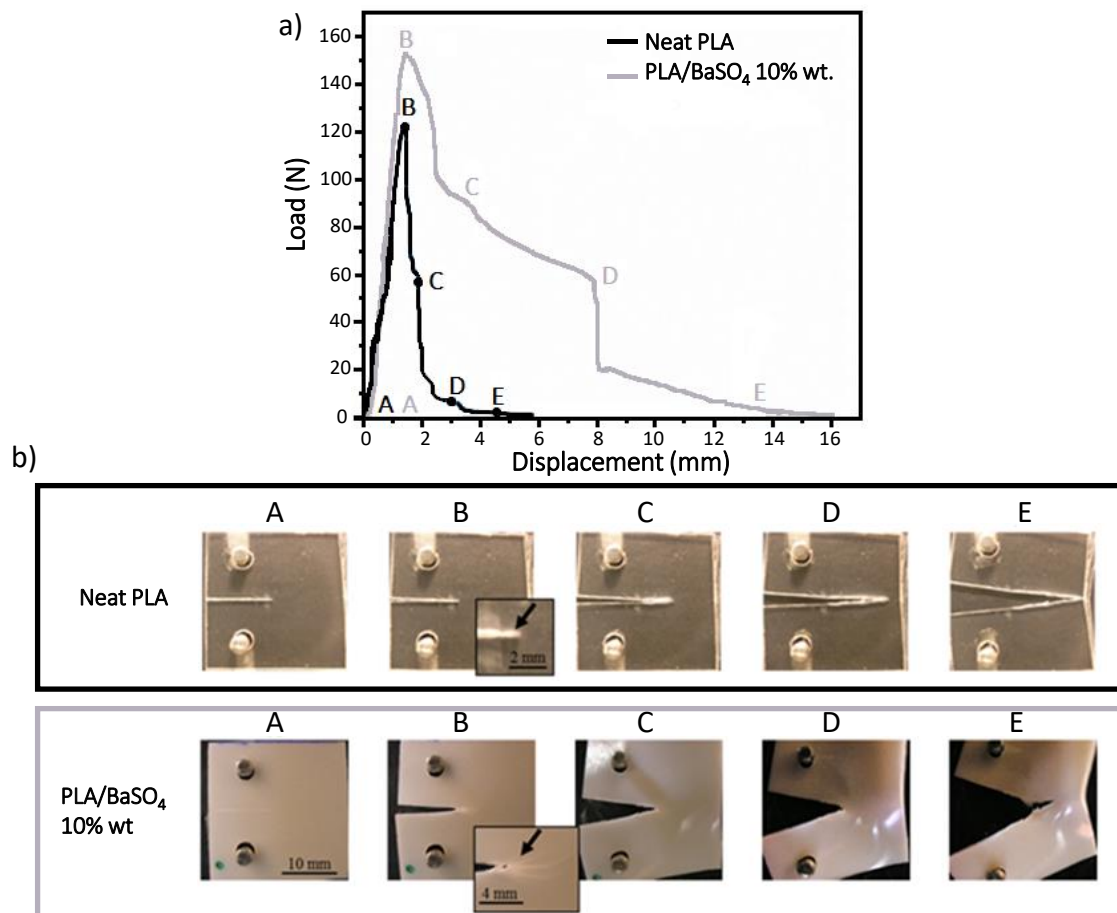


**Figure 3.10.** (a) Fracture tests of neat PLA and 10 wt.% PLA/BaSO<sub>4</sub>. The force-displacement curves at different stages (A, B, C, D, E) and their corresponding (b) images. Inset in image B points the presence or not of fibrils.

In this section, the mechanical characterization of composites were presented. The obtained results shed light on these composites being use as scaffolds for tissue engineering applications. Therefore, in the next section the 3D- printability of these materials and the cytotoxicity will be analyzed.

### 3.3. 3D printing of radiopaque materials

Fused deposition modeling (FDM) technique which is based on extrusion printing is proved to be used in tissue engineering, for bone reconstruction [6] or to improve antimicrobial properties [46], or even for orthopedic use [47].

Due to the feeding mode of the printer and the degradable nature of the polymer, scaffolds are solution printed (as justified in chapter 2). Neat PLA, PLA/BaSO<sub>4</sub> 10 wt.% of BaSO<sub>4</sub>, and PLA/PD-BaSO<sub>4</sub> 10 wt.% of PD-BaSO<sub>4</sub> were dissolved in chloroform during 48 h and printed at 20 °C. The printing conditions are shown in **Table 3.4**. Reproducibility of the PLA, PLA/BaSO<sub>4</sub>, and PLA/PD-BaSO<sub>4</sub> support frames was ensured by using the same CAD model, and by the high XYZ axis resolution of the Bioplotter (0.001 mm)

**Table 3.4.** Printed condition for the neat PLA and composites PLA/BaSO<sub>4</sub> 10 wt.% of BaSO<sub>4</sub> and PLA/PD-BaSO<sub>4</sub> 10 wt.% of PD-BaSO<sub>4</sub>

MATERIAL	TEMPERATURE (°C)	PRESSURE (ATM)	SPEED (MM/s)	POST-FLOW (s)	PRE-FLOW (s)
PLA	25	5	3.5	0.11	0.04
PLA/BaSO <sub>4</sub>	25	5	4.8	0.03	-0.02
PLA/PD-BaSO <sub>4</sub>	25	4.4	4.1	0.11	0.01

The scaffolds were design in order to filaments have 0.25 mm. For that purpose a needle having 0.25mm of diameter was employed. The geometry design of the scaffolds was cylindrical with an internal geometry of 90° (printed layer oriented perpendicular) and with a pore size of 500 µm. The dimensional stability of the scaffold was checked by using an optical microscope. Positive results were obtained (see Figure 3.11).

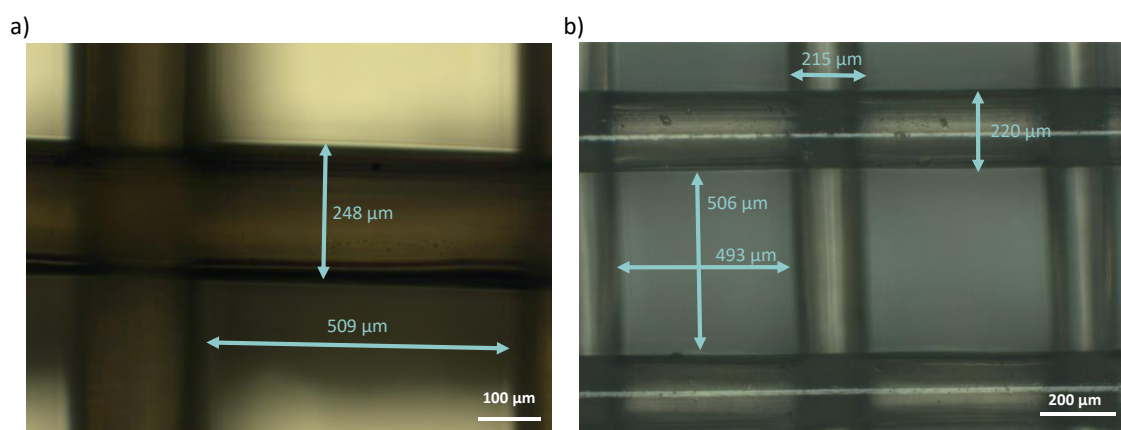


**Figure 3.11.** Images of optical microscopy of PLA scaffolds showing filament and gap dimensions.

Once the scaffolds were fabricated the mechanical properties were analyzed. In this case, mechanical properties were measured in compression to mimic the working conditions of the device. Non-reinforced polylactide (as reference) and the 10 wt. % PLA/PD-BaSO<sub>4</sub> scaffolds with 55% of porosity were tested.

Figure 3.12 shows the stress–strain curves under compression of neat PLA scaffolds and those of its 10 wt. % PLA/PD-BaSO<sub>4</sub> composite counterpart. As can be observed the 3D printed PLA and PLA/PD-BaSO<sub>4</sub> scaffolds do show different regimes and each regime corresponds to a specific mechanism of a porous structured material, in agreement with bibliography. In the first stage (region I), the walls contribute to the resistance of the scaffolds under compressive load, which results in an elastic response region at initial loads and corresponding strains. In the second stage (II), the pores collapse by buckling of the walls (barreling effect). The third stage (III) is featured by a large increase in stress over strain which may be explained by the fact that scaffolds are now compressed to a size that the scaffold becomes denser and furthermore more strain resistant to the applied load [48–50].

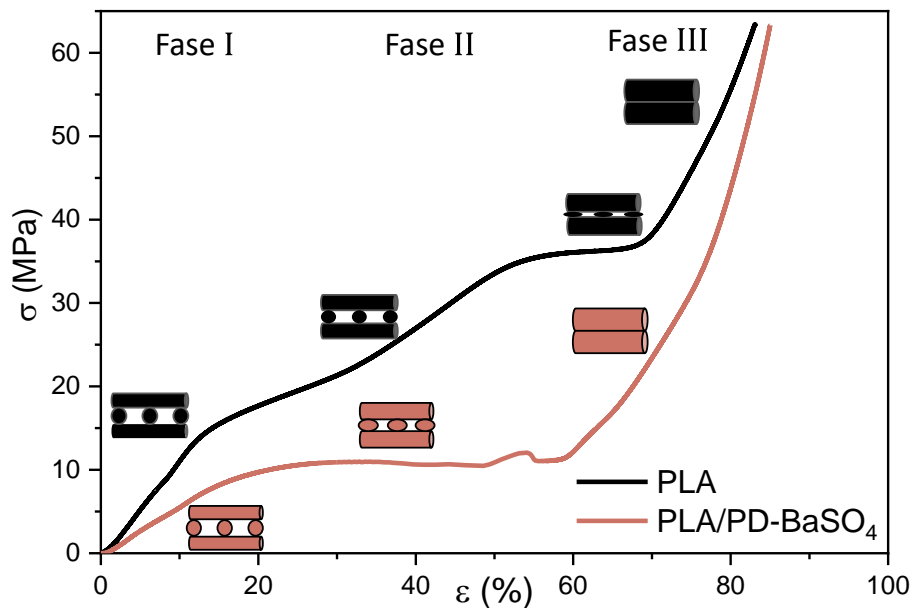


**Figure 3.12.** Compression stress ( $\sigma$ )–strain ( $\epsilon$ ) curves of scaffolds for neat polylactide (PLA) and composite of polylactide with coated polydopamine barium sulfate particles (PLA/PD-BaSO<sub>4</sub>) 10 wt. %.

Despite the fact that both scaffolds have the same porosity (55%), in Figure 3.12 the neat PLA behaved like a more rigid structure [51], while PLA/PD-BaSO<sub>4</sub> shows again a flexible and more ductile behavior. Therefore, it can be concluded that the particles confer flexibility to the scaffolds also in compression tests.

### 3.4. Viability of radiopaque materials for biomedical applications

In this section our materials are demonstrated to be non-cytotoxic based on metabolic activity and proliferation results. Therefore, they might be valid substrates for cells attachment and proliferation. In addition, the levofloxacin adsorption/release ability of polydopamine coated particles reveal these polymeric systems as a smart material for using in biomedical implants.

#### 3.4.1. Cytotoxicity and metabolic activity of particles

In vitro compatibility studies were performed to determine the possible toxicity of BaSO<sub>4</sub> and PD-BaSO<sub>4</sub> particles and their resulting PLA composites

using Human dermal fibroblasts (HDFs) as a basic toxicity test Figure 3.13 shows the metabolic activity of Human dermal fibroblasts (HDFs) in the presence of 10, 50, 100 or 500  $\mu\text{g}/\text{mL}$  of  $\text{BaSO}_4$  or PD- $\text{BaSO}_4$  particles. The metabolic activity displayed in this figure was normalized at each time-point with respect to the metabolic activity of HDFs seeded in the absence of particles, which was used as a control. The presence of  $\text{BaSO}_4$  and PD- $\text{BaSO}_4$  particles slightly reduced the metabolic activity of HDFs with respect to the control. However, in all the cases, the metabolic activity was higher than 80 %, demonstrating that HDFs were able to maintain a normal metabolic activity in the presence of particles. At day 1, the metabolic activity of HDFs seeded with 10, 50, 100 and 500  $\mu\text{g}/\text{mL}$  of  $\text{BaSO}_4$  particles was 95, 94, 90 and 90 %, respectively, relative to that of the control. In the case of HDFs seeded with 10, 50, 100 and 500  $\mu\text{g}/\text{mL}$  of PD- $\text{BaSO}_4$  particles, the metabolic activity was 89, 86, 89 and 83 % that of the control, respectively. At day 3, the metabolic activity of those cells seeded with 10 or 50  $\mu\text{g}/\text{mL}$  of  $\text{BaSO}_4$  particles, as well as 10  $\mu\text{g}/\text{mL}$  of PD- $\text{BaSO}_4$  particles was not significantly different from the metabolic activity of the control. At this day, the metabolic activity in all the cases was higher than 90 %, suggesting a negligible effect of the particles in the metabolic activity of HDFs.

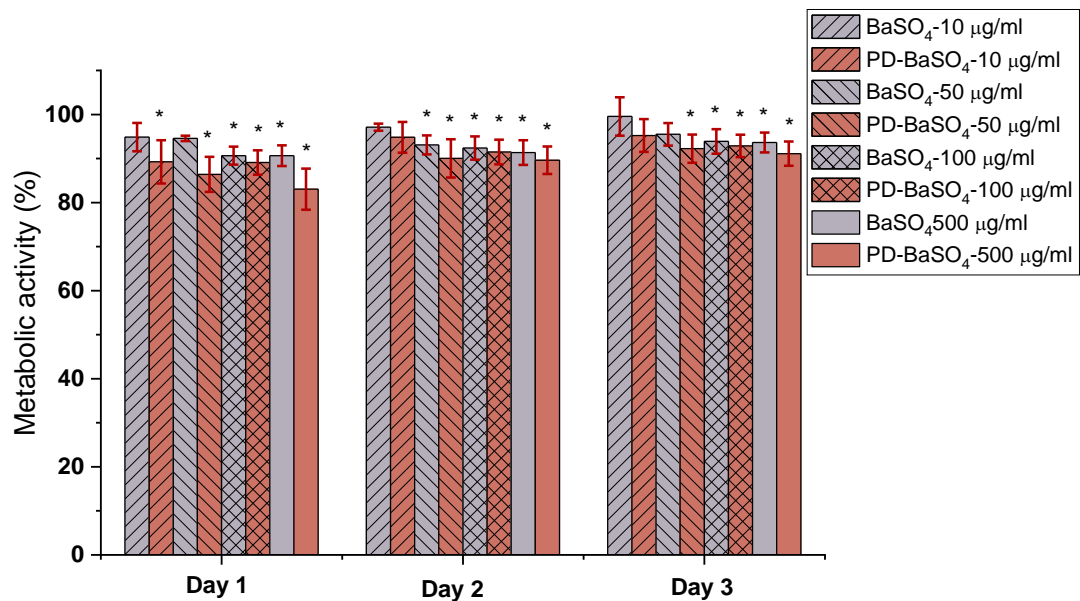


**Figure 3.13.** Metabolic activity of Human dermal fibroblasts (HDFs) seeded in the presence of 10, 50, 100 or 500  $\mu\text{g}/\text{mL}$  of barium sulfate particles ( $\text{BaSO}_4$ ) or barium sulfate particles coated with polydopamine (PD- $\text{BaSO}_4$ ). Asterisks indicate significant differences ( $p < 0.05$ ) with respect to the control.

Additionally, cells observed under an inverted microscope showed normal morphology and the  $\text{BaSO}_4$  and PD- $\text{BaSO}_4$  particles seemed to be internalized by cells and located around the nuclei see Figure 3.14.

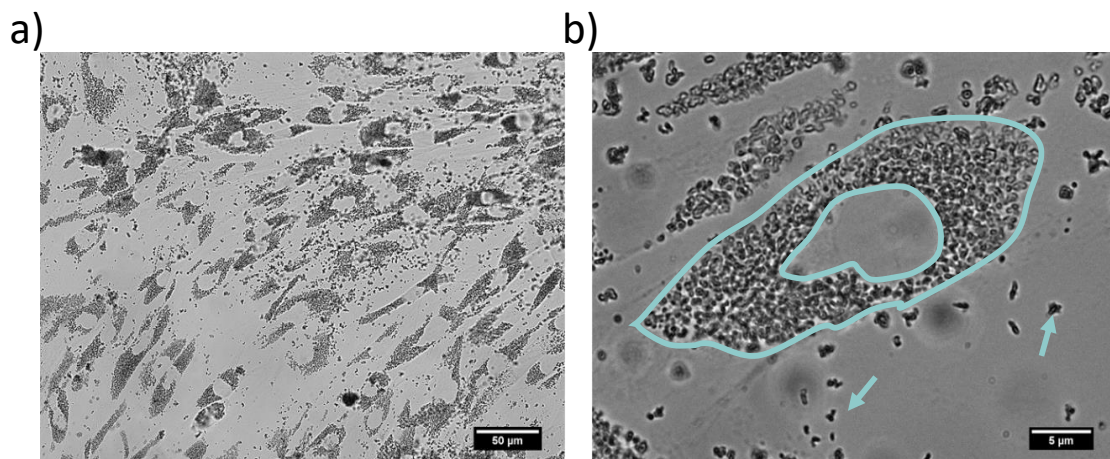


**Figure 3.14.** HDFs seeded in the presence of 500  $\mu\text{g}/\text{mL}$  of  $\text{BaSO}_4$  showing normal morphology and suggesting the internalization of the particles. Particles inside of HDF (blue circle) and outside of HDF (blue arrow)

### 3.4.2. Cytotoxicity and metabolic activity of composites

Figure 3.15 shows metabolic activity of cells seeded in PLA, PLA/ $\text{BaSO}_4$ , PLA/PD- $\text{BaSO}_4$  composites with 10 wt.% of filler and control tissue culture



plastic (TCP). The metabolic activity was normalized at each time-point with the metabolic activity of HDFs seeded onto the TCP, which was used as a control. Except for cells seeded on PLA after 3 days of culture no significant differences were observed in the metabolic activity of HDFs with respect to the control, indicating normal metabolic activity of cells seeded on the composites developed in this work.

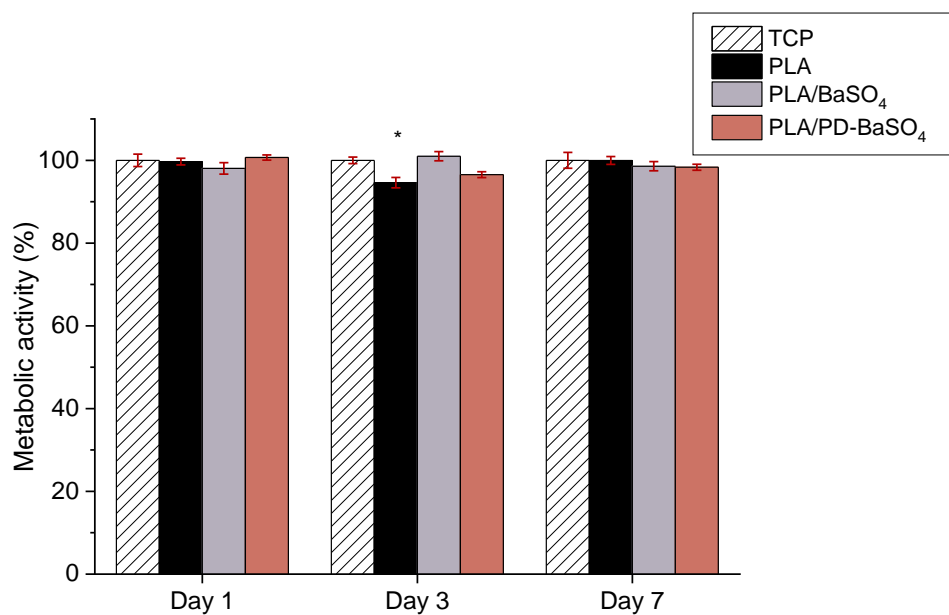


**Figure 3.15.** Metabolic activity of Human dermal fibroblasts (HDFs) seeded on polylactide (PLA), composite of polylactide and barium sulfate particles (PLA/BaSO<sub>4</sub>) and composite of polylactide and coated with polydopamine barium sulfate particles (PLA/PD-BaSO<sub>4</sub>) with respect to the control at day 1, 3 and 7. Asterisks indicate significant differences ( $p < 0.05$ ) with respect to the cells seeded on tissue culture plastic (TCP).

The proliferation of HDFs on PLA, PLA/BaSO<sub>4</sub> and PLA/PD-BaSO<sub>4</sub> composites was evaluated via DNA quantification. As can be seen in Figure 3.16, DNA content increased over culture time in all experimental and control conditions. Accordingly, significant differences were observed between DNA content observed at day 7 and that observed at day 1 for all the samples studied. For example, the calculated proliferation rates between day 1 and day 7 were 1.6, 3.2 and 2.4 for PLA, PLA/BaSO<sub>4</sub> and PLA/PD-BaSO<sub>4</sub>, respectively. The metabolic activity and proliferation results demonstrate

that the materials employed in this work are not cytotoxic and can provide a cytocompatibility substrate for cells to attach and proliferate. A higher proliferation of HDFs was observed in PLA/BaSO<sub>4</sub> or PLA/PD-BaSO<sub>4</sub> composites with respect to pristine PLA samples. Accordingly with literature, it is hypothesized that this higher proliferation rate may be associated to surface characteristic of the samples, such as roughness or hydrophilicity [52,53].

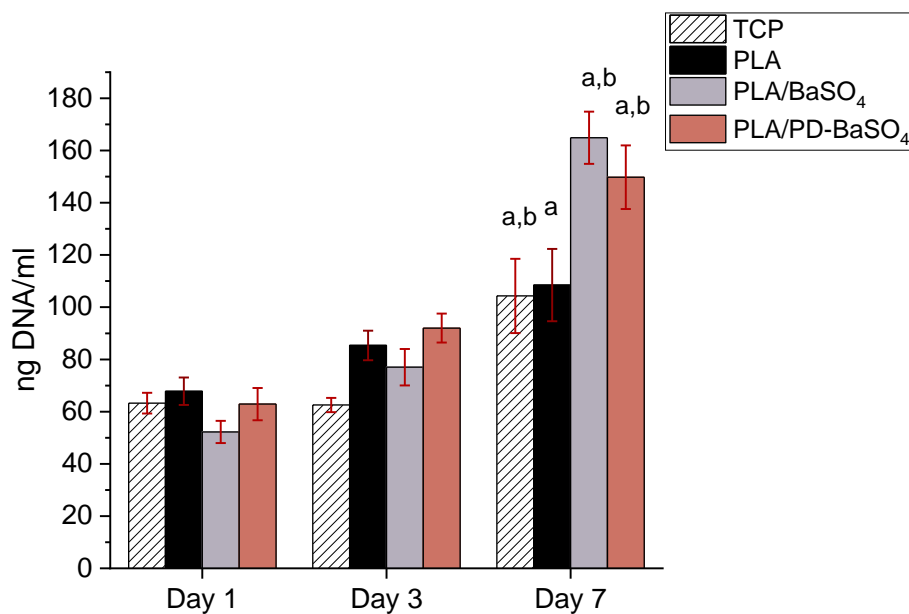


**Figure 3.16.** Proliferation of Human dermal fibroblasts HDFs seeded polylactide (PLA), composite of polylactide and barium sulfate particles (PLA/BaSO<sub>4</sub>) and composite of polylactide and coated with polydopamine barium sulfate particles (PLA/PD-BaSO<sub>4</sub>) a and b indicate significant differences ( $p < 0.05$ ) with respect to day 1 and day 3, respectively.

Moreover, polydopamine coated particles could act as binding site for biologically active molecules such as proteins or drugs increasing widely the use of this composite as internal devices for biomedical applications.

### 3.4.3. Adsorption/release of levofloxacin *in vitro*

Once the cytocompatibility was assessed, the potential for antibiotic delivery with 3D printed scaffolds of PLA/PD-BaSO<sub>4</sub> was evaluated *in vitro*, with the aim of preventing an infection due to the insertion surgery (open wound)

and the consequent rejection of the device [54]. To this end, levofloxacin was incorporated into the material via PD-BaSO<sub>4</sub> particle functionalization as a local drug delivery system for avoiding the oral administration common in this kind of surgeries. Levofloxacin is used for fighting and preventing osteomyelitis, since it is a fluoroquinolone with anti-*staphylococcal* activity in osteoarticular tissues [55].

Here, in order to compare the levofloxacin loading efficiency of the developed composites a polydopamine coated neat PLA sample (termed PD-PLA) is introduced. The release was performed at pH 5 to simulate the state of infection and at body temperature of 37 °C.

PLA shows a non-detectable release of drug, as shown in Figure 3.17. This is because the scaffolds have been previously washed. However, a very low level of drug was retained in the PLA scaffolds pores, reflecting also that PLA does not adsorb the antibiotic and consequently does not release it either. In the case of PD-PLA a burst release was observed during the first 24 h; almost 80 % of levofloxacin eluted. The remaining amount of drug (20 %) was eluted in the following 4 days. This type of release profile is adequate in the context of an infection, since at the beginning a high rate of drug release is desirable followed by a slower drug release. When the PLA/PD-BaSO<sub>4</sub> was analyzed, a more moderate burst release was observed. Initially almost 60 % of levofloxacin eluted and, 30 % of drug during the next 3 days. In the last two days a very slow release with an 8 % release was observed. Comparing the three profiles of Figure 3.17, it is easily observed that at the end of the release process PLA only released 0.43 µg/mL (which is the drug trapped in the holes), while PD-PLA 3.12 µg/mL which is the highest amount of drug released, and the PLA/PD-BaSO<sub>4</sub> composite released a 2.4 µg/mL.

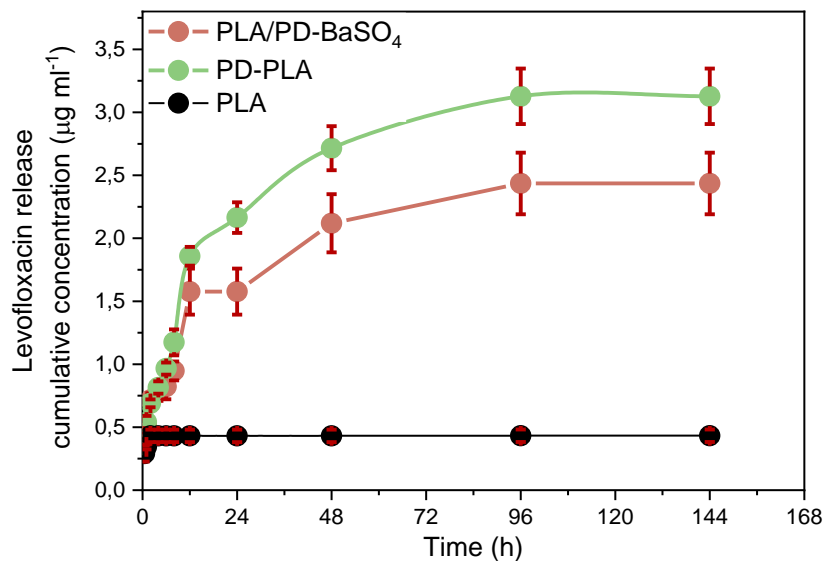


**Figure 3.17.** Release profiles over time of levofloxacin in neat PLA, polydopamine coated neat PLA (PD-PLA) and PLA/PD-BaSO<sub>4</sub>. These release results in global show that PD-PLA and PLA/PD-BaSO<sub>4</sub> display potential antimicrobial properties. Comparing these two materials, the release profile of PLA/PD-BaSO<sub>4</sub> composites was more interesting as it generated a second elution stage with greater release, 40 % versus 20 % in PD-PLA. It is remarked finally that these scaffolds were immersed in trizma buffer (pH 10) prior to analysis so the results of Figure 3.17 correspond to bound levofloxacin after adsorption.

#### 3.4.4. Effectiveness of the antibiotic in bacteria inhibition

To analyze the antibiotic efficacy of the 3D printed scaffolds the Agar Disk Diffusion tests against *Staphylococcus aureus* (*S. aureus*) were carried out. *S. aureus* was chosen because it is one of the most important pathogens in bone infections due to its ability to adhere and form biofilms when in contact with tissue [55]. Figure 3.18 shows the Agar disk diffusion test corresponding to 3D printed scaffolds of PLA/PD-BaSO<sub>4</sub> with levofloxacin, PLA/PD-BaSO<sub>4</sub> scaffold as a negative control without levofloxacin and the disk of levofloxacin (5 µg) as a positive control. Cicuéndez et al. calculated that the minimum inhibitory concentration (MIC) of levofloxacin has a value of

0.06  $\mu\text{g}/\text{mL}$  [56]. As observed in the release assay (Figure 3.17), the scaffolds release larger amounts of drug and could be valid for bacteria inhibition.

Analyzing the Agar Disk Diffusion tests it is observed that PLA/PD-BaSO<sub>4</sub> scaffolds with levofloxacin effectively inhibit bacterial growth, being the inhibition zone of a diameters of  $38 \pm 4$  mm (Figure 3.18a), while the positive control (5  $\mu\text{g}$  of Levofloxacin) exhibited a diameter average of  $28 \pm 0$  mm (Figure 3.18c). No inhibition zone could be observed for the sample without levofloxacin, PLA/PD-BaSO<sub>4</sub> (negative control, Figure 3.18b). It must be noted that the scaffolds were washed after the drug adsorption, therefore the effective inhibition of bacterial growth is attributed to the amount of levofloxacin bound to polydopamine coating of the particles and not to an unspecified content of drug that could remain in the scaffold holds.

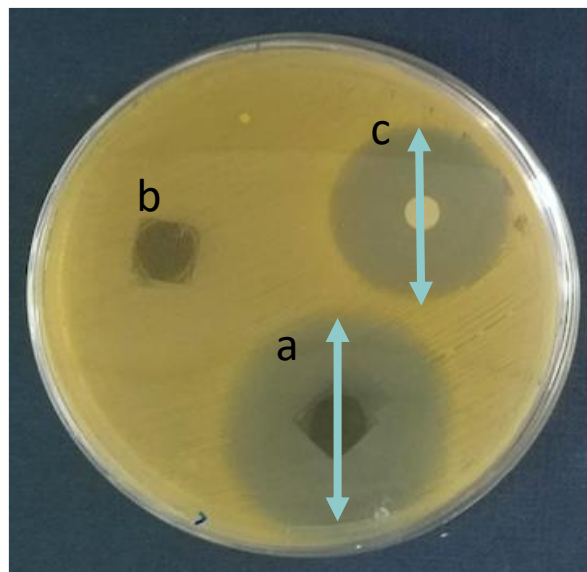


**Figure 3.18.** Agar disk diffusion tests: (a) PLA/PD-BaSO<sub>4</sub> with levofloxacin, (b) PLA/PD-BaSO<sub>4</sub> negative control (no levofloxacin) and (c) levofloxacin disk (5  $\mu\text{g}$ ) as a positive control.

From Agar diffusion tests can be concluded that polydopamine coating of BaSO<sub>4</sub> particles used for drug tethering within the PLA composites is effective and facilitates the release of the drug inhibiting the *S. aureus* growth.

### 3.5. Conclusion

The addition and coating of inorganic and rigid BaSO<sub>4</sub> radiopaque particles in a polylactide matrix has been proved to be a good strategy in order to obtain non-toxic, functional and mechanical properties improved biomedical devices.

For both composites, PLA/ BaSO<sub>4</sub> and PLA/PD-BaSO<sub>4</sub>, the presence of finely dispersed submicron size particles increases impressively the ductility and consequently the toughness of polylactides. For PLA/BaSO<sub>4</sub> system the elongation at break increased by a minimum of 996 % (0.5 wt.% BaSO<sub>4</sub>) and a maximum of 1416 % (5 wt.% BaSO<sub>4</sub>). Whereas for PLA/ PD-BaSO<sub>4</sub> the increase is greater (min. 1341 % for 0.5 wt.% BaSO<sub>4</sub> ) reaching its maximum value of 1887 % for lower particle content (2 wt.% BaSO<sub>4</sub>). The stress-whitening and necking, as well as SEM images, showed that the mechanism by which toughness improves, was based on the debonding and crack deflection between the matrix and particles. This mechanism was directly responsible for the ductile behavior of composites. Obtaining an improvement with the coated particles.

The radiopacity is improved by the BaSO<sub>4</sub> particles incorporation. Moreover, polydopamine coating has no effect in the radiopacity. Furthermore, these composites were proved to be printable. This fact makes them good candidates for radiopaque scaffold fabrication with a variety of geometries; expanding their range of applications.

In this work, dopamine plays a key role. Its presence not only improves matrix and particle interactions leading to better mechanical properties, but also enables interactions between antibacterial drugs such as levofloxacin. This latter fact enables the scaffolds to be used as controlled release devices

for bacteria growth inhibition. For that purpose, the described method is simple and allows the addition of the antibiotic after a 3D printing process of scaffolds. This fact has two advantages since the drug is not processed with the scaffold avoiding either the contact with organic solvents nor high processing temperatures that could degrade the molecules, and, on the other hand, the adsorption of the drug by a scaffold or implant can be done when clinically necessary, *in situ*.

In summary, composites show suitable properties for use as implants due to an improvement in toughness, adhesion of the drug and traceability of polylactide devices.

### **3.6. Material and experimental methods**

#### **3.6.1. Materials**

Commercial poly(D-lactide) ( $100,000 \text{ g mol}^{-1}$ ) and poly(L-lactide) ( $100,000 \text{ g mol}^{-1}$ ) (PLA) have been supplied by from Purac-Corbion. Dopamine chloride, barium sulfate ( $\text{BaSO}_4$ ) inorganic salt, Dulbecco's modified Eagle's medium (DMEM), fetal bovine serum (FBS), Hank's balanced salt solution (HBSS) and penicillin-streptomycin (PS) solution Human dermal fibroblasts (HDFs)) were purchased from Sigma-Aldrich (Ireland). Quant-IT™ PicoGreen® dsDNA kit was from Invitrogen (Ireland) and AlamarBlue® was from ThermoFisher Scientific (Ireland).

#### **3.6.2. Coating of particles and blending**

Coating of particles with polydopamine (PD- $\text{BaSO}_4$ ) has been performed as in previous published researches at trizma base pH 8.5 for 24 hours and then filtered and dried in a vacuum oven for overnight [18]. The size of  $\text{BaSO}_4$  and PD- $\text{BaSO}_4$  particles was measuring by HORIBA Laser Scattering Particle Size Distribution Analyzer LA-350.

A series of biodegradable composites PLA/BaSO<sub>4</sub> and PLA/PD-BaSO<sub>4</sub> were carried out containing in both cases 0.5, 1.0, 2.0, 5.0, 10.0 wt. % of BaSO<sub>4</sub> and PD-BaSO<sub>4</sub>. The blend of composites (PLA/BaSO<sub>4</sub> and PLA/PD-BaSO<sub>4</sub>) and neat polymer (PLA) were prepared by melt-mixing by DSM Xplore micro-compounder (Netherlands) at 200 °C and speed of 150 rpm during 2 minutes.

### 3.6.3. Radiopacity

Radiographs were taken to determine the radiopacity (RO) of the polymer with a standard clinical machine. Five specimens with 1 mm of thickness were irradiated with the X-radiographic standard clinical machine to get a radiograph. The relative RO was determined by comparing the RO exhibited by a 90 % of BaSO<sub>4</sub> specimen with samples of the same thickness of the samples. The remaining 10 % was PLA. The free image editing software ImageJ was used to measure the gray values of the BaSO<sub>4</sub> and composites (PLA/BaSO<sub>4</sub> and (PLA/PD-BaSO<sub>4</sub>) in the resulting image. The relative radiopacity (RO) of the disc was calculated by using the following equation:

$$RO = \left[ \frac{G_c - G_b}{(0.9 \times G_{BaSO_4}) - G_b} \right] \times 100\% \quad (3.1)$$

$G_c$ ,  $G_b$ , and  $G_{BaSO_4}$  are the gray values of PLA/BaSO<sub>4</sub> and PLA/PD-BaSO<sub>4</sub>, background and 90% BaSO<sub>4</sub> respectively, for the same specimen thickness.

### 3.6.4. Thermal properties

Thermal properties were evaluated by differential scanning calorimetry, DSC 2920 model, and thermogravimetric analysis under a nitrogen atmosphere of 20 ml/min to verify the amount of particles (BaSO<sub>4</sub> and PD-BaSO<sub>4</sub>) in each composite



### 3.6.5. 3D printing of radiopaque composite

Scaffolds were fabricated in a 3D-Bioplotter from Envision TEC. The 3D computer aided drawing (CAD) model of scaffolds. The CAD model was uploaded to the slicing software (Prefactory RP) where it was modified before being uploaded to the Bioplotter software (version 3.0.713.1406, Envision TEC), which enables slicing of the model, before 3D-printing. The frame-like structures used to support the implanted tissue were 3D-printed using an.

### 3.6.6. Mechanical Properties

The mechanical properties were performed on the unprinted material to know its properties and on the printed material. To know the properties of the material, tensile tests were carried out. Tensile tests were performed on specimens of 1 mm thickness using an Instron 5565 testing machine with a 500 N maximum loading and a crosshead displacement rate of 5 mm min<sup>-1</sup> (leading into a % strain/time of 12.5 %/min). The mechanical properties of the specimens were measured at 21 ± 2 °C and 50 ± 5 % relative humidity (RH) following ISO 527-2/5A/5/1995 (see Figure 3.19 a) one day after being processed to assure that all the samples have been the same short of time between process and test. The mechanical properties reported for each material correspond to average values of at eight experiments.

Fracture tests were performed on a miniature loading machine (E. Fullam, NY) at a rate of 1.2 mm min<sup>-1</sup>, where the tensile force was transmitted by two points (see the specimen in Figure 3.19 b)

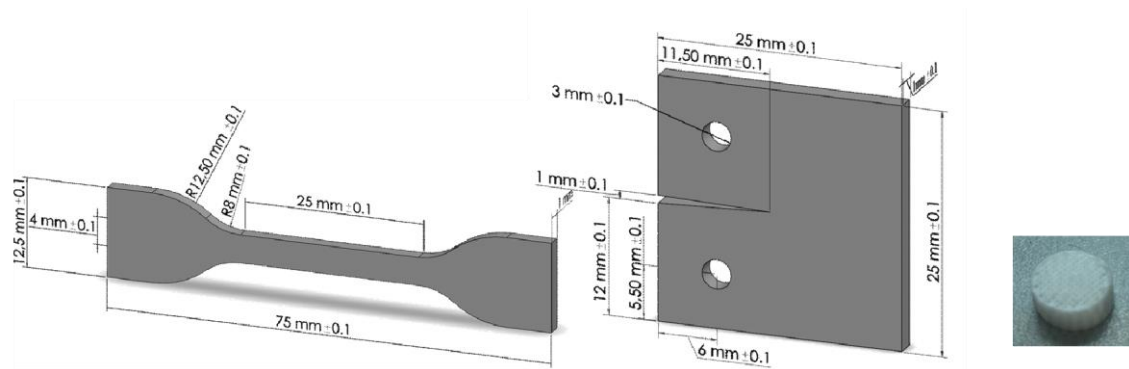


**Figure 3.19.** Specimen geometry for (a) uniaxial tensile tests (dumbbell-shaped sample) , (b) fracture toughness tests (compact tension sample) with a thickness of 1 mm in both cases; (c) compression test in scaffold sample.

In the case of scaffolds properties were following ISO 604 (see Figure 3.19 c). In all cases, tensile tests were performed at 22 °C and 50 % of relative humidity (RH) with an Instron 5565 testing machine with a load cell of 500 N at a crosshead displacement rate of 5 mm min<sup>-1</sup>. The mechanical properties reported for each material correspond to average values of at least 5 determinations.

### 3.6.7. Morphological analysis by microscopy

Scanning Electron Microscope (SEM) and Transmission Electron Microscopy (TEM) were measuring the dispersion of the particles inside of the polymer matrix and the surface fracture. SEM images collected by primary (backscattered) electrons highlight high mass elements and, consequently, location of BaSO<sub>4</sub> particles within the polymer matrix was easily determined. In contrast, when SEM images were acquired with secondary electrons, the morphology of the surface was revealed, which was employed to study the fracture mechanism. For observation of stress direction, samples were cryogenically sectioned by immersing them in liquid nitrogen for 2-3 minutes, then quickly marked with a razor blade in the stress direction, and further hit with a hammer to fracture the sample.

### 3.6.8. Adsorption/Release test

Before starting the release test, the adsorption of levofloxacin in the scaffolds has been carried out. For that, the scaffolds were submerged in a buffer at pH 10 with levofloxacin (2 mg/mL) [40] for 24 h for facilitate the adsorption. Then, the scaffolds were washed with buffer at pH 10 and dried. The washing was done to eliminate the drug from the holes of the scaffolds, and in this way obtain the amount of drug that is absorbed by the material itself.

Levofloxacin release was evaluated using a UV-vis spectrophotometer (BMG Labtech FLUOstar Omega). The band in  $\lambda = 287$  nm for levofloxacin was employed to build a standard curve with known concentrations of the drug in PBS and the measurements were carried out at concentrations lower than 25 ppm. Release of levofloxacin from the scaffolds was tested in 3 mL of PBS at 37 °C, under mild agitation (220 rpm) at pH 5. In all materials, three independent tests were carried out.

### 3.6.9. Cell culture

#### Human Dermal Fibroblasts

HDFs were grown in T75 flasks using DMEM with 10% FBS and 1% PS. The cells were incubated at 37 °C in an atmosphere of 5% CO<sub>2</sub>. The culture medium was changed every 3 days. The cells were then harvested and sub-cultured when >90% confluence was observed.

#### Cell Seeding

To study the metabolic activity of HDFs seeded in the presence of BaSO<sub>4</sub> or PD-BaSO<sub>4</sub>, HDFs were seeded at a density of 25,000 cells/cm<sup>2</sup> in a 96 well tissue culture plate and incubated in 0.5 mL of DMEM with 10% FBS and 1%

PS (37 °C, 5% CO<sub>2</sub>). After 1 day in culture, the media was replaced by complete media containing 0, 10, 50, 100 or 500 µg/mL of BaSO<sub>4</sub> or PD-BaSO<sub>4</sub> particles that were previously autoclaved.

HDFs were also seeded on sterilized PLA, PLA/BaSO<sub>4</sub> and PLA/PD-BaSO<sub>4</sub> samples (7 mm in diameter) at a density of 25,000 cells/cm<sup>2</sup> in a 48 well tissue culture plate and incubated in DMEM with 10% FBS and 1% PS. First, HDFs were suspended in 40 µL of culture medium, seeded onto each sample and incubated for 2 h to allow cell attachment (37 °C, 5% CO<sub>2</sub>, 95% relative humidity). When cells were attached, an additional 0.5 mL of culture medium was added into each well. The culture medium was replaced at day 3 after seeding.

### Cell Viability Studies

AlamarBlue<sup>®</sup> assay was performed to quantify the metabolic activity of HDFs in the presence of BaSO<sub>4</sub> or PD-BaSO<sub>4</sub> particles or seeded on PLA, PLA/BaSO<sub>4</sub> and PLA/PD-BaSO<sub>4</sub>. At the selected time points (1, 2 and 3 days for HDFs in the presence of BaSO<sub>4</sub> or PD-BaSO<sub>4</sub> particles and 1, 3 and 7 days for HDFs seeded on PLA, PLA/BaSO<sub>4</sub> and PLA/PD-BaSO<sub>4</sub>), the cells were washed with HBSS and subsequently incubated (6 h, 37 °C, sheltered from light) in 0.5 mL of fresh culture media with AlamarBlue<sup>®</sup> (10% v/v). Then, 100 µL of assay media was transferred to a 96 well plate, the absorbance at 550 and 595 nm was read on a microplate reader (VarioskanFlash) and the percentage reduction of the dye was calculated.

To quantify the DNA amount of cells seeded on PLA, PLA/BaSO<sub>4</sub> and PLA/PD-BaSO<sub>4</sub> a PicoGreen<sup>®</sup> assay was then performed on the same samples used for AlamarBlue<sup>®</sup>. Cells were repeatedly frozen at -80 °C and thawed to lyse

the cells and release the entire DNA content. Finally, fluorescence was measured at 480 nm.

### Statistics

Statistical differences were analyzed using one-way analysis of variance (ANOVA) and p-values of <0.05 were considered significant. Experiments were performed in triplicate and each assay was repeated three times.

### 3.7. Bibliography

1. Hamad, K.; Kaseem, M.; Yang, H.W.; Deri, F.; Ko, Y.G. Properties and medical applications of polylactic acid: A review. *Express Polym. Lett.* **2015**, *9*, 435–455, doi:10.3144/expresspolymlett.2015.42.
2. Tajbakhsh, S.; Hajiali, F. A comprehensive study on the fabrication and properties of biocomposites of poly(lactic acid)/ceramics for bone tissue engineering. *Mater. Sci. Eng. C* **2017**, *70*, 897–912, doi:10.1016/J.MSEC.2016.09.008.
3. Martínez De Arenaza, I.; Sadaba, N.; Larrañaga, A.; Zuza, E.; Sarasua, J.R. High toughness biodegradable radiopaque composites based on polylactide and barium sulphate. *Eur. Polym. J.* **2015**, *73*, 88–93, doi:10.1016/j.eurpolymj.2015.10.005.
4. Sarasua, J.R.; Arraiza, A.L.; Balerdi, P.; Maiza, I. Crystallinity and mechanical properties of optically pure polylactides and their blends. *Polym. Eng. Sci.* **2005**, *45*, 745–753, doi:10.1002/pen.20331.
5. Sadaba, N.; Martini, R.; Barthelat, F.; Martínez de Arenaza, I.; Larrañaga, A.; Sarasua, J.R.; Zuza, E. Understanding the toughness mechanism prompted by submicron rigid particles in polylactide/barium sulfate composites. *Polym. Test.* **2018**, *69*, 340–

- 349, doi:10.1016/j.polymertesting.2018.05.041.
6. Grémare, A.; Guduric, V.; Bareille, R.; Heroguez, V.; Latour, S.; L'heureux, N.; Fricain, J.C.; Catros, S.; Le Nihouannen, D. Characterization of printed PLA scaffolds for bone tissue engineering. *J. Biomed. Mater. Res. - Part A* **2018**, *106*, 887–894, doi:10.1002/jbm.a.36289.
  7. Nuutinen, J.-P.; Clerc, C.; Törmälä, P. Mechanical properties and in vitro degradation of self-reinforced radiopaque bioresorbable polylactide fibres. *J. Biomater. Sci. Polym. Ed.* **2003**, *14*, 665–676, doi:10.1163/156856203322274923.
  8. Chang, W.-J.; Pan, Y.-H.; Tzeng, J.-J.; Wu, T.-L.; Fong, T.-H.; Feng, S.-W.; Huang, H.-M. Development and Testing of X-Ray Imaging-Enhanced Poly-L-Lactide Bone Screws. *PLoS One* **2015**, *10*, e0140354, doi:10.1371/journal.pone.0140354.
  9. Noor Azman, N.Z.; Musa, N.F.L.; Nik Ab Razak, N.N.A.; Ramli, R.M.; Mustafa, I.S.; Abdul Rahman, A.; Yahaya, N.Z. Effect of Bi<sub>2</sub>O<sub>3</sub> particle sizes and addition of starch into Bi<sub>2</sub>O<sub>3</sub>–PVA composites for X-ray shielding. *Appl. Phys. A* **2016**, *122*, 818, doi:10.1007/s00339-016-0329-8.
  10. Abunahel, B.M.; Mustafa, I.S.; Noor Azman, N.Z. Characteristics of X-ray attenuation in nano-sized bismuth oxide/epoxy-polyvinyl alcohol (PVA) matrix composites. *Appl. Phys. A* **2018**, *124*, 828, doi:10.1007/s00339-018-2254-5.
  11. Meagher, M.J.; Leone, B.; Turnbull, T.L.; Ross, R.D.; Zhang, Z.; Roeder, R.K. Dextran-encapsulated barium sulfate nanoparticles prepared for aqueous dispersion as an X-ray contrast agent. *J. Nanoparticle Res.*

- 
- 2013**, *15*, doi:10.1007/s11051-013-2146-8.
12. Zuza, E.; Meaurio, E.; Sarasua, J.-R. Biodegradable Polylactide-Based Composites. In *Composites from Renewable and Sustainable Materials*; InTech, 2016.
  13. Xiu, H.; Qi, X.; Liu, Z.; Zhou, Y.; Bai, H.; Zhang, Q.; Fu, Q. Simultaneously reinforcing and toughening of polylactide/carbon fiber composites via adding small amount of soft poly(ether)urethane. *Compos. Sci. Technol.* **2016**, *127*, 54–61, doi:10.1016/J.COMPSCITECH.2016.02.025.
  14. Wang, X.; Jiang, M.; Zhou, Z.; Gou, J.; Hui, D. 3D printing of polymer matrix composites: A review and prospective. *Compos. Part B Eng.* **2017**, *110*, 442–458, doi:10.1016/J.COMPOSITESB.2016.11.034.
  15. Parandoush, P.; Lin, D. A review on additive manufacturing of polymer-fiber composites. *Compos. Struct.* **2017**, *182*, 36–53, doi:10.1016/J.COMPSTRUCT.2017.08.088.
  16. Poh, P.S.P.; Chhaya, M.P.; Wunner, F.M.; De-Juan-Pardo, E.M.; Schilling, A.F.; Schantz, J.-T.; van Griensven, M.; Hutmacher, D.W. Polylactides in additive biomanufacturing. *Adv. Drug Deliv. Rev.* **2016**, *107*, 228–246, doi:10.1016/J.ADDR.2016.07.006.
  17. Liu, Y.; Ai, K.; Lu, L. Polydopamine and Its Derivative Materials: Synthesis and Promising Applications in Energy, Environmental, and Biomedical Fields. *Chem. Rev.* **2014**, *114*, 5057–5115, doi:10.1021/cr400407a.
  18. Larrañaga, A.; Ramos, D.; Amestoy, H.; Zuza, E.; Sarasua, J.-R. Coating of bioactive glass particles with mussel-inspired polydopamine as a strategy to improve the thermal stability of poly(L-lactide)/bioactive glass composites. *RSC Adv.* **2015**, *5*, 65618–65626,

doi:10.1039/C5RA09495J.

19. Zou, Z.; Luo, C.; Luo, B.; Wen, W.; Liu, M.; Zhou, C. Synergistic reinforcing and toughening of poly(l-lactide) composites with surface-modified MgO and chitin whiskers. *Compos. Sci. Technol.* **2016**, *133*, 128–135, doi:10.1016/J.COMPSCITECH.2016.07.025.
20. Ahn, B.K. Perspectives on Mussel-Inspired Wet Adhesion. *J. Am. Chem. Soc.* **2017**, *139*, 10166–10171, doi:10.1021/jacs.6b13149.
21. Zhuang, H.; Su, H.; Bi, X.; Bai, Y.; Chen, L.; Ge, D.; Shi, W.; Sun, Y. Polydopamine Nanocapsule: A Theranostic Agent for Photoacoustic Imaging and Chemo-Photothermal Synergistic Therapy. *ACS Biomater. Sci. Eng.* **2017**, *3*, 1799–1808, doi:10.1021/acsbiomaterials.7b00260.
22. Yu, X.; Tang, X.; He, J.; Yi, X.; Xu, G.; Tian, L.; Zhou, R.; Zhang, C.; Yang, K. Polydopamine Nanoparticle as a Multifunctional Nanocarrier for Combined Radiophotodynamic Therapy of Cancer. *Part. Part. Syst. Charact.* **2017**, *34*, 1600296, doi:10.1002/ppsc.201600296.
23. Zhang, J.; Li, J.; Jia, G.; Jiang, Y.; Liu, Q.; Yang, X.; Pan, S. Improving osteogenesis of PLGA/HA porous scaffolds based on dual delivery of BMP-2 and IGF-1 via a polydopamine coating. *RSC Adv.* **2017**, *7*, 56732–56742, doi:10.1039/C7RA12062A.
24. Khoshnood, N.; Zamanian, A.; Massoudi, A. Mussel-inspired surface modification of titania nanotubes as a novel drug delivery system. *Mater. Sci. Eng. C* **2017**, *77*, 748–754, doi:10.1016/j.msec.2017.03.293.
25. Fernandez-Yague, M.A.; Larrañaga, A.; Gladkovskaya, O.; Stanley, A.; Tadayyon, G.; Guo, Y.; Sarasua, J.R.; Tofail, S.A.M.; Zeugolis, D.I.; Pandit, A.; et al. Effects of Polydopamine Functionalization on Boron Nitride Nanotube Dispersion and Cytocompatibility. *Bioconjug. Chem.* **2015**,



- 
- 26, 2025–2037, doi:10.1021/acs.bioconjchem.5b00257.
26. Mu, C.; Zhang, L.; Song, Y.; Chen, X.; Liu, M.; Wang, F.; Hu, X. Modification of carbon nanotubes by a novel biomimetic approach towards the enhancement of the mechanical properties of polyurethane. *Polymer (Guildf)*. **2016**, *92*, 231–238, doi:10.1016/J.POLYMER.2016.03.085.
  27. Luo, C.; Zou, Z.; Luo, B.; Wen, W.; Li, H.; Liu, M.; Zhou, C. Enhanced mechanical properties and cytocompatibility of electrospun poly(l-lactide) composite fiber membranes assisted by polydopamine-coated halloysite nanotubes. *Appl. Surf. Sci.* **2016**, *369*, 82–91, doi:10.1016/J.APSUSC.2016.02.048.
  28. Murariu, M.; Dubois, P. PLA composites: From production to properties. *Adv. Drug Deliv. Rev.* **2016**, *107*, 17–46, doi:10.1016/J.ADDR.2016.04.003.
  29. Wu, T.-Y.; Yang, M.-C.; Hsu, Y.-C. Improvement of cytocompatibility of polylactide by filling with marine algae powder. *Mater. Sci. Eng. C* **2015**, *50*, 309–316, doi:10.1016/J.MSEC.2015.02.020.
  30. Cai, S.; Pourdeyhimi, B.; Lobo, E.G. High-Throughput Fabrication Method for Producing a Silver-Nanoparticles-Doped Nanoclay Polymer Composite with Novel Synergistic Antibacterial Effects at the Material Interface. *ACS Appl. Mater. Interfaces* **2017**, *9*, 21105–21115, doi:10.1021/acsami.7b03793.
  31. Li, M.-X.; Kim, S.-H.; Choi, S.-W.; Goda, K.; Lee, W.-I. Effect of reinforcing particles on hydrolytic degradation behavior of poly (lactic acid) composites. *Compos. Part B Eng.* **2016**, *96*, 248–254, doi:10.1016/J.COMPOSITESB.2016.04.029.

32. Liu, H.; Li, W.; Wen, W.; Luo, B.; Liu, M.; Ding, S.; Zhou, C. Mechanical properties and osteogenic activity of poly(l-lactide) fibrous membrane synergistically enhanced by chitosan nanofibers and polydopamine layer. *Mater. Sci. Eng. C* **2017**, *81*, 280–290, doi:10.1016/J.MSEC.2017.08.010.
33. Shieh, Y.T.; Liu, G.L. Effects of carbon nanotubes on crystallization and melting behavior of poly(L-lactide) via DSC and TMDSC studies. *J. Polym. Sci. Part B Polym. Phys.* **2007**, *45*, 1870–1881, doi:10.1002/polb.21184.
34. Righetti, M.C.; Tombari, E. Crystalline, mobile amorphous and rigid amorphous fractions in poly(L-lactic acid) by TMDSC. *Thermochim. Acta* **2011**, *522*, 118–127, doi:10.1016/j.tca.2010.12.024.
35. Harrats, C.; Groeninckx, G. Deformation mechanisms and toughness of rubber and rigid filler modified semicrystalline polymers. **2016**.
36. Kim, G.M.; Michler, G.H. Micromechanical deformation processes in toughened and particle filled semicrystalline polymers: Part 2. model representation for micromechanical deformation processes. *Polymer (Guildf)*. **1998**, *39*, 5699–5703, doi:10.1016/S0032-3861(98)00169-4.
37. Zuiderduin, W.C.J.; Westzaan, C.; Huétink, J.; Gaymans, R.J. Toughening of polypropylene with calcium carbonate particles. *Polymer (Guildf)*. **2002**, *44*, 261–275, doi:10.1016/S0032-3861(02)00769-3.
38. Gojny, F.H.; Wichmann, M.H.G.; Köpke, U.; Fiedler, B.; Schulte, K. Carbon nanotube-reinforced epoxy-composites: Enhanced stiffness and fracture toughness at low nanotube content. *Compos. Sci. Technol.* **2004**, *64*, 2363–2371, doi:10.1016/j.compscitech.2004.04.002.

- 
39. Smit, T.H.; Engels, T.A.P.; Wuisman, P.I.J.M.; Govaert, L.E. Time-dependent mechanical strength of 70/30 poly(L,DL-lactide): Shedding light on the premature failure of degradable spinal cages. *Spine (Phila. Pa. 1976)*. **2008**, *33*, 14–18, doi:10.1097/BRS.0b013e31815e39df.
  40. Smit, T.H.; Engels, T.A.P.; Söntjens, S.H.M.; Govaert, L.E. Time-dependent failure in load-bearing polymers: A potential hazard in structural applications of polylactides. In Proceedings of the Journal of Materials Science: Materials in Medicine; 2010; Vol. 21, pp. 871–878.
  41. Xu, W.; Raychowdhury, S.; Jiang, D.D.; Retsos, H.; Giannelis, E.P. Dramatic improvements in toughness in poly(lactide-co-glycolide) nanocomposites. *Small* **2008**, *4*, 662–669, doi:10.1002/smll.200701231.
  42. Thio, Y.S.; Argon, A.S.; Cohen, R.E.; Weinberg, M. Toughening of isotactic polypropylene with CaCO<sub>3</sub> particles. *Polymer (Guildf)*. **2002**, *43*, 3661–3674, doi:10.1016/S0032-3861(02)00193-3.
  43. Subramanian, A.S.; Tey, J.N.; Zhang, L.; Ng, B.H.; Roy, S.; Wei, J.; Hu, X. ‘Matthew’ Synergistic bond strengthening in epoxy adhesives using polydopamine/MWCNT hybrids. *Polymer (Guildf)*. **2016**, *82*, 285–294, doi:10.1016/J.POLYMER.2015.11.031.
  44. Tobin, E.J. Recent coating developments for combination devices in orthopedic and dental applications: A literature review. *Adv. Drug Deliv. Rev.* 2017, *112*, 88–100.
  45. Anderson, K.S.; Schreck, K.M.; Hillmyer, M.A. Toughening polylactide. *Polym. Rev.* **2008**, *48*, 85–108, doi:10.1080/15583720701834216.
  46. Mania, S.; Ryl, J.; Jinn, J.R.; Wang, Y.J.; Michałowska, A.; Tylingo, R. The production possibility of the antimicrobial filaments by co-extrusion of

- the pla pellet with chitosan powder for FDM 3D printing technology. *Polymers (Basel)*. **2019**, *11*, doi:10.3390/polym11111893.
47. Ranjan, N.; Singh, R.; Ahuja, I.P.S.; Kumar, R.; Singh, J.; Verma, A.K.; Leekha, A. On 3D printed scaffolds for orthopedic tissue engineering applications. *SN Appl. Sci.* **2020**, *2*, doi:10.1007/s42452-020-1936-8.
48. Rodrigues, N.; Benning, M.; Ferreira, A.M.; Dixon, L.; Dalgarno, K. Manufacture and Characterisation of Porous PLA Scaffolds. *Procedia CIRP* **2016**, *49*, 33–38, doi:10.1016/J.PROCIR.2015.07.025.
49. Ghassemieh, E. Morphology and compression behaviour of biodegradable scaffolds produced by the sintering process. *Proc. Inst. Mech. Eng. Part H J. Eng. Med.* **2008**, *222*, 1247–1262, doi:10.1243/09544119JEIM448.
50. Deplaine, H.; Acosta-Santamaría, V.A.; Vidaurre, A.; Gómez Ribelles, J.L.; Doblaré, M.; Ochoa, I.; Gallego Ferrer, G. Evolution of the properties of a poly(L-lactic acid) scaffold with double porosity during in vitro degradation in a phosphate-buffered saline solution. *J. Appl. Polym. Sci.* **2014**, *131*, 1–10, doi:10.1002/app.40956.
51. Khodaei, M.; Amini, K.; Valanezhad, A. Fabrication and Characterization of Poly Lactic Acid Scaffolds by Fused Deposition Modeling for Bone Tissue Engineering. *J. Wuhan Univ. Technol. Mater. Sci. Ed.* **2020**, *35*, 248–251, doi:10.1007/s11595-020-2250-4.
52. Chung, T.-W.; Wang, Y.-Z.; Huang, Y.-Y.; Pan, C.-I.; Wang, S.-S. Poly (ε-caprolactone) Grafted With Nano-structured Chitosan Enhances Growth of Human Dermal Fibroblasts. *Artif. Organs* **2006**, *30*, 35–41, doi:10.1111/j.1525-1594.2006.00178.x.
53. Navarro, M.; Engel, E.; Planell, J.A.; Amaral, I.; Barbosa, M.; Ginebra,

- 
- M.P. Surface characterization and cell response of a PLA/CaP glass biodegradable composite material. *J. Biomed. Mater. Res. Part A* **2008**, *85A*, 477–486, doi:10.1002/jbm.a.31546.
54. Meaurio, E.; Sanchez-Rexach, E.; Butron, A.; Sarasua, J.R. The conformation of chloramphenicol in the ordered and disordered phases. *Spectrochim. Acta - Part A Mol. Biomol. Spectrosc.* **2019**, *211*, 383–392, doi:10.1016/j.saa.2018.12.021.
55. Ferreira, M.; Rzhepishevskaya, O.; Grenho, L.; Malheiros, D.; Gonçalves, L.; Almeida, A.J.; Jordão, L.; Ribeiro, I.A.; Ramstedt, M.; Gomes, P.; et al. Levofloxacin-loaded bone cement delivery system: Highly effective against intracellular bacteria and *Staphylococcus aureus* biofilms. *Int. J. Pharm.* **2017**, *532*, 241–248, doi:10.1016/j.ijpharm.2017.08.089.
56. Cicuéndez, M.; Doadrio, J.C.; Hernández, A.; Portolés, M.T.; Izquierdo-Barba, I.; Vallet-Regí, M. Multifunctional pH sensitive 3D scaffolds for treatment and prevention of bone infection. *Acta Biomater.* **2018**, *65*, 450–461, doi:10.1016/j.actbio.2017.11.009.



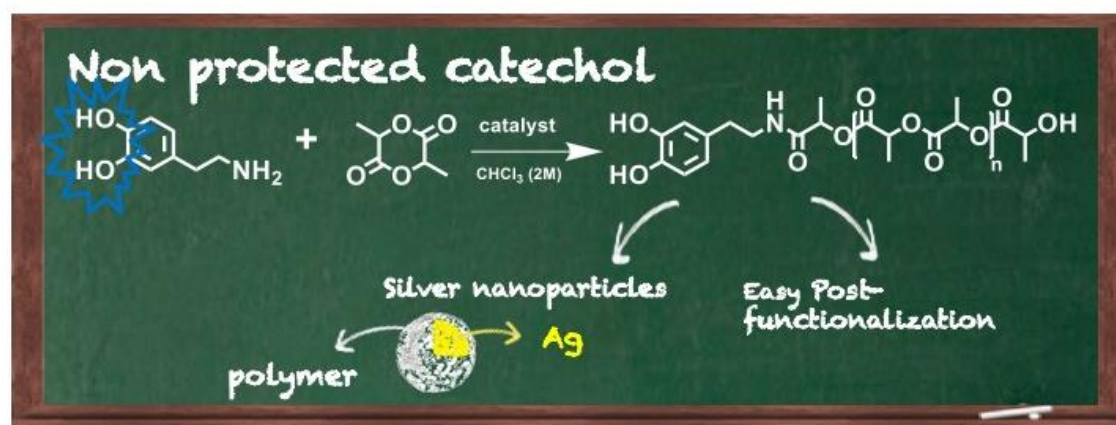


# Chapter 4





## Graphical abstract





## CHAPTER 4: POLYLACTIDE BASED 3D PRINTABLE MATERIALS WITH BIOLOGICAL PERFORMANCE.

In this chapter polylactide (PLA) functionalized with dopamine is presented as an alternative to improve polylactides biological performance. PLA was synthesized using dopamine as initiator obtaining PLA chains with dopamine in the end of the chain (PLA-DA). Blends of PLA/PLA-DA were employed for 3D scaffold fabrication using a 3D printer. Finally the biological performance of these scaffolds was assessed by means of adsorption/release of drug tests, cytotoxicity assessments and antimicrobial test.

### 4.1. Introduction

Catechol-derivatives and their corresponding ortho-quinones represent one of the most important classes of naturally abundant small molecules due to their capacity to mediate fascinating chemical reactions. Indeed, catechol molecules not only have demonstrated to be potent antioxidant, anti-inflammatory, redox active, or to present outstanding adhesion to different substrates but also they could be easily oxidized. When oxidized, this compound possesses the capacity to react towards a wide variety of chemical groups such as amines or thiols. It is not surprising, that these amazing properties of catechols have opened the door to the design of new (multi)functional polymers based on catechols. Catechols are used in several fields, such as tissue engineering, due to biocompatible and non-toxic properties, for surface coating to protect or improve the adhesion of a given material to a substrate [1–5], as redox-active polymers (RAPs) in the battery field to prepare robust energy storage devices [6]. Catechol units can serve also as reducing agent for the preparation of well-dispersed silver nanoparticles (AgNPs) leading to hydrogels with antibacterial behavior [7].

Catechol functionality can be incorporated into polymers using different strategies. The most studied strategy is the direct polymerization of functional

catechols such as dopamine either by oxidative [5] or enzymatic [8] routes. Catechol units can be easily oxidized into highly reactive quinones promoting the auto-polymerization of catechol units and the formation of tridimensional structures. More recently, in order to obtain well-defined linear polymers with pending catechol unit, the free-radical polymerization of vinylic monomers bearing catechol has also been investigated. Although catechols are well-known polymerization inhibitors, their polymerization with no catechol protection has reported the viability of this approach. However, in most of these studies, even using controlled radical polymerization techniques, the potential side reactions of propagating radicals with catechols and their effect on the polymer architecture were rarely discussed. As shown by Detrembleur et al., when vinyl monomers bearing catechols were not protected, high molar mass (hyper)branched polymers were formed at low catechol content [9,10]. At high contents, a crosslinked material was obtained. This has later been further confirmed by Kamperman et al. [11,12]

Besides free radical polymerization, catechol units have been also investigated as interesting synthetic targets in ring-opening polymerization (ROP) reactions. Thus, Deming et al. prepared high molecular weight polypeptides bearing catechols by ROP of  $\alpha$ -amino acid *N*-carboxyanhydrides NCAs containing protected catechols followed by their deprotection [13]. Although, catechol units did not interfere with nucleophilic substitution reactions, their instability under oxygen and basic pH represent difficulties to perform controlled ROP [9]. Thus, it is recommended to protect and unprotect catechol units during the polymerization process in order to avoid its homopolymerization and to carry out a controlled polymerization [14–16].

In the last decade, continuous efforts have been devoted to promote innovations in polymerization towards the convergence of functional group tolerance, fast rates, and selectivity in catalyst design. For instance,

Waymouth et al recently developed an effective catalytic system combining alkoxides with thioureas that catalysed rapid and selective ring-opening polymerizations, while most of the catalysts were subject to find a compromise between polymerization rate and polymerization control [17]. Following this innovation, in this paper, we use for the first time an unprotected catechol containing a pendant amine group (named dopamine) as initiator for the controlled ROP of L-lactide using a weak base as catalyst. We performed the polymerizations in the absence of oxygen and using different solvents in order to reduce the potential of catechol units to autopolymerize [11,18,19]. In this way, a lactide polymer with dopamine in its chain will be obtained.

Due to its biomimetic adhesivity [37], polydopamine has been used to confer anchoring sites for biologically active molecules [38]. In our case, the presence of dopamine will help to anchor drugs, whereas PLA due to its suitable physical-chemical properties [20] will ensure the use of additive manufacturing process for scaffold fabrication. In the last decade additive manufacturing have received a greater attention, more specifically the 3D printing technology, due to the versatility to process material and facility of reproducing complex and well-defined geometries [21–23]. In the majority of the traditional methods for creating 3D scaffolds including electrospinning [24], freeze-drying [25], gas foaming [26,27], particle or porogen leaching [28,29] only the bulk properties of the scaffolds can control and do not allow precise control of the internal architecture (porosity) and topology (pore shape) [30]. These two facts are of vital importance for cell life, as highly porous open structure allows the uninterrupted flow and access of culture media [21,31]. In addition, thanks to 3D printing technology, customized implants can be reproduced [32,33]. This is one of the main reasons why this

technology is used in biomedical applications and especially in tissue engineering.

Moreover, 3D porous structures are also used to transport/release drugs [34,35]. In drug delivery systems it is important to achieve reproducible well-defined inner structures. In this sense, 3D printing allows the fabrication of scaffolds having always the same porosity and interconnections; thus always promoting the same results. The addition of drugs within the scaffolds, prevents the latter from being rejected by the body, since the drug is released and prevents inflammation of the cells. The addition of the drug within the matrix of the scaffolds could be carried out in two different ways: (1) by incorporating it into the material, that is, a mixture or blend of drug/polymer and (2) by adding it by covalent bonds or secondary bonds. In order for the drug to be released, it is preferable electrochemical or secondary bonds.

The aim of this work was to develop PLA based polymeric systems with capability of adsorbing/releasing drug for antimicrobial applications. For this purpose, mussel inspired adhesive (polydopamine) was employed as drug-adsorbed/drug-desorbed binding point. Dopamine was added in two ways in the materials, (1) by attaching it to the end of lactide chain (PLA-DA) as explained above and (2) by incorporating it as a polydopamine coating into PLA (PD-PLA) which is a simple method for surface modification published by Messersmith's group [5,36]. The different way of drug adsorption capability and the drug release behaviour in different conditions have been studied. Finally to check the effectiveness (antibacterial properties) and non-toxicity of the drug a Kirby Bauer test and cell viability test was carried out, respectively.

## 4.2. Synthesis and characterization of PLA-DA

Catechol-derivatives and their corresponding ortho-quinones represent one of the most important classes of naturally abundant small molecules due to their capacity to mediate fascinating chemical reactions. When oxidized, this compound possesses the capacity to react towards a wide variety of chemical groups such as amines or thiols. Catechols are used in several fields, such as tissue engineering, due to biocompatible and non-toxic properties, for surface coating to protect or improve the adhesion of a given material to a substrate [1–4,39], as redox-active polymers (RAPs) in the battery field to prepare robust energy storage devices [6].

Free radical polymerization, catechol units have been also investigated as interesting synthetic targets in ring-opening polymerization (ROP) reactions. Thus, Deming et al. prepared high molecular weight polypeptides bearing catechols by ROP of  $\alpha$ -amino acid *N*-carboxyanhydrides NCAs containing protected catechols followed by their deprotection [13]. Although, catechol units did not interfere with nucleophilic substitution reactions, their instability under oxygen and basic pH represent difficulties to perform controlled ROP [9]. Thus, it is recommended to protect and unprotect catechol units during the polymerization process in order to avoid its homopolymerization and to carry out a controlled polymerization [14–16]

In the last decade, continuous efforts have been devoted to promote innovations in polymerization towards the convergence of functional group tolerance, fast rates, and selectivity in catalyst design. For instance, Waymouth et al. recently developed an effective catalytic system combining alkoxides with thioureas that catalysed rapid and selective ring-opening polymerizations, while most of the catalysts were subject to find a compromise between polymerization rate and polymerization control [40]

Following this innovation, in this chapter , we use for the first time an unprotected catechol containing a pendant amine group (named dopamine) as initiator for the controlled ROP of L-lactide (L-LA) using a weak base as catalyst. We performed the polymerizations in the absence of oxygen and using different solvents in order to reduce the potential of catechol units to autopolymerize [11,18,19]

As a first test, the catalyst free ROP of L-LA in the presence of dopamine initiator (Figure 4.1) was investigated.

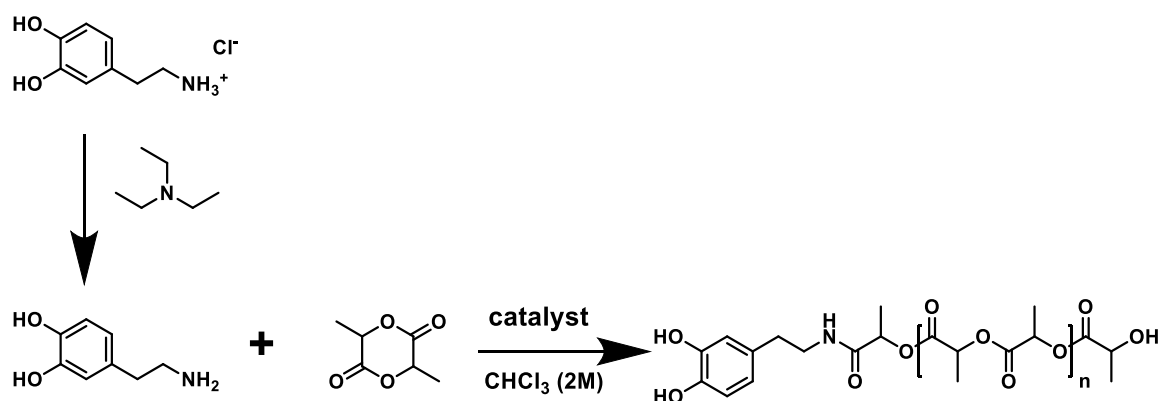


**Figure 4.1.** Ring-opening polymerization for dopamine end-capped polylactide (PLA-DA).

In order to prepare the free amine and allow the initiation process, 1.0 equiv. of triethylamine (TEA) must be added to a solution of dopamine hydrochloride (1 equiv.) followed by the addition of L-lactide monomer and chloroform. Although amines can act as initiator, the reaction did not lead to any polymerization even using different solvents such as chloroform ( $\text{CHCl}_3$ ), tetrahydrofuran (THF) or N,N-Dimethylformamide (DMF) and temperatures (Table 4.1).

**Table 4.1.** Different synthesis rout for the polymerization L-lactide initiate by dopamine.



Entry	Solvent	Temperature (°C)	catalyst	Time (h)	[M]/[I]/[Cat]	DP <sub>NM</sub> <sub>R</sub>
1	DCM	25	-	96	10/1/0	8
2	CHCl <sub>3</sub>	25	-	96	10/1/0	12
3	DMF	25	-	48	10/1/0	9
5	THF	25	-	96	10/1/0	7
6	THF	50	-	48	10/1/0	7
7	DMF+CHCl <sub>3</sub>	25	-	144	10/1/0	-
8	DMF+CHCl <sub>3</sub>	25	TEA	24	10/1/1	11
9	DMF+CHCl <sub>3</sub>	25	DBU	48	10/1/1	

After this unsuccessful attempt, we envisioned a more efficient ROP using an organic base inspired by the work of Bourissou and co-workers which explored 1,8-diazabicyclo[5.4.0]undec-7-ene (DBU) catalyst for the use of amines as initiators for the preparation of amide end-capped PLA [14]. Two different bases were explored as potential catalyst for the catechol initiated controlled polymerization of L-LA, triethylamine (TEA) a weak base (Table 4.1, entry 8) and DBU a strong base (Table 4.1, entry 9, Figure 4.2).

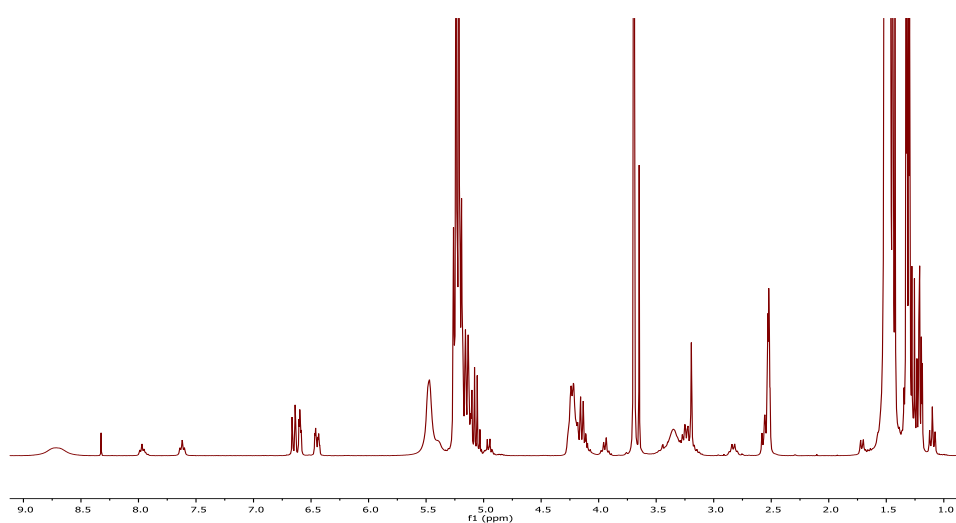


**Figure 4.2.** <sup>1</sup>H NMR of PLA-DA for degree of polymerization. Dp = 10. Reaction conditions: 2 mol L<sup>-1</sup> solution of L-lactide in CHCl<sub>3</sub> at 25 °C using DBU as catalyst. (entry 9 of Table 4.1).

With the DBU the reaction continued without success, for that, it was decided to continue with the TEA, using different percentages of this and different percentages of lactide/dopamine, in all cases both solvent was used  $\text{CHCl}_3$  and DMF (see Table 4.2)

**Table 4.2.** Different synthesis routes for the polymerization L-lactide initiated by dopamine using TEA as catalyst and DCM and  $\text{CHCl}_3$  like a solvents.

Entry	Initiator	Time (h)	Conv. <sup>1</sup> (%)	$([M]_0/[I]_0/[Cat])$	$M_n$ (Theo) <sup>2</sup> (kg/mol)	$M_n$ (Exp) <sup>3</sup> (kg/mol)	$\bar{D}$ <sup>3</sup>
1	DA	96	1	10/1/0	0	-	-
2	DA	24	93	10/1/0.25	1.5	3.8	1.2
3	DA	24	93	10/1/0.5	1.5	3.5	1.1
4	DA	12	94	10/1/0.75	1.5	3.4	1.2
5	DA	12	94	10/1/1	1.5	3.6	1.1
6	DA	24	93	25/1/0.25	2.8	4.0	1.2
7	DA	48	92	50/1/0.25	6.9	9.5	1.2
8	DA	48	91	100/1/0.25	13.4	21.0	1.4
9	P	24	90	10/1/0.25	1.5	1.6	1.2

Reaction conditions: 2 mol·L<sup>-1</sup> solution of L-lactide in  $\text{CHCl}_3$  at 25 °C using TEA as catalyst. <sup>1</sup> Conversion by <sup>1</sup>H NMR; <sup>2</sup> Calculated from the molar mass of L-lactide (144 g·mol<sup>-1</sup>) × conversion × [the initial monomer]/[initiator ratio] plus the molar mass of the initiator. <sup>3</sup> Molecular weight ( $M_n$ ) and dispersity ( $\bar{D}$ ) obtained from size exclusion chromatography analysis in tetrahydrofuran relative to polystyrene standards.

For catalyst screening, polymerization of L-LA was performed at room temperature in chloroform using a 2 M concentration of L-LA and an initial monomer-to-initiator-to-catalyst ratio of ( $[M]_0/[I]_0/[catalyst]$ ) of 10/1/0.25). The polymerization was monitored by <sup>1</sup>H NMR and the conversion was calculated by determining the ratio of the signals related to the monomer methine protons at 5.4 ppm from and L-LA, and comparing them to the signal of the polymer methine protons at 5.2 ppm from poly(L-lactide) (Figure 4.3).

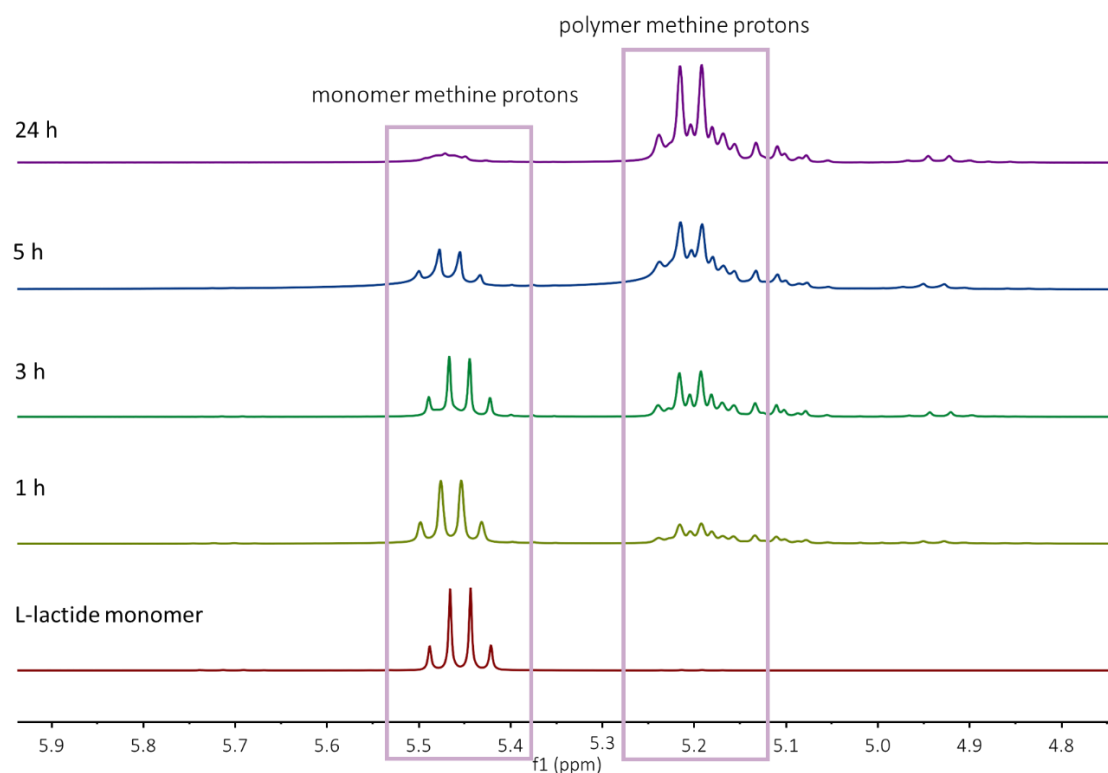


**Figure 4.3.** Kinetics of polylactide followed by  $^1\text{H}$  NMR ( monomer 5.45 ppm polymer 5.20 ppm) (entry 2 of Table 4.2).

We found that in the presence of 0.25 equiv. of DBU polymer was formed but the molecular weight was lower than expected and some extra signals observed in the  $^1\text{H}$  NMR suggested that the polymerization was not controlled and some side reactions were occurring (Figure 4.2). When using 0.25 equiv. of TEA, although the polymerization was slower only the signals attributed to dopamine initiated PLA were observed. The catalyst concentration was increased from 0.25 to 1.00 and we did not observe any significant change in the polymerization kinetics (Table 4.2, entry 2-5 and Figure 4.4). Therefore, the minimum amount of catalyst used to carry out the polymerization was 0.25.

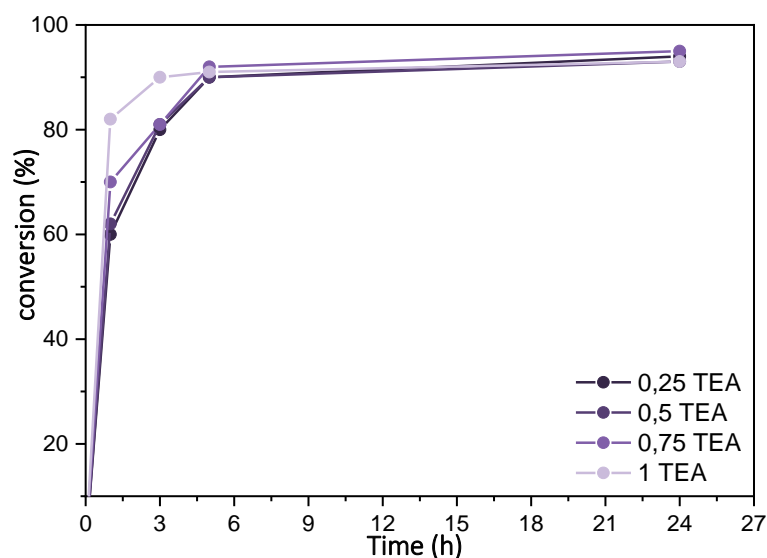


**Figure 4.4.** Kinetic plots for the different experiments runned with different TEA concentratios.

Moreover, the diagnostic peak of dopamine units remain is the low-field shift of the  $\text{CH}_2\text{N}$  signal (from  $\delta$  3.05 ppm in the amine to  $\delta$  3.25 ppm in the adduct). In addition to the characteristic signals associated with the  $\text{CH}_2\text{-NH}$  and  $\text{CH-OH}$  moieties (at  $\delta$  3.25 and 4.21 ppm, with relative integrations of 2 and 1, respectively), a  $\text{NHCO}$  signal is observed at  $\delta$  7.96 ppm (relative integration 1), as seen in Figure 4.5a.

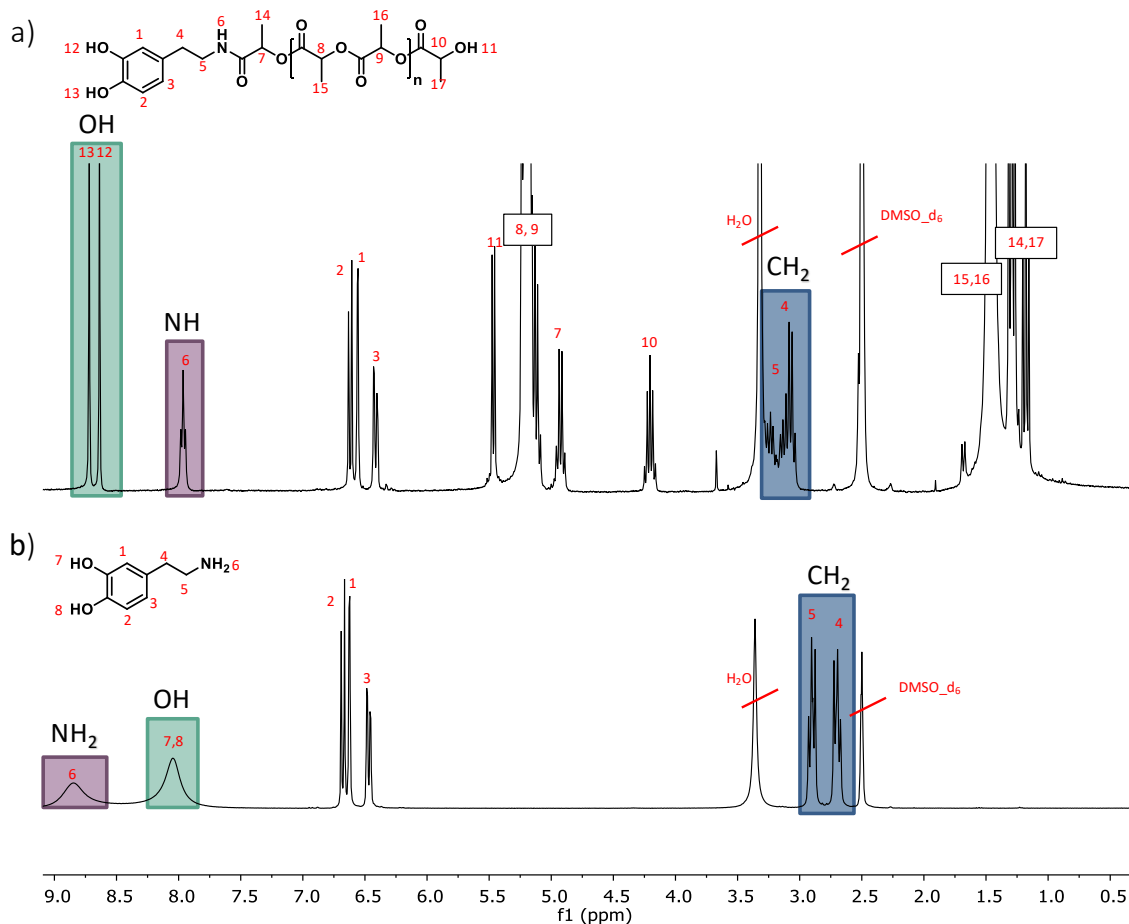


**Figure 4.5.**  $^1\text{H}$  NMR spectra in  $\text{DMSO-d}_6$  for a) Catechol end-functional PLLA with DP 10 and b) Dopamine initiator.

The average  $M_n$  calculated by comparing the integration of protons from the catechol groups with that from the polymer backbones was  $1700 \text{ g}\cdot\text{mol}^{-1}$ , which was similar to the theoretical ones. The absence of side reactions was confirmed by carefully evaluating the carbonyl and the methine region in the  $^{13}\text{C}$  NMR where we did not observe any presence of racemization (Figure 4.6).

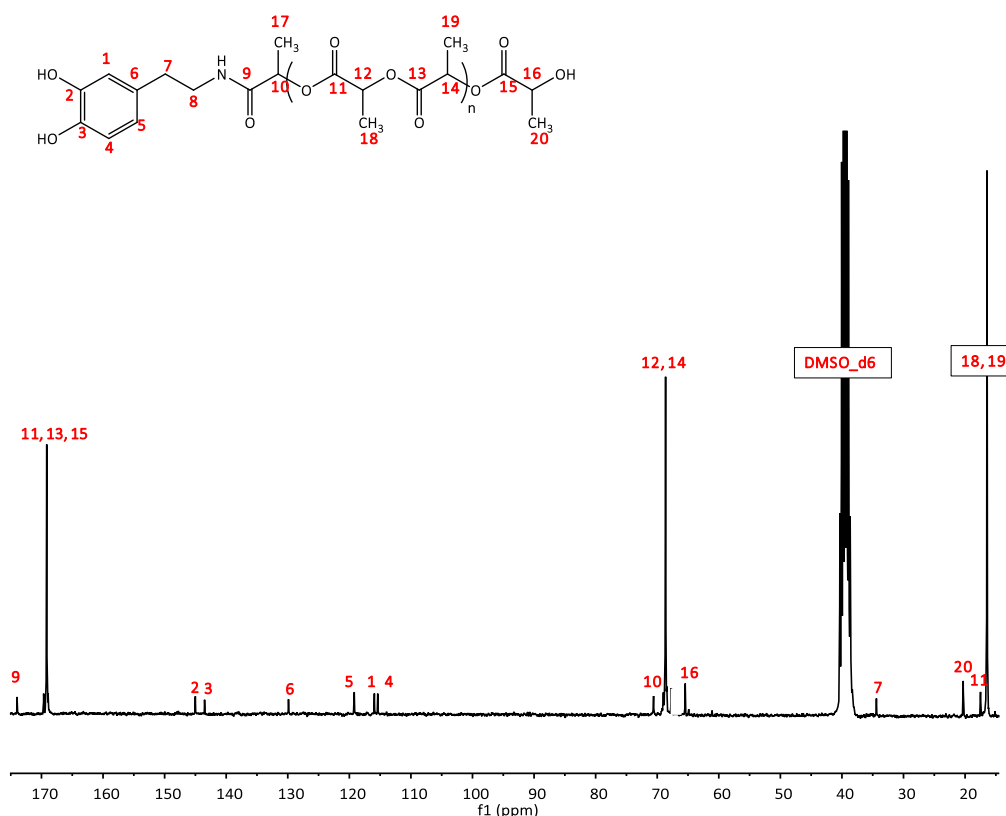


**Figure 4.6:**  $^{13}\text{C}$  NMR of Catechol-PLLA for degree of polymerization  $DP = 10$ . (entry 2 of table 4.2).

As seen in Figure 4.7a, a linear relationship between molecular weight characterized by SEC and conversion was observed. In order to further confirm end-group fidelity and the absence of side reactions we analyzed the SEC traces using both ultraviolet/visible (UV-vis) and refractive index (RI) signals. As dopamine is UV active at 289 nm, all the polymer chains initiated with dopamine should overlap with the RI signal. As shown in Figure 4.7b, the UV-vis and RI SEC traces for PLLA overlay, indicating that dopamine is on the chain end, confirming that the catechol group is attached to the polymer chain. In order to further verify the polymerization, MALDI-TOF results were carried out (Figure 4.7c) where the corresponding end groups and only one set of peaks or distributions separated by  $144 \text{ g}\cdot\text{mol}^{-1}$  (associated with the lactide monomer unit) were detected.

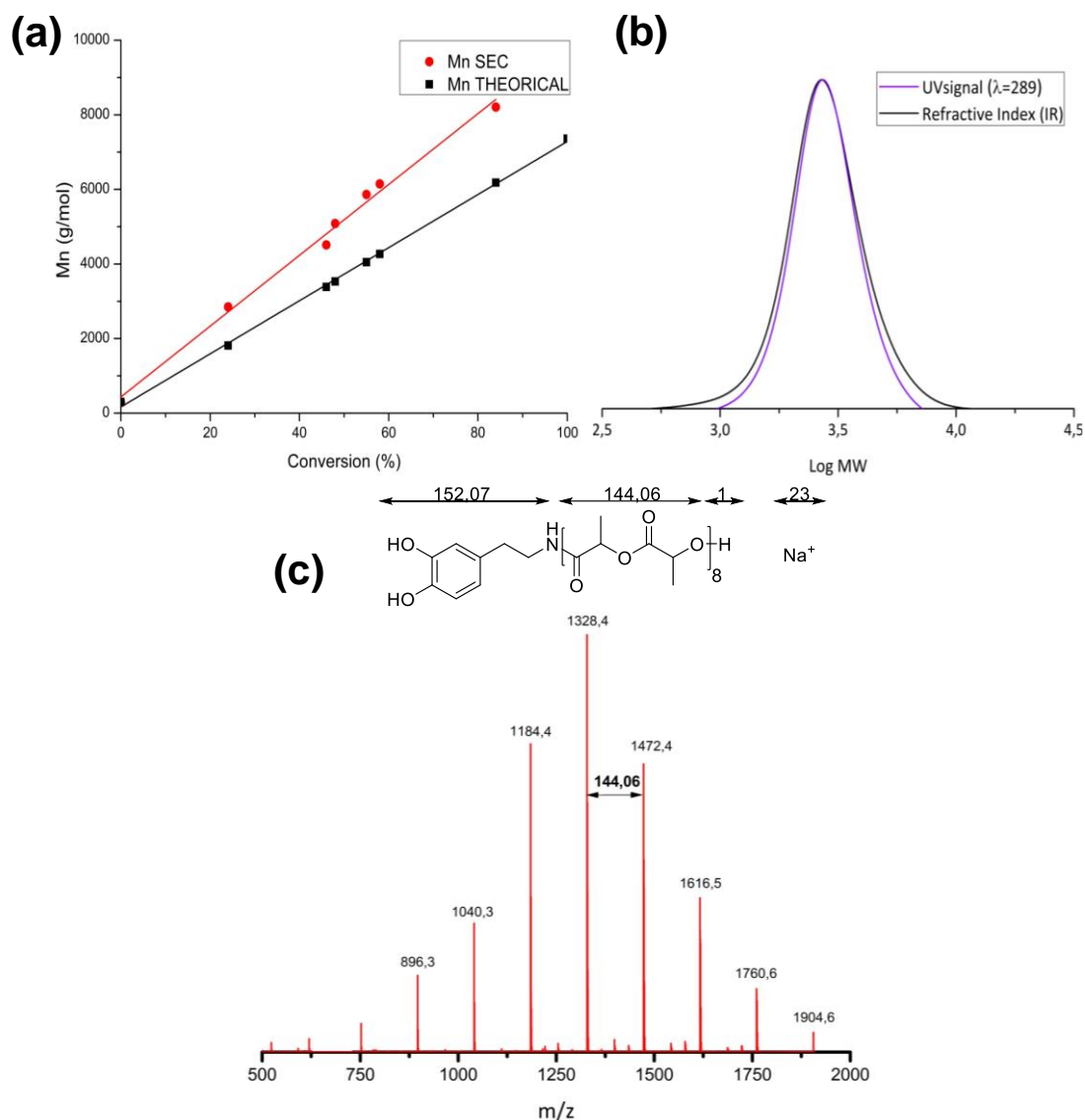


**Figure 4.7.** (a) Molecular weight vs. conversion graph of PLLA using dopamine as initiator, [(a) entry 7]; (b) SEC trace with UV (289 nm wavelength) and refractive-index signals for semitelechelic catechol PLLA; (c) MALDI-TOF spectra for semitelechelic catechol-PLA. [(b) and (c) Entry 2].

Moreover, we investigated the potential of TEA to prepare higher-molecular-weight Dopamine-PLA. Therefore, the targeted degree of polymerization,  $[M]_0/[I]_0$  was varied from 10 to 50 (Figure 4.8). We found that the experimental molecular weight in both cases was similar to the targeted one (Table 4.2, entry 6 and 7) and still only the signals attributed to dopamine chain ends were observed in  $^1\text{H}$  NMR.

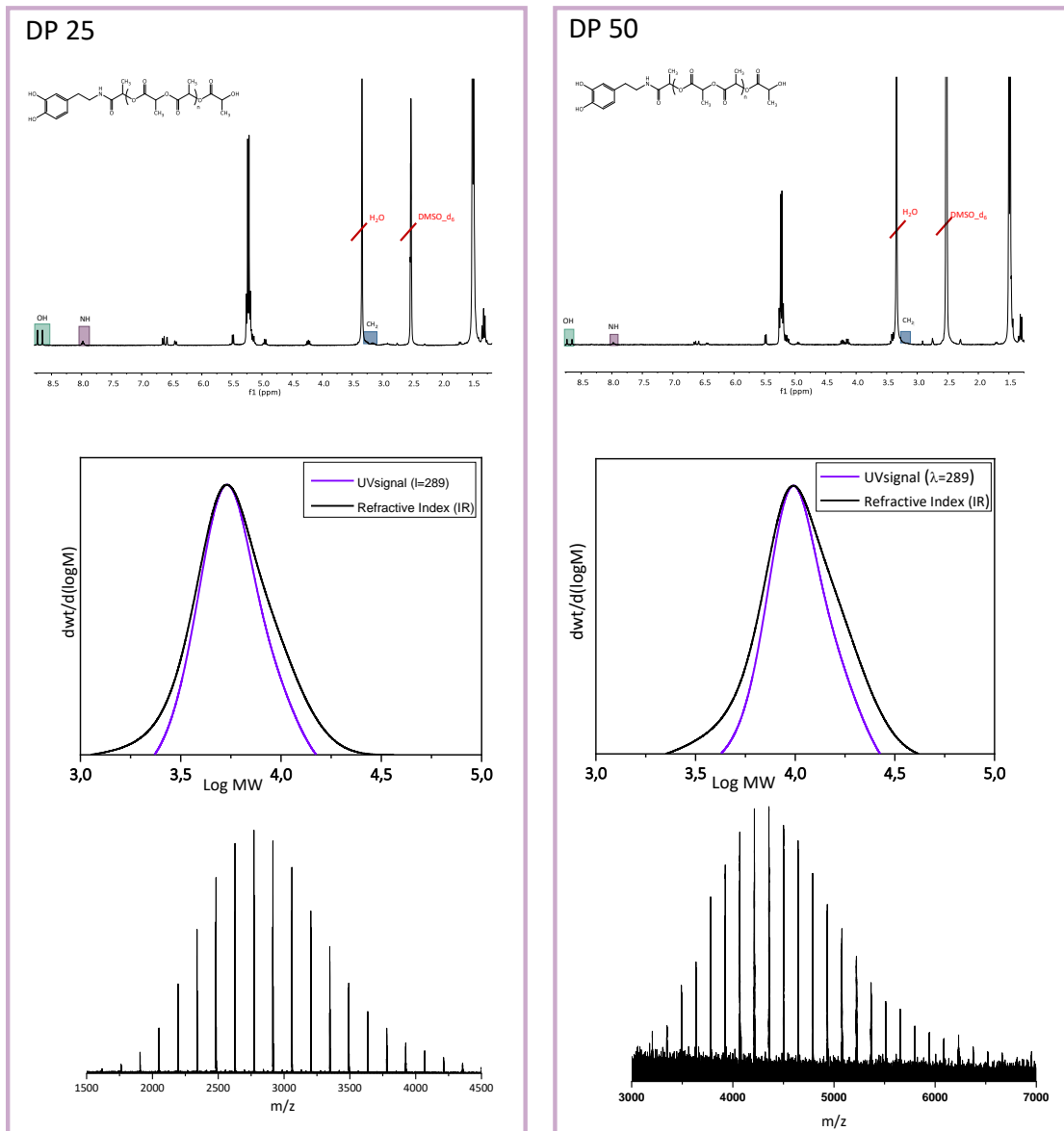


**Figure 4.8.** Left figure for DP 25 and right figure for DP 50.  $^1\text{H}$  NMR spectra in  $\text{DMSO-d}_6$  for Catechol end-functional PLLA, SEC trace with UV (289 nm wavelength) and refractive-index signals for semitelechelic catechol PLLA. And finally MALDI-TOF spectra for semitelechelic catechol-PLLA.

It is shown that the synthesis of semitelechelic catechol-PLA can be carried out, now it will be tested if this new one can be post-functionalized. One of the advantages of catechol units is their ability to be easily oxidized into highly reactive o-quinones allowing its functionalization either by Michael addition or Schiff base reaction. The reaction between catechols and amines is vital in biological processes such as the crosslinking of adhesive proteins by marine organism[41]. In order to convert the catechol to ortho-quinone,



the catechol was oxidized using 2,3-Dichloro-5,6-dicyano-1,4-benzoquinone (DDQ) (1 equiv.) in  $\text{CDCl}_3/\text{CH}_3\text{OH}$  solution. The solution changes color indicating that some reactions might have been taking place. To verify the quinone formation, we followed the change in the characteristic signals of dopamine aromatic region by  $^1\text{H}$  NMR spectroscopy. We found that due the higher electron-withdrawing property of the carbonyl groups there is an effect in the shielding effect on the protons confirming that the catechol was converted to ortho-quinone. Figure 4.9 show the representative  $^1\text{H}$  NMR spectra of the reaction of oxidized catechol and hexylamine. As soon as the reagents were mixed, the solution turned dark red. The amine can react through two different mechanisms with the o-quinone via the Michael addition or via Schiff base reaction. When the Michael addition is carried out, the amine attach to the quinone in beta position, and via Schiff base an imine group is formed[9,42]As expected hexamine has been introduced through two mechanisms, on the one hand the peaks corresponding to the Michael addition (5.1 and 5.5 ppm) are observed together with the peaks attributed to the formation of imine (5.7, 5.8 and 6.6 ppm).

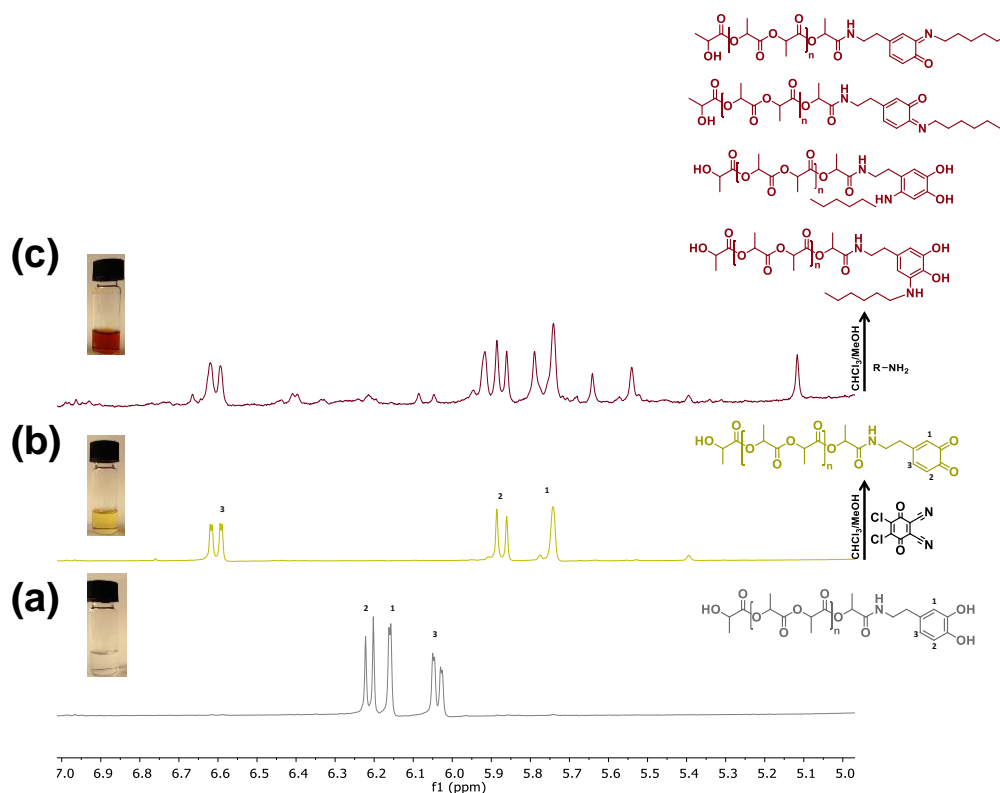


**Figure 4.9.** Scale spanned  $^1\text{H}$  NMR of catechol-PLLA (a) before oxidation; (b) after oxidation and (c) after post-functionalization with hexamethylenamine.

Other ability of catechol is reduce metal ions to metal nanoparticles. For instance, elemental AgNPs ( $\text{Ag}^0$ ) with small particle sizes were already prepared by adding a silver nitrate ( $\text{AgNO}_3$ ) aqueous solution to a catechol containing polymers<sup>10</sup>. Indeed, the catechol can reduce the  $\text{Ag}^+$  into  $\text{Ag}^0$  while the polymer can stabilize the so-formed nanoparticles. Therefore, we explored the utilization of catechol end-functional PLLA for the synthesis of AgNPs using the catechol group as reducing agent and the PLLA with a degree of polymerization of 50 polymer chain as steric stabilizer. For comparative purposes PLLA without catechol units was also investigated as precursor for the synthesis of AgNPs. In this regard, PLLA with a degree of polymerization of 50 was synthesized using phenethylamine as initiator (Table 4.2, entry 9). The formation of the silver NPs was monitored with respect to time by extinction spectroscopy. A single, narrow surface plasmon

resonance band (SPRB) with a maximum at 402 nm and a full width at half maximum (FWHM) of 89 nm was obtained for the polymer-Ag system, which is indicative of the formation of non-aggregated, uniformly-sized nanoparticles (Figure 4.10a). A yellowish coloration of the dispersion as well as the transmission electron microscopy (TEM) images confirmed the synthesis of these AgNPs (Figure 4.10a). The nanoparticles size distribution was studied using the ImageJ software where particles smaller than 50 nm were observed (Figure 4.10a). In the control experiment without catechol units we did not observe any nanoparticles formation (Figure 4.10b).

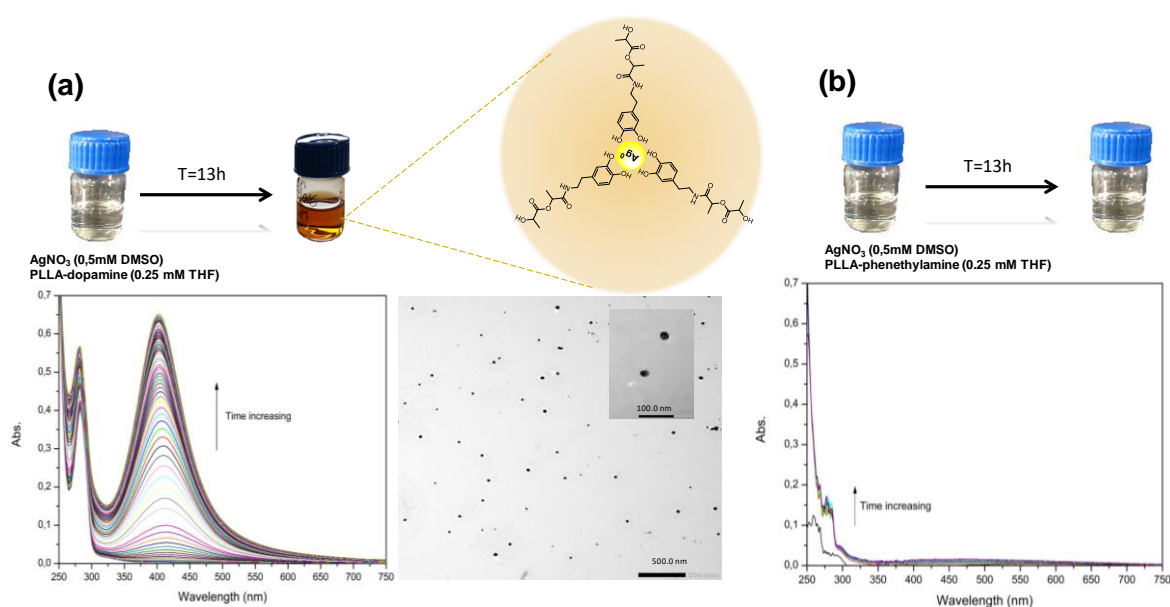


**Figure 4.10.** (a) The progress of the  $\text{Ag}^+$  reduction in the presence of catechol-PLLA studied by extinction spectroscopy and TEM image of AgNPs stabilized by the polymer; (b) The progress of the  $\text{Ag}^+$  reduction in the presence of PLLA-phenethylamine studied by extinction spectroscopy.

### 4.3. 3D printing of PLA/PLA-DA blends

The synthesis of polylactide with dopamine (PLA-DA) was carried out according to the previous section. Low molecular weight of PLA-DA was obtained from the synthesis resulting in poor mechanical properties.

Therefore, PLA-DA was blended with higher molecular weight PLA to improve its mechanical properties.

Due to the difference in molecular weights, it was not possible to print these blends by melt-printing. Low molecular weight PLA-DA degrades before the high molecular weight PLA melts. Therefore, blends were printed by solution-printing method.

Before the 3D printing process the miscibility of the blends was analyzed. When blends are miscible, they behave like a single-phase material [20,43] showing a single transition temperature. Therefore, the thermal properties of the blends were analyzed. As shown in Figure 4.11, blends with 30 wt. % of PLA-DA or more showed two enthalpic peaks related to both of the polymer melt energies. However, blends having 10 wt. % and 20 wt. % of PLA-DA show a single melting peak. This peak was lower than 175 °C, a small displacement respecting to neat PLA, demonstrating the miscibility of both polymers.

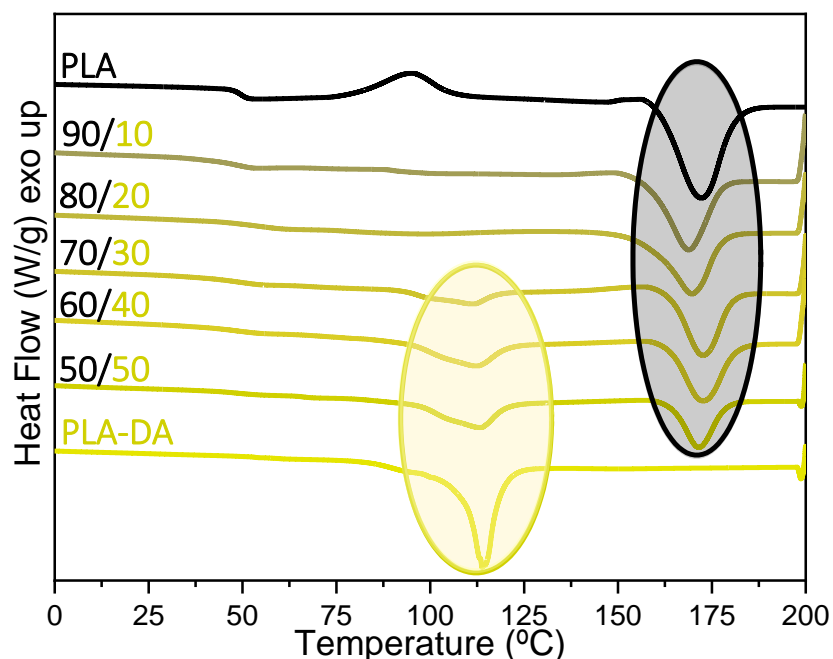


Figure 4.11. DSC spectrum for blends of PLA/PLA-DA and neat PLA.

Once analyzed the thermal behavior the homogeneous blend having the most dopamine/polylactide proportion was selected for 3D printing, the 80/20 blend.

As mentioned before, materials were printed in solution. To prepare the polymer blend, first the high molecular weight PLA was dissolved in chloroform (30 wt %) for 48 h, then, a few hours before starting the impression, the PLA-DA was added in the PLA. In this way, the oxidation of catechol during the dissolution of the material was avoided. Once both materials (PLA and PLA-DA) were dissolved, the blend was introduced into the low temperature cartridge and was printed at 20 °C. Scaffolds for drug-release were built in 9 min. The printing conditions are shown in Table 4.3. Reproducibility of the scaffolds for both cases, neat PLA and PLA/PLA-DA, is ensured by using the same computer aided design (CAD) model for each frame, and by the high XYZ axis resolution of the Bioplotter (0.001 mm).

**Table 4.3.** Printed condition for the neat PLA and Blend PLA/PLA-DA 80/20.

MATERIAL	TEMPERATURE (°C)	PRESSURE (ATM)	SPEED (MM/SEG)	POST-FLOW (SEG)	PRE-FLOW (SEG)
PLA	25	5	3.5	0.11	0.04
PLA/PLA-DA(80/20)	25	5	3.1	0.03	-0.02

The scaffold of 55% porosity was obtained by printing a 500 µm interconnected 90 ° square-like inner morphology. The filament used had 0.25 mm.

#### 4.4. Biological activity of PLA/PLA-DA scaffolds

In drug delivery, most of union bonds between drug and material were attained by either physical or secondary chemical bonds, the predominant interaction being hydrogen bonding. Consequently, several functional groups such as hydroxyl, carboxyl and other hydrogen bond-forming

functional groups can contribute to union with the drug and material. Blends of PLA/PLA-DA were able to adsorb/release drug thanks to the adhesiveness of catechol group. As previously observed, the polymer alone has the ability to generate silver nanoparticles or even to oxidize. In this case, levofloxacin will be used again since it has a fluoroquinone group which can be attached at catechol groups, and thus promote drug adsorption/release from these materials.

To analyze the unions between drug and the material a quartz crystal microbalance (QCM) was used. This technique is a high sensitive instrument to measure the mass and structural changes occurring to a layer. When the drug is adsorbed into the polymer films, simultaneous changes in the Frequency and Dissipation (the frequencies corresponding with the harmonic frequencies of crystal) of quartz crystal can be detected. The (QCM) has the ability to sequentially measure multiple frequencies, i.e. it measures different frequency/dissipation harmonics, allowing to measure the depth to which the drug penetrates into the material, that is, each harmonic shows specific depth within the material [44].

In order to be able to compare the results obtained by means of QCM, the characteristics of the films have to be as similar as possible, because the thicknesses of the films can affect the QCM results. Therefore, the films were prepared by spin-coating and subsequently characterized by Atomic Force Microscopy (AFM). In order to control the thickness of the samples, first of all samples of different concentrations prepared at different rotational speeds were characterized by AFM. Thickness of 60 nm was found to be common for the three materials, neat PLA, PLA-DA and PLA/PLA-DA (see Figure 4.12). Therefore, a solution of 0.5 Vol % was used for the case of neat PLA and 80/20 blend, while 2 Vol % for PLA-DA.

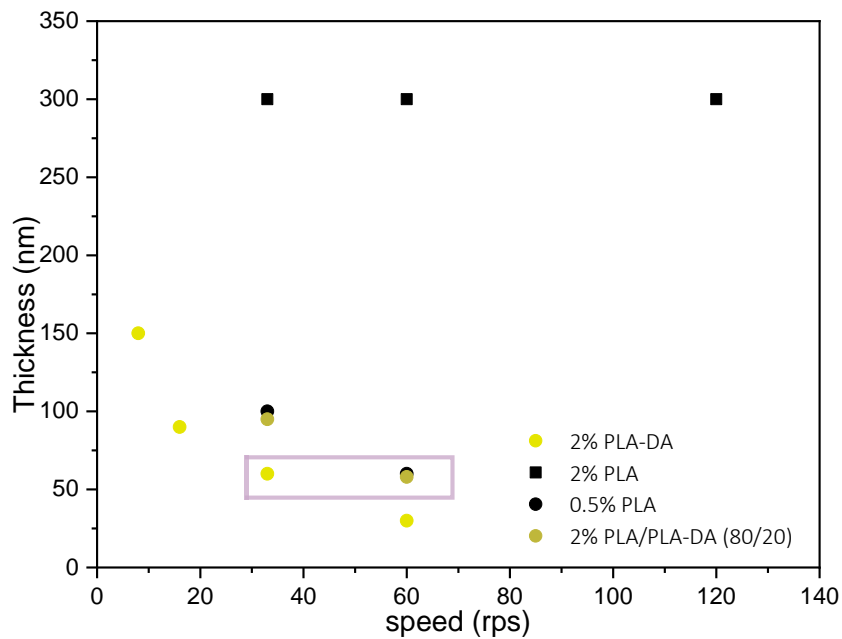


**Figure 4.12.** Thickness of neat PLA, neat PLA-DA and blend of PLA/PLA-DA (80/20).

Once the common thicknesses were obtained the QCM tests were carried out. If the drug is deposited or penetrates the surface of the film, a change in frequency and dissipation will be observed. In this case, except for the first harmonic, which had high noise levels, the higher harmonics overlapped each other, thus only the third harmonic was represented as shown in the Figure 4.13.

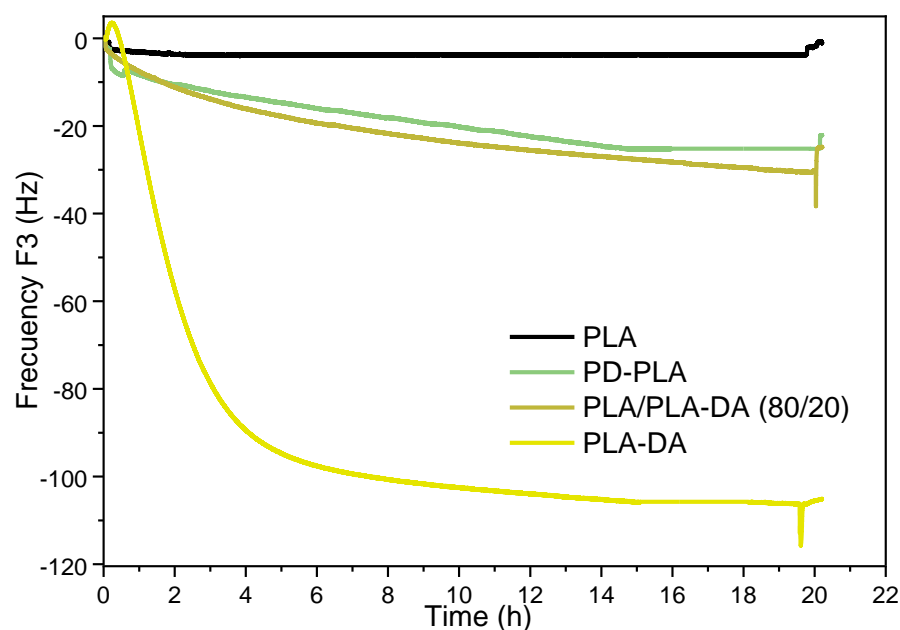


**Figure 4.13.** Third harmonic Frequency (F3) versus time.

Figure 4.13 shows the changes in frequency as a function of time. The drug adsorption process on the polymer-coated gold QCM-D crystal was observed. The results show an initial decrease in frequency (F3), followed by a slower shift until a plateau was obtained. When the chamber is rinsed with buffer, a small increase of frequency was observed.

In addition, the Sauberry equation allows to calculate the amount of drug that each system is able to adsorb. As expected, the neat PLA does not have the capacity to drug adsorption, while the functional PLA with dopamine (PLA-DA) has the highest drug adsorption capacity, adsorbing  $462 \pm 27 \text{ ng cm}^{-2}$ . While the PLA coated with polydopamine (PD-PLA) has an adsorption capacity of  $121 \pm 2 \text{ ng cm}^{-2}$ .

Surprisingly, the PLA-DA even having less dopamine have a greater capacity to absorb drugs than the polydopamine coated one. This result might indicate polydopamine uses some catechol groups to adhere to the polymer (by either -OH and pi-pi bonds) leaving others free to interact with the drug, while PLA-DA has all catechol groups free to interact with the drug (see Figure 4.14). When PLA-DA was blended with high molecular PLA very similar drug adsorption ( $159 \pm 7 \text{ ng cm}^{-2}$ ) as that of the polydopamine-coated system was observed.

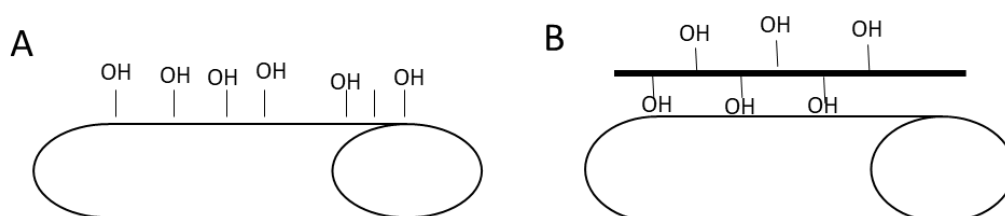


**Figure 4.14.** A) Functional polymer (PLA-DA) B) PLA coated with polydopamine.

Once the adsorption of the polymers at pH 10 was analyzed the release behavior was analyzed. The assays confirm the weak bonds established



between the drug and the polymer, such as Van der Waals, TT-TT or hydrogen bonds.

The *in vitro* drug release assays of PLA/PLA-DA and PLA scaffolds (as control) with levofloxacin were carried out at different pH values: a buffer at pH 5 for simulating an infectious process, and PBS at pH 7.4 for simulating normal physiological conditions.

After finishing the adsorption process, all the scaffolds were washed with a trizma buffer (pH 10) to remove the drug inside of the porous, thus drug release only refers to the bonding of levofloxacin with dopamine.

Figure 4.15 shows the drug release of pH 5 and pH 7. In pH 5 the drug release of both systems (PLA/PLA-DA (80/20) and PD-PLA) showing similar behavior is observed. A burst release releasing 60% of the drug during the first 24 h is observed followed by a slower release until the maximum is reached. As expected, the release of PLA/PLA-DA is slightly higher due to higher drug adsorption (Figure 4.13), but there is no great difference between one system and another despite the difference in the addition of dopamine into scaffold. In the PLA there is a small release due to the drug that was trapped in the porous.

At pH 7 (Figure 4.15), a small drug release was observed, which occurred during the first 8 h. The drug release was due to the drug that was trapped in the pores of the scaffolds, since, in the 3 systems, a very similar behavior was observed.

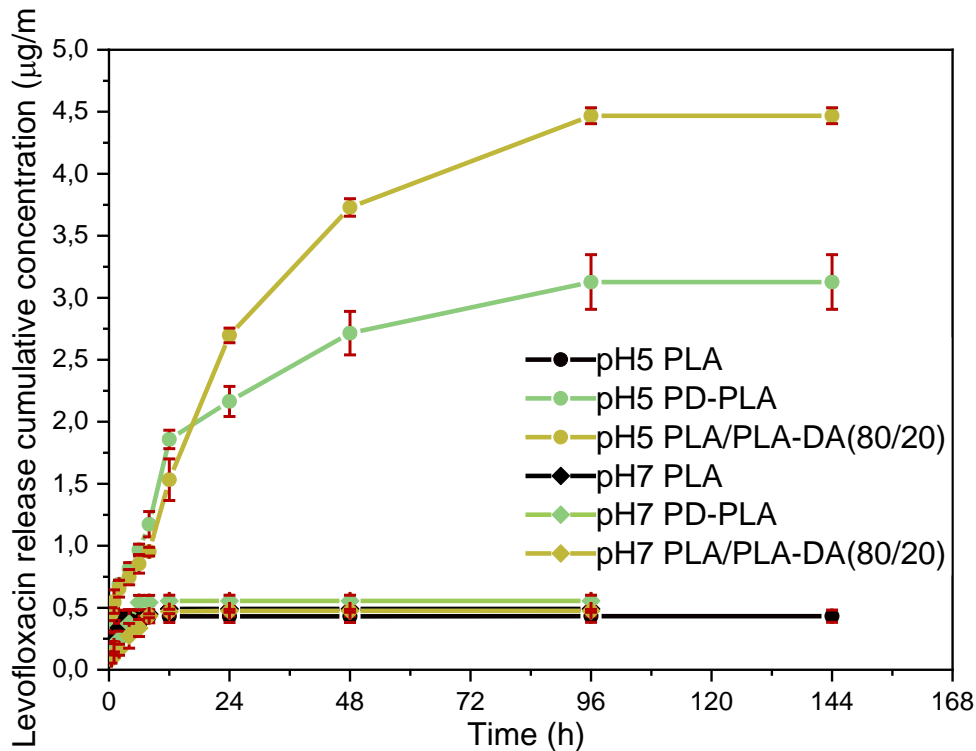


**Figure 4.15.** Release profiles over time of levofloxacin in neat PLA, polydopamine coated neat PLA (PD-PLA) and the blend of PLA/PLA-DA (80/20) at pH 7 and pH 5

At different pH the levofloxacin and dopamine molecules suffer ionic changes. As can be seen in Figure 4.16 in the levofloxacin molecule 6-carboxylic acid and the N4 piperazinyl group are present with pKa values of 6.1 and 8.2, respectively [45]. Concerning to the dopamine, it has a pKa values of:  $pK_{a1} = 8.71$  (phenol);  $pK_{a2} = 10.90$  (amine);  $pK_{a3} = 13.68$  (phenol) (est). Regarding the interactions between the molecules, it can be stated that at pH 10 and 7.4 levo molecules adhere and are retained on the surface of the catechol when cationic forms are stable and at pH 5 the levo molecule is released, probably due to the protonation of the moieties.

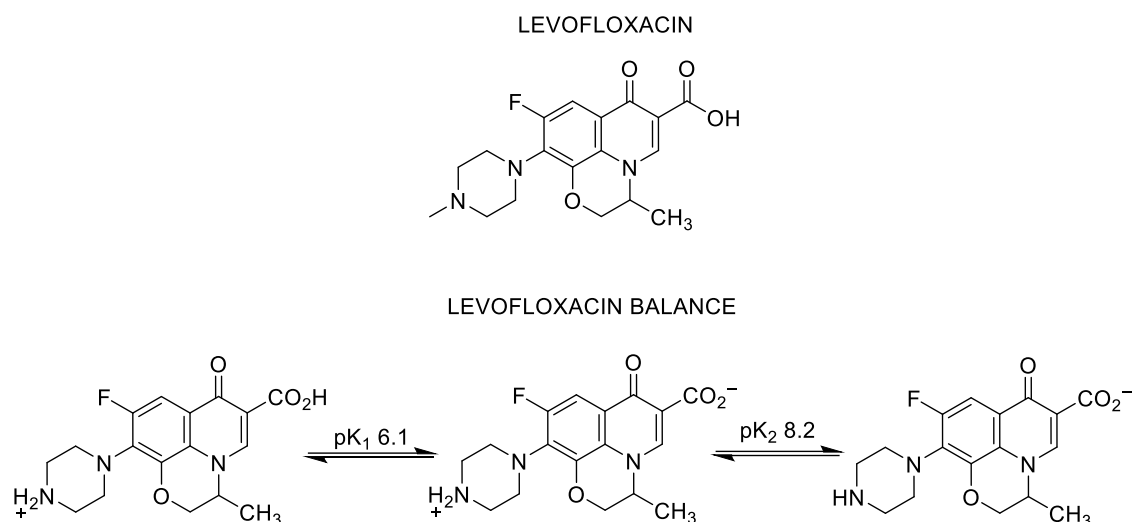
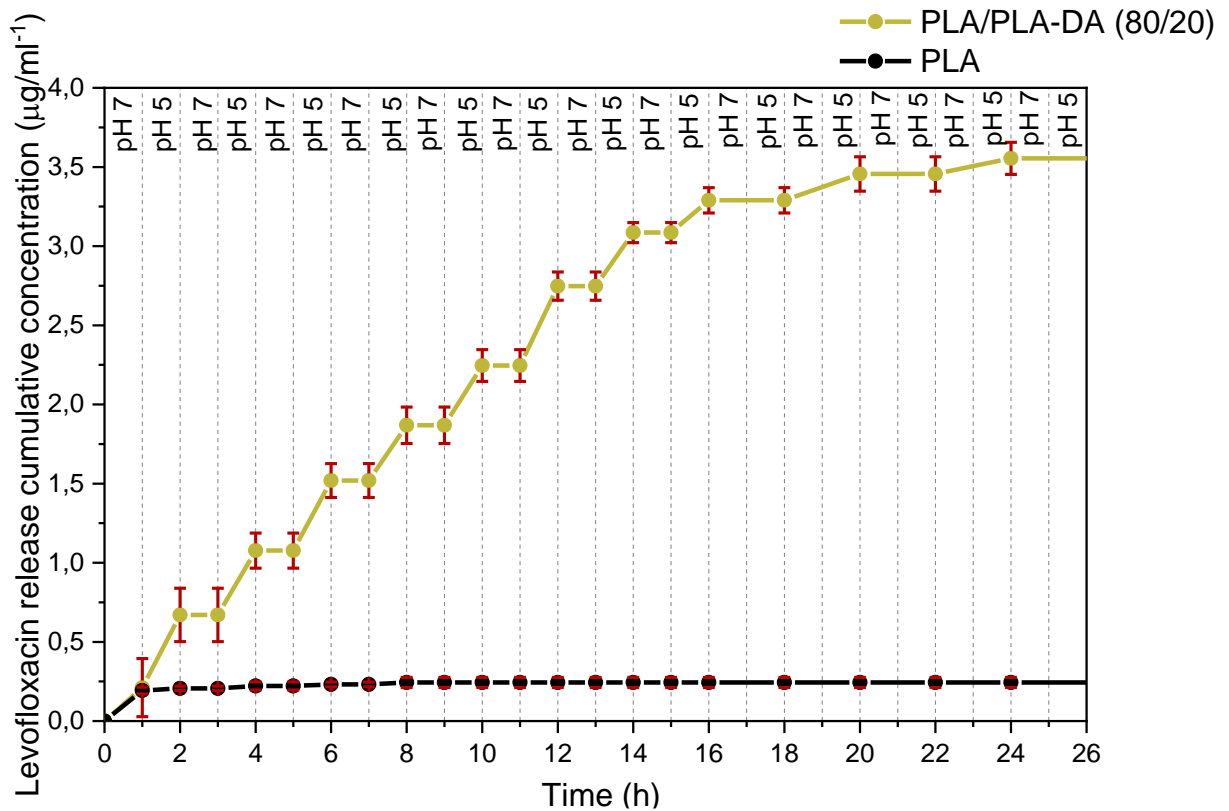


Figure 4.16. Levofloxacin balance in different pH  
In advance, it was decided to continue analyzing drug release only with the PLA/PLA-DA system, due to the better mechanical properties.

Therefore, it was decided to do a test with pH changes every hour, to check if the drug release could be triggered and stopped with the pH change. The scaffolds were first immersed in pH 7 and kept for one hour and then immersed at pH 5 for another hour and so on successively.

Figure 4.17 shows a selective release as previously predicted. It is observed how there is a small release during the first immersion at pH 7, being this phenomenon associated to the drug which has been retained inside the pores. But in general, the curve of the release stops even it is submerged at a pH 7 and the tendency has a more marked release in the first 14 hours.



**Figure 4.17.** Selective release profiles over time of levofloxacin in neat PLA and PLA/PLA-DA (80/20) at pH7 and pH 5

Summarizing, the release of levofloxacin from PLA/PLA-DA scaffolds was pH dependent. It is possible to control the drug release with the pH: specifically drug release occurs in acidic pH (at pH5, as in infection conditions) and do not occurs in neutral pH (at pH 7, as normal conditions). The drug-scaffold interaction is smart and reversible: allowing levofloxacin only to be released when it is necessary.

Figure 4. 18 shows metabolic activity of cells seeded in scaffolds of blends of PLA/PLA-DA with and without levofloxacin (the last one as control). The metabolic activity displayed in this figure was normalized at each time-point with the metabolic activity of HeLa. No significant differences were observed in the metabolic activity of Hela with respect to the control, indicating normal metabolic activity of cells seeded on the samples developed in this work.

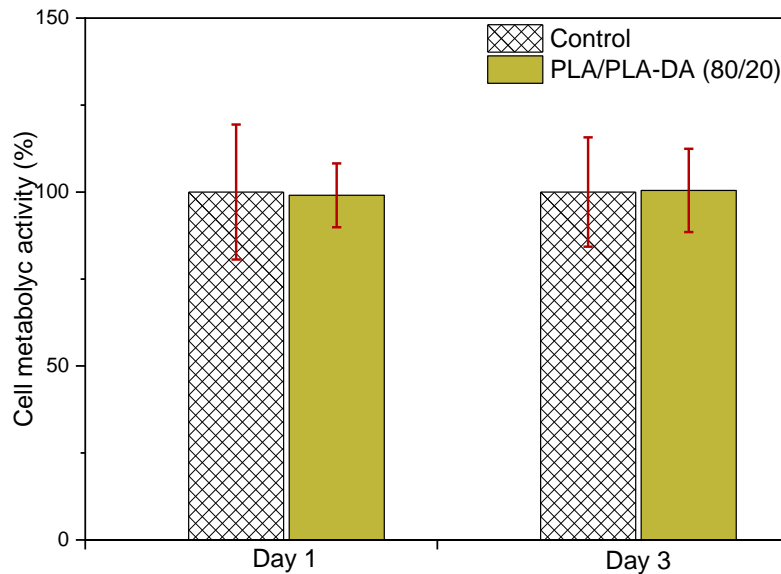


Figure 4. 18. Metabolic activity of HeLa cells.

Figure 4.19 shows cells onto the levofloxacin contained scaffolds under fluorescence microscopy. The cells are attached to the material and have similar size and quantity. In contrast the pores of scaffolds are free of cells. Therefore, it can be concluded that the presence/release of levofloxacin does not have influence in the metabolic activity of cells.

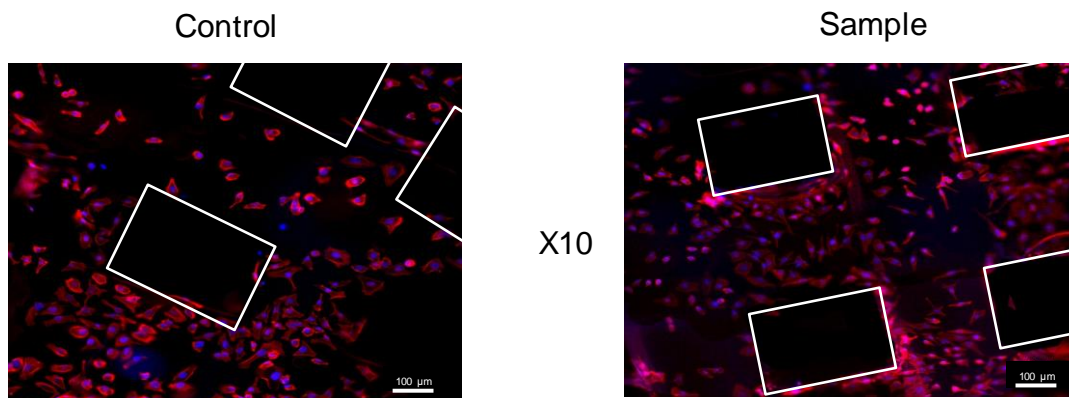


Figure 4.19. Cells onto scaffolds with levofloxacin.

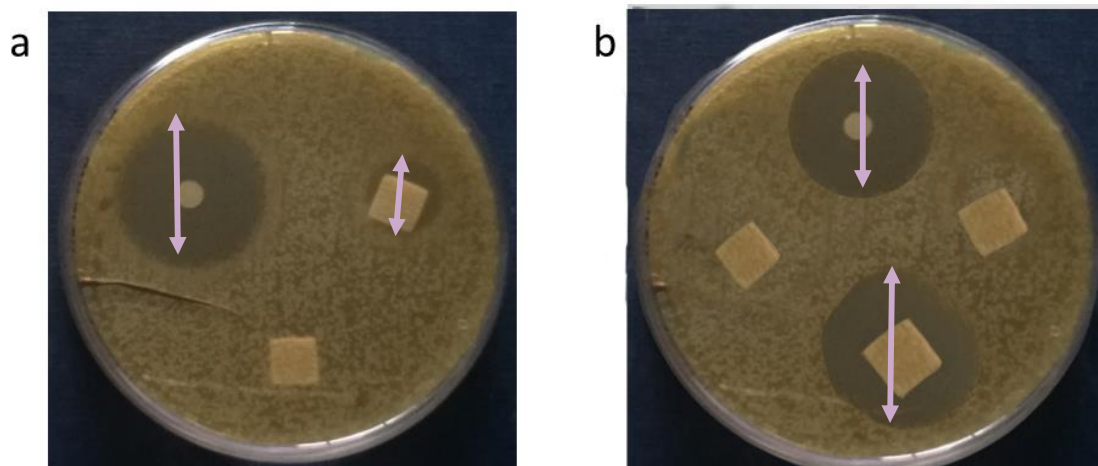
Finally the efficacy of the drug was analyzed using the Agar diffusion test. This test was carried out with *Staphylococcus aureus* (*S.aureus*) bacteria. The *S.aureus* was chosen due to its ability to adhere and form biofilms (both in implants and bone) among bone-associated infections [46].

Table 4.4 shows the results of agar diffusion test to neat PLA (as negative control), neat PLA-levofloxacin, blend of PLA/PLA-DA (as negative control), blend of PLA/PLA-DA-Levofloxacin and a disk of 5µg of levofloxacin (as a positive control). It can be observed how the samples with attached levofloxacin show a big area of inhibition, while the samples that do not contain antibiotics do not show this area of inhibition.

**Table 4.4.** Inhibition zone diameter for PLA, PLA-Levofloxacin, PLA/PLA-DA and (PLA/PLA-DA)-Levofloxacin

Sample	Inhibition zone diameter (mm)
(PLA/PLA-DA)-Levofloxacin	39±1
PLA/PLA-DA	0
PLA-Levofloxacin	17±4
PLA	0
Levofloxacin disk (5 µg)	28±0

PLA-levofloxacin has a small zone of inhibition despite not adsorbing the drug (see Figure 4.20a). This is due to the drug trapped inside of porous. No inhibition zone is observed for the sample (PLA/PLA-DA scaffold) (Figure 4.20b) without antibiotic adsorption (negative control).



**Figure 4.20.** Agar diffusion test for a) PLA and b) PLA/PLA-DA

Regarding the agar test, it can be concluded that PLA/PLA-DA blend with levofloxacin inhibits the bacterial growth demonstrating the validity of this polymer as a smart drug delivery and 3D printable system.

## 4.5. Conclusion

To improve the biological activity of the polylactides, it was decided to introduce a catechol at the end of the chain.

In this work, the controlled organocatalyzed ROP of L-Lactide using dopamine as initiator is shown. It was demonstrated that the dopamine can be used as initiator for the ring-opening polymerization of cyclic monomers such as L-Lactide in the presence of triethylamine as catalyst. The polymers were analyzed by  $^1\text{H}$  NMR, SEC-IR and MALDI-TOF and the results confirmed the controlled nature of the polymerization and end-group fidelity. We show that this catechol end-functional PLA polymer can be easily converted to highly reactive ortho-quinone using 3-Dichloro-5,6-dicyano-1,4-benzoquinone oxidizer. After the oxidation step, we confirmed that the catechol-PLA polymer can be post-functionalized with amines. Besides the ability of catechol to be post-functionalized, we also confirmed the ability of catechol functionalized PLA to reduce metal ions to metal nanoparticles, studying the formation of silver nanoparticles.

Not only this, it was shown that adding dopamine to lactide creates an ideal polymer to adhere and release drugs, but due to the low molecular weight this polymer could not be printed. Therefore, it was blended with a high molecular weight PLA. Different blends were analyzed to obtain optimal properties. The best blend was 80/20 since it was the one with the highest content of dopamine and it was still homogeneous (miscible), which allowed printing it having the same mechanical and biological properties. It was

observed how this blend was effective to adsorb and release drugs in a controlled manner at pH 5 and not at pH 7, which means that the drug is going to be released when there is an infection, that is, when it is necessary. Moreover, it also showed an antibacterial effect without damaging the cells.

## 4.6. Material and experimental method

### 4.6.1. Materials

High molecular polylactide ( $100,000 \text{ gmol}^{-1}$ ) (PLA) have been supplied by from Purac-Corbion. L-lactide (LA) was obtained from Futerro (Escanaffles, Belgium), and it was recrystallized and dried prior to use. Triethylamine (TEA), dopamine hydrochloride benzoic acid, Levofloxacin, Dulbecco's modified Eagle's medium (DMEM), fetal bovine serum (FBS), Hank's balanced salt solution (HBSS) and penicillin-streptomycin (PS) solution were purchased from Sigma Aldrich (St. Louis, MO, USA) and were dried under vacuum for 24 h. Dichloromethane (DCM) ( $\geq 99\%$ ) and tetrahydrofuran (THF) ( $\geq 99\%$ ), chloroform, 99% extra dry, methanol and AlamarBlue<sup>®</sup> were attained from ThermoFisher Scientific (Madrid, Spain) and used as received. *N,N*-Dimethylformamide (DMF) was acquired from SeccoSolv (St. Louis, MO, USA). Finally the Human cervical cancer cells (HeLa).

### 4.6.2. Synthesis of L-Lactide

#### Synthesis of L-lactide Initiate by dopamine.

All reaction is carry out in a nitrogen-purged glovebox. Dopamine hydrochloride was dissolved in the DMF, then the TEA is added to a solution of dopamine, and L-lactide in  $\text{CHCl}_3$ . The solution was stirred at room temperature for 24 hours till complete de O-ring polymerization ( $^1\text{H}$  NMR monitoring). The reaction catalyst was quenched with an excess of benzoic



acid and the polymer solution was precipitate into cold methanol, centrifuged and dried to obtain a white solid (yield 80%).  $^1\text{H}$  NMR (300 MHz, Chloroform- $d$ )  $\delta$  6.89 – 6.55 (m, 2H), 6.27 (t,  $J$  = 5.7 Hz, 1H), 5.20 (ddt,  $J$  = 8.8, 7.9, 7.0 Hz, 20H), 4.38 (q,  $J$  = 6.9 Hz, 1H), 3.49 (d,  $J$  = 6.0 Hz, 1H), 2.73 (s, 1H), 1.66 – 1.54 (m, 62H).

### **Synthesis of L-lactide Iniciate by phenethylamine.**

The reaction is carry out in a nitrogen-purged glovebox. Phenethylamine was dissolved in the DMF, them L-lactide was mixed whit phenethylamine and TEA (0.25) finally it was added  $\text{CHCl}_3$  during 24 hours still complete de ROP. The reaction was precipitate into cold methanol, centrifugate and dried to obtain a white solid.

### **Synthesis of Silver Nanoparticles (AgNPs)**

The synthesis of AgNPs was carried out by the reduction of  $\text{Ag}^+$  to  $\text{Ag}^0$ . The polymer Catechol-PLA (DP = 50) acted as both the reducing agent and the stabilizer of AgNPs. The polymer solution with a 0.25 mM effective dopamine concentration was obtained by dissolving Catechol-PLA (2.8 mg) in 3 mL of THF.  $\text{AgNO}_3$  (0.5 mM, 0.25 mg, 0.0015 mmol of  $\text{Ag}^+$ ) dissolved in 100  $\mu\text{L}$  of DMSO was then added to the polymer solution and the mixture stirred for 13 h at 25 °C. Extinction spectroscopy and transmission electron microscopy (TEM), were used to study the formation of the AgNPs over time (PLA dopamine-Ag dispersions were obtained).

#### **4.6.3. Characterization of the PLA-DA polymer**

**$^1\text{H}$  and  $^{13}\text{C}$  Nuclear Magnetic Resonance (NMR):**  $^1\text{H}$  and  $^{13}\text{C}$  NMR spectra were recorded at room temperature on Bruker spectrometers (Bruker, Billerica, MA, USA) operating at 300 MHz, using deuterated chloroform ( $\text{CDCl}_3$ ) as solvent

**Size exclusion chromatography (SEC):** SEC was performed in THF at 30 °C using a Waters chromatograph (waters chromatography, Milford, MA, USA) equipped with four 5 mm Waters columns (300 mm × 7.7 mm) connected in series with increasing pore sizes (100, 1000, 105, 106 Å). Toluene was used as a marker. Polystyrene of different molecular weights, ranging from 2100 g·mol<sup>-1</sup> to 1,920,000 g·mol<sup>-1</sup>, were used for the SEC calibration.

**MALDI-TOF:** Mass Spectrometry measurements were performed on a Bruker Autoflex Speed system (Bruker, Billerica, MA, USA) instrument equipped with a 355 nm Nd:YAG laser. All spectra were acquired in the positive-ion reflection mode (accelerating voltage 20 kV, pressure 5 × 10<sup>-6</sup> mbar). Samples were dissolved at concentration of 10 g·L<sup>-1</sup> in THF.

**UV-Vis spectroscopy:** UV-Vis spectroscopy was performed on a Shimadzu UV-2550 spectrophotometer using 1 cm path length quartz cells. The polymer Catechol-PLA acted as both the reducing agent and the stabilizer of AgNPs. The polymer solution with a 0.25 mM effective dopamine concentration was obtained by dissolving Catechol-PLA (2.8 mg) in 3 mL of THF. AgNO<sub>3</sub> (0.5 mM, 0.25 mg, 0.0015 mmol of Ag<sup>+</sup>) dissolved in 100 μL of dimethyl sulfoxide (DMSO) was then added to the polymer solution and the mixture stirred for 13 h at 25 °C.

**Cyclic Voltammetry:** electrochemical measurements were performed on an Autolab PGSTAT302N potentiostat (Metrohm Autolab, Utrecht, The Netherlands) using the standard three-electrode cell with a glassy carbon electrode (GC, 0.07 cm<sup>2</sup> area) and platinum plate as working (WE) and counter (CE) electrodes, respectively and an Ag/AgCl (3 M KCl) reference electrode. The PLA-catechol electrodes were drop-casted on GC electrode from a dichloromethane solution. Cyclic voltammetry (CV) was performed

from  $-0.25$  V to  $1.0$  V vs. Ag/AgCl at various scan rates in  $0.1$  M perchloric acid aqueous solution ( $\text{HClO}_4$ , Sigma-Aldrich, St. Louis, MO, USA).

#### 4.6.4. Characterization of blends

Due to the low molecular weight of the PLA-DA obtained during the synthesis, blends with commercial and high molecular weight PLA were obtained to improve the mechanical properties. Blends of PLA/PLA-DA were carried out by solvent/casting, for avoiding the degradation of the polymer with lower molecular mass, in 90/10, 80/20, 70/30, 60/40 and 50/50 weight proportions.

**Differential scanning calorimetry:** Thermal analysis was carried out with a DSC 2920 (Waters-TA Instruments) under a nitrogen atmosphere at a velocity of  $20$  °C/min to verify the miscibility of the blends.

The blends were miscible as they behave like a single-phase material.

**3D printing of Polylactides:** Scaffolds were fabricated in a 3D-Bioplotter from Envision TEC. The 3D computer aided drawing (CAD) model of scaffolds was employed. The CAD model was modified before being uploaded to the Bioplotter software (version 3.0.713.1406, Envision TEC), which enables slicing of the model, before 3D-printing.

The geometry of scaffolds for biological test were square-like with  $10 \times 10 \times 10$  mm (length X width X height) dimensions. Pore size was  $500$   $\mu\text{m}$  and it was used a plastic conic needle of  $0.25$  mm inner diameter (layer dimension) for printing. The resulting file was uploaded to the software Visual Machines (version 2.8.126) that allows the user to input the various parameters that control the printer.

The coating of scaffolds of PLA covered with polydopamine (PD) to obtain PD-PLA were obtained as in our previous article using basic pH 8.5 for 24 h followed by filtration and drying in a vacuum oven overnight [47].

#### 4.6.5. Biological activity characterization

**Adsorption/Release test:** To analyze the adsorption of the materials, Quartz Cristal Microbalance (QCM) (Q-sense E4, Gothenburg, Sweden) technique was performed. Gold QCM-D sensors were spin-coated with 40  $\mu\text{l}$  of 5 mg  $\text{ml}^{-1}$  polymer solution (in chloroform), for 20 s at 66 rps. The sensor were used immediately after solvent evaporation for experiments.

Technique of QCM-D was used to analyze the drug adsorption. This technique simultaneously monitors mass and energy dissipation from changes in the resonant frequency and the damping of a vibrating sensor. The Sauerbrey equation[48] was used to calculate the adsorbed levofloxacin mass per unit area.

$$\Delta m = -c \frac{\Delta F}{n} \quad (\text{equation 1})$$

Where:  $\Delta m$  represents the mass Surface density ( $\text{ng cm}^{-2}$ ),  $C$  is a proportionality constant that depends only on the intrinsic properties of the sensor ( $-17.7 \text{ ng Hz}^{-1} \text{ cm}^{-2}$  for this AT-cut quartz sensor),  $\Delta F$  is the frequency shift, and  $n$  is the overtone number.

Release of levofloxacin from scaffolds was tested in two different solution; one of PBS (pH 7) and the other one in buffer saline to simulate an infection (pH 5). In both case, it was used 3 ml of solution at 37 °C in a shaker incubator at 220 rpm. Levofloxacin distribution, throughout 3D scaffolds was evaluated using Lambda 265 from PerkinElmer.

Samples were taken in the following times: 30min, 1h, 2h, 4h, 6h, 8h, 24h, 28h, 32h, 48h, 52h, 72h, 96h, 120h and 144. In all materials, three independent tests were carried out.

**Kirky Bauer (Agar Diffusion test ):**The diffusion disk agar tests were performed under the Clinical and Laboratory Standards (CLSI)[49]. The inoculum was swabbed on Mueller Hinton Agar (Biokar Diagnostics) plates and the scaffolds (one without drug as a negative control) were tested, as well as 5 mg of levofloxacin (positive control). Petri dishes were further incubated (Ultima, Revco) at 37 °C for 24 h. Assays were performed in three independent experiments.

**Cell culture:** Human cervical cancer cells (HeLa) were grown in Dulbecco's Modified Eagle Medium (DMEM) supplemented with 10% fetal bovine serum (FBS) and 1% penicillin and streptomycin (PS). The cells were incubate at 37 °C in an atmosphere of 5% CO<sub>2</sub>.

**Cell Viability Studies:**AlamarBlue® assay was performed to quantify the metabolic activity of HeLA cells in the presence of Levofloxacin. At the selected time points (1 and 3 days), the cells were washed with HBSS and subsequently incubated (6 h, 37 °C, sheltered from light) in 0.5 ml of fresh culture media with AlamarBlue® (10% v/v). Then, 100 µl of assay media was transferred to a 96 well plate, the absorbance at 550 and 595 nm was read on a microplate reader (VarioskanFlash) and the percentage reduction of the dye was calculated.

**Statistics:** Statistical differences were analysed using one-way analysis of variance (ANOVA) and p-values of <0.05 were considered significant. Experiments were performed in triplicate and each assay was repeated three times

## 4.7. Reference

1. Lee, B.P.; Messersmith, P.B.; Israelachvili, J.N.; Waite, J.H. Mussel-Inspired Adhesives and Coatings. *Annu. Rev. Mater. Res.* **2011**, *41*, 99–132, doi:10.1146/annurev-matsci-062910-100429.
2. Kord Forooshani, P.; Lee, B.P. Recent approaches in designing bioadhesive materials inspired by mussel adhesive protein. *J. Polym. Sci. Part A Polym. Chem.* **2017**, *55*, 9–33, doi:10.1002/pola.28368.
3. Moulay, S. Dopa/catechol-tethered polymers: Doadhesives and biomimetic adhesive materials. *Polym. Rev.* **2014**, *54*, 436–513, doi:10.1080/15583724.2014.881373.
4. Ye, Q.; Zhou, F.; Liu, W. Bioinspired catecholic chemistry for surface modification. *Chem. Soc. Rev.* **2011**, *40*, 4244–4258.
5. Lee, H.; Dellatore, S.M.; Miller, W.M.; Messersmith, P.B. Mussel-inspired surface chemistry for multifunctional coatings. *Science (80-. )*. **2007**, *318*, 426–430, doi:10.1126/science.1147241.
6. Patil, N.; Aqil, A.; Ouhib, F.; Admassie, S.; Inganäs, O.; Jérôme, C.; Detrembleur, C. Bioinspired Redox-Active Catechol-Bearing Polymers as Ultrarobust Organic Cathodes for Lithium Storage. *Adv. Mater.* **2017**, *29*, doi:10.1002/adma.201703373.
7. Ribeiro, M.; Ferraz, M.P.; Monteiro, F.J.; Fernandes, M.H.; Beppu, M.M.; Mantione, D.; Sardon, H. Antibacterial silk fibroin/nanohydroxyapatite hydrogels with silver and gold nanoparticles for bone regeneration. *Nanomedicine Nanotechnology, Biol. Med.* **2017**, *13*, 231–239, doi:10.1016/j.nano.2016.08.026.
8. Jus, S.; Kokol, V.; Guebitz, G.M. Tyrosinase-catalysed coupling of

- functional molecules onto protein fibres. *Enzyme Microb. Technol.* **2008**, *42*, 535–542, doi:10.1016/j.enzmictec.2008.02.012.
9. Faure, E.; Falentin-Daudré, C.; Jérôme, C.; Lyskawa, J.; Fournier, D.; Woisel, P.; Detrembleur, C. Catechols as versatile platforms in polymer chemistry. *Prog. Polym. Sci.* 2013, *38*, 236–270.
  10. Charlot, A.; Sciannaméa, V.; Lenoir, S.; Faure, E.; Jérôme, R.; Jérôme, C.; Van De Weerd, C.; Martial, J.; Archambeau, C.; Willet, N.; et al. All-in-one strategy for the fabrication of antimicrobial biomimetic films on stainless steel. *J. Mater. Chem.* **2009**, *19*, 4117–4125, doi:10.1039/b820832h.
  11. Yang, J.; Keijsers, J.; Van Heek, M.; Stuiver, A.; Cohen Stuart, M.A.; Kamperman, M. The effect of molecular composition and crosslinking on adhesion of a bio-inspired adhesive. *Polym. Chem.* **2015**, *6*, 3121–3130, doi:10.1039/c4py01790k.
  12. Yang, J.; Cohen Stuart, M.A.; Kamperman, M. Jack of all trades: Versatile catechol crosslinking mechanisms. *Chem. Soc. Rev.* 2014, *43*, 8271–8298.
  13. Yu, M.; Deming, T.J. Synthetic polypeptide mimics of marine adhesives. *Macromolecules* **1998**, *31*, 4739–4745, doi:10.1021/ma980268z.
  14. Alba, A.; Du Boullay, O.T.; Martin-Vaca, B.; Bourissou, D. Direct ring-opening of lactide with amines: Application to the organo-catalyzed preparation of amide end-capped PLA and to the removal of residual lactide from PLA samples. *Polym. Chem.* **2015**, *6*, 989–997, doi:10.1039/c4py00973h.
  15. Liu, Z.; Hu, B.H.; Messersmith, P.B. Acetonide protection of dopamine for the synthesis of highly pure N-docosahexaenoyldopamine.

- Tetrahedron Lett.* **2010**, *51*, 2403–2405, doi:10.1016/j.tetlet.2010.02.089.
16. Patil, N.; Cordella, D.; Aqil, A.; Debuigne, A.; Admassie, S.; Jérôme, C.; Detrembleur, C. Surface- and Redox-Active Multifunctional Polyphenol-Derived Poly(ionic liquid)s: Controlled Synthesis and Characterization. *Macromolecules* **2016**, *49*, 7676–7691, doi:10.1021/acs.macromol.6b01857.
17. Zhang, X.; Jones, G.O.; Hedrick, J.L.; Waymouth, R.M. Fast and selective ring-opening polymerizations by alkoxides and thioureas. *Nat. Chem.* **2016**, *8*, 1047–1053, doi:10.1038/nchem.2574.
18. Zhang, Q.; Nurumbetov, G.; Simula, A.; Zhu, C.; Li, M.; Wilson, P.; Kempe, K.; Yang, B.; Tao, L.; Haddleton, D.M. Synthesis of well-defined catechol polymers for surface functionalization of magnetic nanoparticles. *Polym. Chem.* **2016**, *7*, 7002–7010, doi:10.1039/c6py01709f.
19. Tavasi, V.; Bettens, R.P.A.; Leong, L.P. Temperature and solvent effects on radical scavenging ability of phenols velmurugan thavasi. *J. Phys. Chem. A* **2009**, *113*, 3068–3077, doi:10.1021/jp806679v.
20. Sarasua, J.R.; Arraiza, A.L.; Balerdi, P.; Maiza, I. Crystallinity and mechanical properties of optically pure polylactides and their blends. *Polym. Eng. Sci.* **2005**, *45*, 745–753, doi:10.1002/pen.20331.
21. Salah, M.; Tayebi, L.; Moharamzadeh, K.; Naini, F.B. Three-dimensional bio-printing and bone tissue engineering: technical innovations and potential applications in maxillofacial reconstructive surgery., doi:10.1186/s40902-020-00263-6.
22. Derby, B. Printing and prototyping of tissues and scaffolds. *Science* (80-



- . ). 2012, 338, 921–926.
23. Zhang, Q.; Luo, H.; Zhang, Y.; Zhou, Y.; Ye, Z.; Tan, W.; Lang, M. Fabrication of three-dimensional poly( $\epsilon$ -caprolactone) scaffolds with hierarchical pore structures for tissue engineering. *Mater. Sci. Eng. C* **2013**, 33, 2094–2103, doi:10.1016/j.msec.2013.01.025.
  24. Fong, E.L.S.; Lamhamedi-Cherradi, S.E.; Burdett, E.; Ramamoorthy, V.; Lazar, A.J.; Kasper, F.K.; Farach-Carson, M.C.; Vishwamitra, D.; Demicco, E.G.; Menegaz, B.A.; et al. Modeling Ewing sarcoma tumors in vitro with 3D scaffolds. *Proc. Natl. Acad. Sci. U. S. A.* **2013**, 110, 6500–6505, doi:10.1073/pnas.1221403110.
  25. Lee, M.K.; Rich, M.H.; Lee, J.; Kong, H. A bio-inspired, microchanneled hydrogel with controlled spacing of cell adhesion ligands regulates 3D spatial organization of cells and tissue. *Biomaterials* **2015**, 58, 26–34, doi:10.1016/j.biomaterials.2015.04.014.
  26. Jiang, J.; Carlson, M.A.; Teusink, M.J.; Wang, H.; MacEwan, M.R.; Xie, J. Expanding Two-Dimensional Electrospun Nanofiber Membranes in the Third Dimension by a Modified Gas-Foaming Technique. *ACS Biomater. Sci. Eng.* **2015**, 1, 991–1001, doi:10.1021/acsbomaterials.5b00238.
  27. Bajaj, P.; Schweller, R.M.; Khademhosseini, A.; West, J.L.; Bashir, R. 3D Biofabrication Strategies for Tissue Engineering and Regenerative Medicine. *Annu. Rev. Biomed. Eng.* **2014**, 16, 247–276, doi:10.1146/annurev-bioeng-071813-105155.
  28. Zhang, J.; Yin, H.M.; Hsiao, B.S.; Zhong, G.J.; Li, Z.M. Biodegradable poly(lactic acid)/hydroxyl apatite 3D porous scaffolds using high-pressure molding and salt leaching. *J. Mater. Sci.* **2014**, 49, 1648–1658, doi:10.1007/s10853-013-7848-x.

29. Park, H.J.; Lee, O.J.; Lee, M.C.; Moon, B.M.; Ju, H.W.; Lee, J. min; Kim, J.H.; Kim, D.W.; Park, C.H. Fabrication of 3D porous silk scaffolds by particulate (salt/sucrose) leaching for bone tissue reconstruction. *Int. J. Biol. Macromol.* **2015**, *78*, 215–223, doi:10.1016/j.ijbiomac.2015.03.064.
30. Hribar, K.C.; Soman, P.; Warner, J.; Chung, P.; Chen, S. Light-assisted direct-write of 3D functional biomaterials. *Lab Chip* 2014, *14*, 268–275.
31. Hollister, S.J. Scaffold design and manufacturing: From concept to clinic. *Adv. Mater.* 2009, *21*, 3330–3342.
32. Jardini, A.L.; Larosa, M.A.; Filho, R.M.; Zavaglia, C.A.D.C.; Bernardes, L.F.; Lambert, C.S.; Calderoni, D.R.; Kharmandayan, P. Cranial reconstruction: 3D biomodel and custom-built implant created using additive manufacturing. *J. Cranio-Maxillofacial Surg.* **2014**, *42*, 1877–1884, doi:10.1016/j.jcms.2014.07.006.
33. Memon, A.R.; Wang, E.; Hu, J.; Egger, J.; Chen, X. A review on computer-aided design and manufacturing of patient-specific maxillofacial implants. *Expert Rev. Med. Devices* 2020, *17*, 345–356.
34. Yang, Y.; Wang, H.; Li, H.; Ou, Z.; Yang, G. 3D printed tablets with internal scaffold structure using ethyl cellulose to achieve sustained ibuprofen release. *Eur. J. Pharm. Sci.* **2018**, *115*, 11–18, doi:10.1016/j.ejps.2018.01.005.
35. Urgan, I.; Chiu, L.; Pierce, A. Three-dimensional drug printing: A structured review. *J. Am. Pharm. Assoc.* **2013**, *53*, 136–144, doi:10.1331/JAPhA.2013.12217.
36. Ryu, J.H.; Messersmith, P.B.; Lee, H. Polydopamine Surface Chemistry: A Decade of Discovery. *ACS Appl. Mater. Interfaces* 2018, *10*, 7523–

- 7540.
37. Ahn, B.K. Perspectives on Mussel-Inspired Wet Adhesion. *J. Am. Chem. Soc.* **2017**, *139*, 10166–10171, doi:10.1021/jacs.6b13149.
  38. Liu, Y.; Ai, K.; Lu, L. Polydopamine and Its Derivative Materials: Synthesis and Promising Applications in Energy, Environmental, and Biomedical Fields. *Chem. Rev.* **2014**, *114*, 5057–5115, doi:10.1021/cr400407a.
  39. Lee, H.; Dellatore, S.M.; Miller, W.M.; Messersmith, P.B. Mussel-Inspired Surface Chemistry for Multifunctional Coatings., doi:10.1126/science.1147241.
  40. Zhang, X.; Jones, G.O.; Hedrick, J.L.; Waymouth, R.M. Fast and selective ring-opening polymerizations by alkoxides and thioureas. *Nat. Chem.* **2016**, *8*, 1047–1053, doi:10.1038/nchem.2574.
  41. Yang, J.; Saggiomo, V.; Velders, A.H.; Cohen Stuart, M.A.; Kamperman, M. Reaction Pathways in Catechol/Primary Amine Mixtures: A Window on Crosslinking Chemistry. *PLoS One* **2016**, *11*, e0166490, doi:10.1371/journal.pone.0166490.
  42. Faure, E.; Lecomte, P.; Lenoir, S.; Vreuls, C.; Van De Weerd, C.; Archambeau, C.; Martial, J.; Jérôme, C.; Duwez, A.S.; Detrembleur, C. Sustainable and bio-inspired chemistry for robust antibacterial activity of stainless steel. *J. Mater. Chem.* **2011**, *21*, 7901–7904, doi:10.1039/c1jm11380a.
  43. Meaurio, E.; Zuza, E.; Sarasua, J.R. Miscibility and specific interactions in blends of poly(L-lactide) with poly(vinylphenol). *Macromolecules* **2005**, *38*, 1207–1215, doi:10.1021/ma047818f.

44. (1) (PDF) Optimal design for studying mucoadhesive polymers interaction with gastric mucin using a quartz crystal microbalance with dissipation (QCM-D): Comparison of two different mucin origins | Sejin Oh - Academia.edu Available online: [https://www.academia.edu/18337552/Optimal\\_design\\_for\\_studying\\_mucoadhesive\\_polymers\\_interaction\\_with\\_gastric\\_mucin\\_using\\_a\\_quartz\\_crystal\\_microbalance\\_with\\_dissipation\\_QCM-D\\_Comparison\\_of\\_two\\_different\\_mucin\\_origins](https://www.academia.edu/18337552/Optimal_design_for_studying_mucoadhesive_polymers_interaction_with_gastric_mucin_using_a_quartz_crystal_microbalance_with_dissipation_QCM-D_Comparison_of_two_different_mucin_origins) (accessed on Apr 20, 2020).
45. Cicuéndez, M.; Doadrio, J.C.; Hernández, A.; Portolés, M.T.; Izquierdo-Barba, I.; Vallet-Regí, M. Multifunctional pH sensitive 3D scaffolds for treatment and prevention of bone infection. *Acta Biomater.* **2018**, *65*, 450–461, doi:10.1016/j.actbio.2017.11.009.
46. Ferreira, M.; Rzhepishevskaya, O.; Grenho, L.; Malheiros, D.; Gonçalves, L.; Almeida, A.J.; Jordão, L.; Ribeiro, I.A.; Ramstedt, M.; Gomes, P.; et al. Levofloxacin-loaded bone cement delivery system: Highly effective against intracellular bacteria and Staphylococcus aureus biofilms. *Int. J. Pharm.* **2017**, *532*, 241–248, doi:10.1016/j.ijpharm.2017.08.089.
47. Larrañaga, A.; Ramos, D.; Amestoy, H.; Zuza, E.; Sarasua, J.-R. Coating of bioactive glass particles with mussel-inspired polydopamine as a strategy to improve the thermal stability of poly(L-lactide)/bioactive glass composites. *RSC Adv.* **2015**, *5*, 65618–65626, doi:10.1039/C5RA09495J.
48. Lopez, A.E.; Moreno-Flores, S.; Pum, D.; Sleytr, U.B.; Toca-Herrera, J.L. Surface Dependence of Protein Nanocrystal Formation. *Small* **2010**, *6*, 396–403, doi:10.1002/sml.200901169.

49. *M02-A12 Performance Standards for Antimicrobial Disk Susceptibility Tests; Approved Standard-Twelfth Edition; 2015;*



## GENERAL CONCLUSION





## General conclusion

In this thesis, two main variants have been studied, firstly, an exhaustive study of extrusion 3D printing for lactide. Secondly, an exhaustive study of PLA/BaSO<sub>4</sub>, PLA/PD-BaSO<sub>4</sub>, and PLA/PLA-DA composites for their use in bone tissue engineering and for their subsequent use in bone fixation implants has been carried out.

Although conclusions are displayed at the end of each chapter, next the general and most important conclusions derived from the results of the research carried out are compiled:

First, for the 3D printing analysis, a rigorous rheological study was carried out, followed by a study of filament welding, ending with a visual study of the scaffolds, for different percentages of PLA inks with chloroform and 1,4-Dioxane. During this work, two rheology models are obtained, which predict the 3D printing parameters. Furthermore, it is shown that, in both cases, the most suitable inks for printing scaffolds were the more concentrated ones. Although PLA/chloroform inks were only suitable for small and low height geometries, as this material shrinks as the layers are printed. Whereas PLA/1,4-dioxane inks are suitable for all geometries and heights.

After learning how to print PLA, improvements to the PLA material are started. Firstly, the toughness and radiopacity were improved. For this goal, the PLA composite is analyzed with different percentages of BaSO<sub>4</sub>, providing the PLA/BaSO<sub>4</sub> blends with radiopacity. Regarding the mechanical properties, it is observed that the tensile modulus and tensile strength remained constant or had a small improvement, while the elongation of these composites increased up to a maximum of 1416%. Once both radiopacity and toughness were improved, dopamine is added to the BaSO<sub>4</sub>

particles to provide the material with biological activity. The dopamine is added in the form of Polydopamine, coating the particulate, and polydopamine allowed the adsorption and release of drug. The adsorbed drug is released in a controlled manner, initially with a more abrupt release and later with a smoother release. In addition, the amount of drug released was effective against *S.aureus* bacteria. Not only that, polydopamine also improved the adhesion between the matrix and the particles, obtaining higher elongations (1887 % respect to PLA) than with the uncoated particles or neat PLA.

Finally, to improve adhesion and drug release, it is decided to add dopamine into the PLA chain. Dopamine is added at the end of the PLA chain. Dopamine is used as an initiator of ROP of lactide. In addition, an organocatalyst (TEA) is used to carry out this synthesis, so that the catalyzer can be completely removed from the polymer. Nevertheless, the most important aspect of this synthesis is realized in one-step synthesis without the OH protection of the catechols.

Different molecular weights of PLA-DA are synthesized, choosing the one with the lowest molecular weight to have the highest amount of dopamine; in addition, blends were made with PLA of high molecular weight to improve the mechanical properties. The miscible blend with the highest amount of dopamine was the PLA/PLA-DA 80/20.

The drug absorption of the 80/20 scaffolds and the PLA scaffolds coated with polydopamine showed the same adsorption, although the 80/20 blends have lower amount of dopamine. Drug release was shown to be pH controllable in the 80/20 blends, for instance, the drug was released only at acidic pH while at neutral pH it was not released. Furthermore, this release

stops if the pH changes to pH 7 and restarts again if the pH drops to acidic values (pH 5). It is confirmed that the amount of drug released was effective against *S. aureus* bacteria, and was not toxic to HeLa cells.

In conclusion, the new systems proposed throughout this thesis PLA/basor4pd and PLA/PLA-da show improved radiopacity, tenacity and biological improvements of PLA thanks to dopamine/polydopamine. Although there is still work to be done to use them as bone fixation devices, it is observed that they are very promising composites for use in tissue engineering and especially as bone fixation devices.



# APPENDIX



## A1. List of Figures

<b>Figure 1.1.</b> Areas involved in tissue engineering .....	30
<b>Figure 1.2.</b> 3D printing process scheme, from the CAD model to the printed object.....	34
<b>Figure 1.3.</b> Schematic of the 3D printing process by material extrusion (FDM) .....	36
<b>Figure 1.4.</b> Schematic of the 3D printing process by material extrusion (DIW) .....	38
<b>Figure 1.5.</b> Different synthesis routes for the production of LA.....	40
Figure 1.6. Enantiomers of lactide acid .....	40
<b>Figure 1.7.</b> The three possible configurations of PLA chain.....	41
<b>Figure 1.8.</b> Life cycle of PLAs; synthesis and degradation.....	42
<b>Figure 1.9.</b> Scheme of the methodology that has been followed to achieved the objectives of the thesis .....	47
<b>Figure 2.1.</b> <i>Schematic diagram of the 3D Bioplotter a) Melted polymer in a high temperature cartridge and b) polymer ink in low temperature cartridge.</i>	
68	
<b>Figure 2.2.</b> Molecular weight change during printing time. The temperature of the cartridge was 195 °C .....	69
<b>Figure 2.3.</b> <i>Viscosity as a function of shear rate for a) PLA solution in chloroform at room temperature and b) PLA solution in 1,4-Dioxane at 50 °C</i> .....	71
<b>Figure 2.4.</b> Printing pressure and rate of PLA inks in chloroform. Real data and predictive data.....	76
<b>Figure 2.5.</b> Printing pressure and rate of PLA inks in 1,4-dioxane. Real data and predictive data.....	77

**Figure 2.6.** Frequency sweep for PLA inks in chloroform at 22 °C. The red line represents the cross-point between  $G'$  and  $G''$  ..... 79

**Figure 2.7.** Frequency sweep for PLA inks in 1,4-dioxane at 10 °C (up) and at 50 °C (bottom). The red line represents the cross-point between  $G'$  and  $G''$ . ..... 80

**Figure 2.8.** Normalized solvent content as a function of the time for C9, C15, D9 and D15 solutions. C#: Chloroform solutions and D#: 1,4-Dioxane solutions. .... 81

**Figure 2.9.** Schematic of simple specimen preparation for *trouser tearing* test..... 82

**Figure 2.10.** Propagation force obtained for different filament length on the samples (C9, C10, C11 and C17). .... 83

**Figure 2.11.** Longitudinal and cross section images of samples C17, C15, C11 and C9 for a filament length of 10 cm ..... 84

**Figure 2.12.** Longitudinal and cross section images of samples D15, D11, D10 and D9 for a filament length of 10 cm ..... 85

**Figure 2.13.** Propagation force obtained for different filament length on the samples (C9, D8, D9 and D10)..... 85

**Figure 2.14.** Crystallinity fraction for different (a) PLA/chloroform inks and (b) PLA/1,4-Dioxane inks. .... 87

**Figure 2 15.** SEM images of PLA inks in chloroform, up images top view of scaffold and bottom images cross section of scaffolds. .... 88

**Figure 2.16** SEM images of PLA inks in 1,4-dioxane, up images top view of scaffold and bottom images cross section of scaffolds. .... 89

**Figure 2.17.** a) Image of C9 scaffold after printing process and b) image of D8 scaffold before and after drying. .... 90



<b>Figure 3.1.</b> Particle size of BaSO <sub>4</sub> (gray) and PD-BaSO <sub>4</sub> (pink) .....	109
<b>Figure 3.2.</b> TEM microscopy images of composites containing 10 wt. % of particles of a) PLA/BaSO <sub>4</sub> and b) PLA/PD-BaSO <sub>4</sub> . .....	110
<b>Figure 3.3.</b> X-radiographies neat PLA, PLA/BaSO <sub>4</sub> and PLA/PD-BaSO <sub>4</sub> composites with 2, 5 and 10 wt. % of BaSO <sub>4</sub> and PD-BaSO <sub>4</sub> . .....	111
<b>Figure 3.4.</b> Stress concentrations in rigid particles (a) induce debonding (b) and shear yielding (c) mechanism.....	113
<b>Figure 3.5.</b> Values obtained from tensile stress-strain behavior of neat PLA, PLA/BaSO <sub>4</sub> and PLA/PD-BaSO <sub>4</sub> composites with 0.5, 1.0, 2.0, 5.0 and 10.0 wt. % of particles. a) Tensile modulus b) elongation at break and c) tensile toughness. ....	115
<b>Figure 3.6.</b> Tensile test specimen after a tensile test, (a) PLA/BaSO <sub>4</sub> 10 wt. % of BaSO <sub>4</sub> and (b) PLA/PD-BaSO <sub>4</sub> 10 wt. % of PD-BaSO <sub>4</sub> . Blue arrows represent stress whitening and blue circles the necking.....	116
<b>Figure 3.7.</b> SEM images of PLA/BaSO <sub>4</sub> composites with (a) 5 and (b) 10 wt.% of BaSO <sub>4</sub> . blue circle pointed voids created by particles. ....	117
<b>Figure 3.8.</b> SEM image of PLA/PD-BaSO <sub>4</sub> composite 10 wt.% of PD-BaSO <sub>4</sub> taken with dispersion of (left) secondary electrons and (right) backscattered electrons. Blue arrows pointed anchored and stretched threads between particles and blue circle particles in threads.....	118
<b>Figure 3.9.</b> Schematic representation of the steps involved in crazing process. 1) earlier stage: debonding and cavitation of the voids; 2) advanced stage: deformed voids initiate craze formation. ....	119
<b>Figure 3.10.</b> (a) Fracture tests of neat PLA and 10 wt.% PLA/BaSO <sub>4</sub> . The force-displacement curves at different stages (A, B, C, D, E) and their corresponding (b) images. Inset in image B points the presence or not of fibrils. ....	121

**Figure 3.11.** Images of optical microscopy of PLA scaffolds showing filament and gap dimensions. .... 123

**Figure 3.12.** Compression stress ( $\sigma$ )–strain ( $\epsilon$ ) curves of scaffolds for neat polylactide (PLA) and composite of polylactide with coated polydopamine barium sulfate particles (PLA/PD-BaSO<sub>4</sub>) 10 wt. %. .... 124

**Figure 3.13.** Metabolic activity of Human dermal fibroblasts (HDFs) seeded in the presence of 10, 50, 100 or 500  $\mu\text{g}/\text{mL}$  of barium sulfate particles (BaSO<sub>4</sub>) or barium sulfate particles coated with polydopamine (PD-BaSO<sub>4</sub>). Asterisks indicate significant differences ( $p < 0.05$ ) with respect to the control. .... 126

**Figure 3.14.** HDFs seeded in the presence of 500  $\mu\text{g}/\text{ml}$  of BaSO<sub>4</sub> showing normal morphology and suggesting the internalization of the particles. Particles inside of HDF (blue circle) and outside of HDF (blue arrow) ..... 126

**Figure 3.15.** Metabolic activity of Human dermal fibroblasts (HDFs) seeded on polylactide (PLA), composite of polylactide and barium sulfate particles (PLA/BaSO<sub>4</sub>) and composite of polylactide and coated with polydopamine barium sulfate particles (PLA/PD-BaSO<sub>4</sub>) with respect to the control at day 1, 3 and 7. Asterisks indicate significant differences ( $p < 0.05$ ) with respect to the cells seeded on tissue culture plastic (TCP). .... 127

**Figure 3.16.** Proliferation of Human dermal fibroblasts HDFs seeded polylactide (PLA), composite of polylactide and barium sulfate particles (PLA/BaSO<sub>4</sub>) and composite of polylactide and coated with polydopamine barium sulfate particles (PLA/PD-BaSO<sub>4</sub>) a and b indicate significant differences ( $p < 0.05$ ) with respect to day 1 and day 3, respectively. .... 128

**Figure 3.17.** Release profiles over time of levofloxacin in neat PLA, polydopamine coated neat PLA (PD-PLA) and PLA/PD-BaSO<sub>4</sub>. .... 130

<b>Figure 3.18.</b> Agar disk diffusion tests: (a) PLA/PD-BaSO <sub>4</sub> with levofloxacin, (b) PLA/PD-BaSO <sub>4</sub> negative control (no levofloxacin) and (c) levofloxacin disk (5 μg) as a positive control. ....	131
<b>Figure 3.19.</b> Specimen geometry for (a) uniaxial tensile tests (dumbbell-shaped sample) ,(b) fracture toughness tests (compact tension sample) with a thickness of 1 mm in both cases; (c)compression test in scaffold sample. ....	136
<b>Figure 4.1.</b> Ring-opening polymerization for dopamine end-capped polylactide (PLA-DA). ....	158
<b>Figure 4.2.</b> <sup>1</sup> H NMR of PLA-DA for degree of polymerization. Dp = 10. Reaction conditions: 2 mol L <sup>-1</sup> solution of L-lactide in CHCl <sub>3</sub> at 25 °C using DBU as catalyst. (entry 9 of Table 4.1). ....	159
<b>Figure 4.3.</b> <i>Kinetics of polylactide followed by <sup>1</sup>H NMR ( monomer 5.45 ppm polymer 5.20 ppm)</i> (entry 2 of Table 4.2). ....	161
<b>Figure 4.4.</b> Kinetic plots for the different experiments runned with different TEA concentratios. ....	162
<b>Figure 4.5.</b> <sup>1</sup> H NMR spectra in DMSO-d <sub>6</sub> for a) Catechol end-functional PLLA with DP 10 and b) Dopamine initiator. ....	163
<b>Figure 4.6.</b> <sup>13</sup> C NMR of Catechol-PLLA for degree of polymerization DP = 10. (entry 2 of table 4.2). ....	164
<b>Figure 4.7.</b> (a) Molecular weight vs. conversion graph of PLLA using dopamine as initiator, [(a) entry 7]; (b) SEC trace with UV (289 nm wavelength) and refractive-index signals for semitelechelic catechol PLLA; (c) MALDI-TOF spectra for semitelechelic catechol-PLA. [(b) and (c) Entry 2]. ....	165
<b>Figure 4.8.</b> Left figure for DP 25 and right figure for DP 50. <sup>1</sup> H NMR spectra in DMSO-d <sub>6</sub> for Catechol end-functional PLLA, SEC trace with UV (289 nm	

wavelength) and refractive-index signals for semitelechelic catechol PLLA.  
 And finally MALDI-TOF spectra for semitelechelic catechol-PLLA. .... 166

**Figure 4.9.** Scale spanned <sup>1</sup> H NMR of catechol-PLLA (a) before oxidation; (b) after oxidation and (c) after post-functionalization with hexamethylenamine. .... 168

**Figure 4.10.** (a) The progress of the Ag<sup>+</sup> reduction in the presence of catechol-PLLA studied by extinction spectroscopy and TEM image of AgNPs stabilized by the polymer; (b) The progress of the Ag<sup>+</sup> reduction in the presence of PLLA-phenethylamine studied by extinction spectroscopy. .... 169

**Figure 4.11.** DSC spectrum for blends of PLA/PLA-DA and neat PLA. .... 170

**Figure 4.12.** Thickness of neat PLA, neat PLA-DA and blend of PLA/PLA-DA (80/20). .... 173

**Figure 4.13.** Third harmonic Frequency (F3) versus time. .... 173

**Figure 4.14.** A) Functional polymer (PLA-DA) B) PLA coated with polydopamine. .... 174

**Figure 4.15.** Release profiles over time of levofloxacin in neat PLA, polydopamine coated neat PLA (PD-PLA) and the blend of PLA/PLA-DA (80/20) at pH 7 and pH 5 ..... 176

Figure 4.16. Levofloxacin balance in different pH ..... 177

**Figure 4.17.** Selective release profiles over time of levofloxacin in neat PLA and PLA/PLA-DA (80/20) at pH7 and pH 5 ..... 178

Figure 4. 18. Metabolic activity of HeLa cells. .... 179

**Figure 4.19.** Cells onto scaffolds with levofloxacin. .... 179

**Figure 4.20.** Agar diffusion test for a) PLA and b) PLA/PLA-DA ..... 181

## A2. List of Tables

<b>Table 1.1.</b> Additive manufacturing technologies overview to ASTM F2792-12a .....	<b>Error! Bookmark not defined.</b>
<b>Table 2.1.</b> The solution of PLA with chloroform and 1,4-Dioxane. The wt. % of solution and the rename of de solution. 69	
<b>Table 2.2.</b> Shear modulus (G), initial viscosity ( $\eta_0$ ) and coporation index (n) of PLA inks with chloroform and 1,4-dioxane.....	73
<b>Table 3.1.</b> Radiopacity of composite PLA/BaSO <sub>4</sub> and PLA/PD-BaSO <sub>4</sub> for 2, 5 and 10 wt. % of BaSO <sub>4</sub> and PD-BaSO <sub>4</sub> respectively 111	
<b>Table 3.2.</b> Mechanical properties of neat PLA and PLA/BaSO <sub>4</sub> composites with respect to wt. % of BaSO <sub>4</sub> . E: tensile modulus, $\sigma_r$ : tensile strength, $\epsilon_r$ : elongation at break and TT: tensile toughness. ....	113
<b>Table 3.3.</b> Mechanical properties of neat PLA and PLA/PD-BaSO <sub>4</sub> composites with respect to wt. % of PD-BaSO <sub>4</sub> . $\sigma_y$ : tensile yield, E: tensile modulus, $\sigma_r$ : tensile strength, $\epsilon_r$ : elongation at break and TT: tensile toughness. ....	114
<b>Table 3.4.</b> Printed condition for the neat PLA and composites PLA/BaSO <sub>4</sub> 10 wt.% of BaSO <sub>4</sub> and PLA/PD-BaSO <sub>4</sub> 10 wt.% of PD-BaSO <sub>4</sub> .....	122
<b>Table 4.1.</b> Different synthesis rout for the polymerization L-lactide initiate by dopamine. 158	
<b>Table 4.2.</b> Different synthesis routes for the polymerization L-lactide initiated by dopamine using TEA as catalyst and DCM and CHCl <sub>3</sub> like a solvents....	160
<b>Table 4.3.</b> Printed condition for the neat PLA and Blend PLA/PLA-DA 80/20. ....	171
<b>Table 4.4.</b> Inibition zone diameter for PLA, PLA-Levofloxacin, PLA/PLA-DA and (PLA/PLA-DA)-Levofloxacin.....	180



### A3. Symbols and Abbreviations

PLA	Polylactide
TE	Tissue engineering
ECM	Extracellular matrix
HA	Hydroxyapatite
TCP	Tricalcium sulfate
LA	Lactic acid
ROP	Ring Opening Polymerization
PLLA	Poly-L-lactic acid
PDLA	Poly-D-lactic acid
PDLLA	Poly-D,L-lactic acid
$T_g$	Glass transition temperature
$T_c$	Crystallization temperature
$T_f$	Melting temperature
AM	Additive manufacturing
CAD	Computer aid design
BJG	Binder jetting
3DP	3D printing
DED	Directed energy deposition
DLF	Directed light fabrication

### A3 Symbols and Abbreviations:

---

DMD	Direct metal deposition
LENS	Laser engineered net shaping
PEEK	Polyether ether ketone
PP	Polypropylene
SHS	Selective heat sintering
SLM	Selective laser melting
EBM	Electron beam melting
DMLS	Direct metal laser sintering
CIJ	Continuous inkjet printing
MJM	Multijet modelling (MJM),
PJM	Polyjet modelling
DoD	Drop-on-demand
UV	Ultra violet
UAM	Ultrasonic additive manufacturing
LOM	Laminated object manufacturing
PVC	Polyvinyl chloride (PVC)
SL	Stereolithography
2PP	Two-photon polymerization
DLP	Digital light processing
CLIP	Continuous liquid interface production



### A3 Symbols and Abbreviations

---

DIW	Robocasting/direct ink writing
PC	Polycarbonate
ABS	Acrylonitrile butadiene styrene
PS	Polystyrene
PVA	Polyvinyl alcohol
CA	Cellulose acetate
MC	1-chloro-2,2,5,5-tetramethyl-4-imidazolidinone
PCL	Polycaprolactone
PHB	Polyhydroxybutyrate
DSC	Differential scanning calorimetry
SEM	Scanning Electron Microscope
$\eta$	Viscosity
$\eta_0$	Initial viscosity
$\sigma$	Shear stress
G	Shear modulus
n	Performance index
Q	Flow rate
L	Needle height
$R_L$	Inner diameter of the needle end zone
$R_0$	Inner diameter of the initial needle area

### A3 Symbols and Abbreviations:

---

$\mu$	Viscosity of PLA ink
$\Delta P$	Change of pressure occurring in the needle
$S_L$	Lateral surface of a truncated cone.
F	Force exerted at the needle inlet.
$G''$	Loss modulus
$G'$	Storage modulus
PTFE	Polytetrafluoroethylene
$BaSO_4$	Barium sulfate
$Fe_3O_4$	Ferrous oxide
$Bi_2O_3$	Bismuth oxide
PD	Polydopamine
BMP-2	Bone morphogenic protein 2
IGF-1	Insulin-like growth factor 1
MWCNT	Multi-walled carbon nanotubes
PU	Polyurethanes
PD- $BaSO_4$	$BaSO_4$ particles coated with polydopamine
RO	Radiopacity
$t_d$	Thermal degradation temperatura
TT	Toughness
E	Tensile Modulus

### A3 Symbols and Abbreviations

---

$\sigma_r$	Tensile strength
$\epsilon_r$	Elongation at break
WOF	Work of fracture
Wt. %	weight percent
HDFs	Human dermal fibroblasts
TCP	Tissue culture plastic
FDM	Fused deposition modelling
$\sigma_y$	Tensile yield







# Curriculum vitae





## Naroa Sadaba Larraona

Date of birth: 09/08/1989  
Nationality: Pamplona, Spain  
Phone: +34 695997909  
Email: [naroasadaba89@gmail.com](mailto:naroasadaba89@gmail.com)

### International Research Experience

July 2019 | December 2019

**University of Washington, (Seattle) USA.**

Alshakim Nelson Research Group.

*Research focus: 3D printing of hydrogel tube*

Research Assistant

March 2019/April 2019

**University of Natural Resources and Life Sciences, Vienna**

*Research focus: attachment of drug in the PLA-Based scaffolds*

PhD Student

February 2018 | March 2018

**Institute for Medicines iMed.ULisboa, Faculty of Pharmacy, Portugal**

*Research focus: Drug delivery and antiviral activity of PLA-based scaffold*

PhD Student

### Education

September 2015 | Present

**PhD Program "Engineering of Materials and Sustainable Processes"**

Universidad del País Vasco (UPV/EHU), POLYMAT, Spain

September 2016 | July 2017

**Master in engineering of advanced Materials Engineering**

Universidad del País Vasco (UPV/EHU), Spain

September 2011 | June 2013

**Material Engineering**

Universidad del País Vasco (UPV/EHU), Spain

October 2007 | June 2011

**Industrial Technical Engineering specialized in industrial chemistry**

Universidad del País Vasco (UPV/EHU), Spain

## Fellowship

September 2015 | June 2019

**Polymat Researcher Fellowship**

Doctorate in "Organocatalysis and Sustainable Polymers"

June 2019 | December 2019

**Global Training International Fellowship**

Basque Government

## Publications

1. I. MARTINEZ DE ARENAZA, N. SADABA, A. LARRAÑAGA, E. ZUZA AND J.R. SARASUA. "**High Toughness Biodegradable Radiopaque Composites Based On Polylactide And Barium Sulphate**". EUR POLYM J 73, 88-93 (2015). [doi:10.1016/j.eurpolymj.2015.10.005]
2. N. SADABA, M. SALSAMENDI, N. CASADO, E. ZUZA, J. MUNOZ, J.R. SARASUA, D. MECERREYES, D. MANTIONE, C. DETREMBLEUR AND H.

- SARDON. "*Catechol End-Functionalized Polylactide By Organocatalyzed Ring-Opening Polymerization*". POLYMERS-10, 2, - (2018). [doi:10.3390/polym10020155]
3. N. SADABA, R. MARTINI, F. BARTHELAT, I. MARTINEZ DE ARENAZA, A. LARRANAGA, J.R. SARASUA AND E. ZUZA. "*Understanding The Toughness Mechanism Prompted By Submicron Rigid Particles In Polylactide/Barium Sulfate Composites*". POLYM TEST 69, 340-349 (2018). [doi:10.1016/j.polymertesting.2018.05.041]
4. M. CALAFEL, R. AGUIRRESAROBÉ, N. SADABA, M. BOIX, J. CONDE, B. PASCUAL AND A. SANTAMARIA. "*Tuning The Viscoelastic Features Required For 3D Printing Of PVC-Acrylate Copolymers Obtained By Single Electron Transfer-Degenerative Chain Transfer Living Radical Polymerization (SET-DTLRP)*". EXPRESS POLYM LETT 12, 9, 824-835 (2018). [doi:10.3144/expresspolymlett.2018.70]
5. N. ZIVIC, N. SADABA, N. ALMANDOZ, F. RUIPEREZ, D. MECERREYES AND H. SARDON. "*Thioxanthone-Based Photobase Generators For The Synthesis Of Polyurethanes Via The Photopolymerization Of Polyols And Polyisocyanates*". MACROMOLECULES 53, 6, 2069-2076 (2020). [doi:10.1021/acs.macromol.9b02648]
6. N. SADABA, A. LARRANAGA, G. ORPELLA-ACERET, A. BETTENCOURT, V. MARTIN, M. BIGGS, I. RIBEIRO, J. UGARTEMENDIA, J.R. SARASUA AND E. ZUZA. "*Benefits Of Polydopamine As Particle/Matrix Interface In Polylactide/PD-BaSO<sub>4</sub> Scaffolds*". INT J MOL SCI 21, 15, 1-15 (2020). [doi:10.3390/ijms21155480]
7. K. O'HARRA, N. SADABA, M. IRIGOYEN, F. RUIPEREZ, R.

AGUIRRESAROBE, H. SARDON AND J. BARA "*Nearly Perfect 3D Structures Obtained By Assembly Of Printed Parts Of Polyamide Lonene Self-Healing Elastomer*". ACS APPL POLYM MATER 2, 11, 4352-4359 (2020). [doi:10.1021/acspapm.0c00799]

### Contribution to conferences Congresses

- **Poster presentation:**, N. Sadaba, E.Zuza, J. Muñoz, H. Sardon. "*Facile synthesis of dopamine initiated immortal ring-opening polymerization of L-lactide*" 2nd SUSPOL-EJD SCHOOL .Bruselas(2016)
- **Oral presentation III** N. Sadaba, I. Martinez de Arenaza, E. Zuza, A. Larrañaga, J.R Sarasua "*Zailtasun handiko polilaktida erradio-opakoak*". **Materialen Zientzia eta Teknologia**. Markina (2016)
- **Oral presentation.** N. Sadaba, M. Fernández, I.Calafell, E. Zuza, J.R. Sarasua, J.Muñoz "*3D PRINTING OPTIMIZATION OF PLLA BASED ON RHEOLOGICAL ANALYSIS*". **Eupoc 2017**Lago di Garda (Italia) (2017)
- **Oral presentation** N. Sadaba, R. H. Aguirresarobe, M. Fernández, J. Muñoz, J.R: Sarasua, E. Zuza. "*RADIOPAQUE MATERIAL FOR 3D PRINTING SCAFFOLDS ANALYSIS*" **JIP** Tarragona (España)(2017)
- **Oral presentation** .N. Sadaba Larraona, M. Fernandez San Martin, I. Calafell Martinez, J.R.Sarasua Oiz, J.Muñoz Ugartemendia, E.Zuza Hernández "*RADIOPAQUE MATERIAL FOR 3D PRINTING SCAFFOLDS*" **XXXV Congreso anual de la Sociedad de la Ingeniería biomédica Española CASEIB-2017** Bilbao (España)(2017)
- **Oral presentation**, N. Sadaba, E. Aldalur, E. Zuza, J.R Sarasua, J. Muñoz "*Funtzio-gradienteak duten zelula-euskarrien fabrikazioa 3D*

*inprimagailuz lotailu-hezur juntura birsortzeko*". **Materialen Zientzia eta Teknologia IV** Donostia-San Sebastian (Spain) (2018)

- **Oral presentation**, N. Sadaba, J. Muñoz, J.R. Sarasua, E. Zuza *Bioresorbable, "Radiopaque and 3d printable scaffolds for bone tissue"* 4th International Conference on Biomedical Polymers & Polymeric Biomaterials ISBPPB2018 Krakow (Poland) (2018).
- **Poster presentation** . N. Sadaba, E. Zuza, J.R. Sarasua, J. Muñoz *"3D para implantes hueso-ligamento"* **"XXXV Congreso anual de la Sociedad de la Ingeniería biomédica Española CASEIB-2018** Ciudad Real (España)(2018)

